UNIVERSITY OF EVRY VAL D'ESSONNE

DOCTORAL SCHOOL SITEVRY

P H D T H E S I S

to obtain the title of

PhD of Science

of the University of Evry Val d'Essonne

Specialty : Robotics

Defended by

Mohamed Guiatni

Design and Control of a Haptic Device for Minimally Invasive Surgery Simulation

Thesis Advisor: Abderrahmane Kheddar

prepared at IBISC Laboratory, Evry

defended on June 22, 2009

Jury :

Reviewers :	André Crosnier	-	Université de Montpellier II
	Gábor Székely	-	ETH Zürich (Suisse)
Advisor :	Abderrahmane Kheddar	-	CNRS
President :	Vincent Hayward	-	Université Paris 6 (Paris)
Examinators :	Jean-Loup Florens	-	ICA-ACROE (Grenoble)
	Christian Duriez	-	INRIA Futur (Lille)

Acknowledgments

D'abord, je remercie Dieu l'Omniscient, le Tout-généreux de m'avoir permis de concrétiser ce projet.

Je tiens tout particulièrement à exprimer ma plus profonde gratitude au Professeur Abderrahmane Kheddar, pour m'avoir fait confiance depuis mon stage de magister, avoir accepté de diriger ces travaux de thèse et m'avoir soutenu tout au long de cette étude. Ses orientations lucides, critiques et expérimentée ont été indispensables à la concrétisation de cette recherche.

J'adresse ma plus respectueuse reconnaissance aux membres du jury de soutenance, pour l'intérêt qu'ils ont porté à ce travail en acceptant de participer dans ce jury. Je remercie ainsi les rapporteurs, messieurs Gabor Szekely et André Crosnier ainsi que les examinateurs, messieurs Jean-Loop Florent et Christian Duriez, qui ont fait l'effort de venir respectivement de Suisse, de Montpelier, de Grenoble et de Lille, et le président du jury M. Vincent Hayward pour leurs remarques pertinentes et les discussions enrichissantes.

Ce travail a été réalisé dans le cadre d'une convention entre l'Université d'Evry Val d'Essonne et l'Ecole Militaire Polytechnique (EMP) d'Alger. Que ces deux institutions trouvent ici le témoignage de ma reconnaissance.

Je remercie le personnel administratif de l'Ecole doctorale de l'Université d'Evry Val d'Essonne et spécialement Mme Florence Hamon et Mme Annie Plazza pour leur gentillesse et pour les services qu'elles m'ont rendu le long de cette thèse. Je remercie le directeur du laboratoire IBISC et son adjoint et également les membres de l'équipe Haptique, Hichem Arioui, Nicholas Séguy, Pierre Julie, Lamri Hehoua et Nadjet Talbi avec lesquels j'ai eu la joie de travailler le long de mes séjours à IBISC. J'adresse un remerciement distingué à Abdelhamid Drif et Vincent Riboulet avec lesquels j'ai eu le plaisir de travailler et de partager de bons moments.

Une grande partie de ce travail a été menée au Laboratoire de Contrôle et Commande de l'EMP à laquelle je dois beaucoup. Je remercie d'abord, le Commandant de l'EMP, le Directeur de la Recherche et de la Formation Post-Graduée, le chef d'UER Automatique, et le chef du Laboratoire de Contrôle et Commande de m'avoir donné la possibilité de faire cette thèse, pour la confiance qu'ils ont mis en moi et pour leurs encouragements. Je suis très reconnaissant à toutes les personnes de l'EMP qui ont contribués à la concrétisation de ce projet ainsi que M. Lehtihet pour ses remarques pertinentes et ses conseils.

Je remercie aussi M. Abdelaziz Benallegue et Tarek Madani de m'avoir accueilli au Laboratoire d'Ingénierie des Systèmes de Versailles (LISV). Je les remercie également pour les nombreuses discussions enrichissantes et pour les bons moments

que j'ai partagés avec eux.

Je remercie également M. Christophe Chaillou, responsable du groupe-projet ALCOVE de l'Institut de Recherche en Composants logiciels et matériels pour l'Information et la Communication Avancée (IRCICA) ainsi que les membres de l'équipe SOFA, Stéphane Cottin, Juan-Pablo et spécialement Christian Duriez de m'avoir agréablement accueilli dans leur équipe. Je les remercie aussi pour l'aide qu'ils m'ont offert et surtout pour leur sympathie.

Je ne peux terminer ces remerciements sans mentionner mes proches, à qui je dédie ce travail et dont l'amour et le soutien et les encouragements m'ont été plus que bénéfiques.
A ma mère d'abord, l'être le plus cher à mon coeur, qui a beaucoup prié pour moi, et dont ses prières ont été exaucées.
A mes frères Amar et Said.
A mes soeurs Nawel, Amel, Fazia et Mounia.
A mes nièces Amira, Fatima, Lina et Doua et mes neuvex, Hakim, Aymen, Houssam et Islam.
A mes beaux frères Tahar, Ahcène et Salim.
Je ne saurais oublier mes amis Meziane, Yacine, Mohamed, Ramzi, Réda, Said, Amar...

...à la mémoire de mon très cher père...

Contents

Chapter 1

Introduction

Contents

1.1 Context

Open surgery traditionally involves making large incisions to visualize the operative field and to access human internal tissues. Minimally invasive surgery (MIS) is an attractive alternative to the open surgery whereby essentially a large number of operations are performed using the specialized instruments designed to fit into the body through several small incisions. MIS offers important advantages: it can minimize trauma and pain, decrease the recovery time thereby reducing the hospital stay and cost. However MIS induces some difficulties for the surgeon. During an intervention, the surgeon cannot directly see the operating site, but must rely on a 2D video image of the site. Since the instruments and the camera are introduced through small holes, their movements are restricted. This makes manipulating them awkward. In addition, biomechanical behavior of the tissue is relayed through the instruments, thus reducing touch sensations. Hence, surgeons have reduced visual and haptic feedback during MIS interventions, and can not rely on traditional hand-eye coordination. Therefore, training a new MIS procedure takes more practice than learning new traditional surgical procedures. Interactive Virtual Reality (VR) surgery simulators are becoming a common useful tool for training surgical procedures. The advent, growth, and development of VR simulation as adjunctive educational, training, and certification modalities in surgery is likely affecting current surgical practice in substantial and various ways.

Unfortunately, constructing such simulations is a technically challenging task. Consider such a system, consisting of a VR graphics simulation connected with a haptic interface that renders reaction forces (a force feedback or haptic device), lets the surgeon manipulate virtual organs, and feel their reactions. In addition, these simulators serve as a test-bed for the evaluation and validation of new instrumentation and procedures, since the advances in these fields have enabled continual growth

in MIS techniques. The operating room is becoming an increasingly complex environment as technology affects the ways in which surgery is practiced, with marked change during the last years and little to suggest otherwise for the future.

Among several medical diagnosis skills, palpation involves the medical personnel interacting directly with skins or tissues. The development of palpation simulators tends to be less common, although palpation is an important technique for the diagnosis of many conditions. Tactile and thermal are the main senses stimulated during a palpation task. However, thermal sensing tends to be ignored, although it is important, especially, for abnormal thermal behavior localization; those are correlated with the presence of tumors detection.

In this research, considerations are made of a system, where thermal information, together with visual and force feedback, is integrated as a new multi-sensory surgical simulation platform. The main issue that must be addressed when trying to introduce surgery simulator in medical training, is the cost and the fragility of haptics with force feedback. Indeed, such a device makes the surgery simulator four times more expensive and requires frequent repairs during normal use.

1.2 Objectives

The main objective of this research is to make a contribution in the field of surgery simulation. It focuses on the creation of a new interface for MIS training. This interface allows the followings:

1. ***Force feedback rendering:*** Beyond the functional role of haptics in surgery simulation, the design of a new haptic device for MIS training will help understanding the technological issues, reducing cost, implementing, testing algorithms, etc.

2. ***Thermal rendering:*** Particular emphasis has to be placed in presenting the user with the thermal cues of a manipulated object in Telepresence and VR systems. In the context of surgery, the palpated organ will have not only visual features and biomechanical behavior, but also thermal characteristics. This thermal cue has to be reproduced to the user fingertip when interacting with virtual organs.

3. ***Integrating multi-cues feedback:*** The incorporation of novel broadband sensory modalities, with visual, haptics and thermal technology, into the evolution of the next generation of surgical robotic and surgical simulator will be investigated.

4. ***Improving the immersion and realism of simulators:*** Since dexterous manipulation and haptic sensation are especially interrelated in surgery, the final objective is to meet the different challenges in order to interface successfully this multi-modal interface with the typical environmental characteristics found in surgery.

1.3 Thesis outline

This thesis is organized as follows:

The first chapter introduces the MIS-surgery techniques and briefly recalls its specificity, evolution and nowadays use. We discuss problems and limitations encountered in MIS procedures teaching for skill when using cadavers, animals or pelvi-trainers. We present an alternative technique for MIS skill acquisition using VR technology and discuss several other advantages which make VR-MIS a nearly standard mean. Building a VR surgery simulator requires first the understanding of the expert surgeon's dexterity (i.e. gesture, sensory-motor behaviors, procedures, etc.) during a given operation. Therefore, the particular contribution of the haptic, tactile and thermal senses is discussed. We also list and compare a chosen set of commercially available simulators developed for MIS training (some advanced laboratory prototypes are also evoked). Then, we present recent investigation results concerning the use of VR simulator as a reliable tool for the assessment of skills in surgery.

The second chapter discusses general requirements for designing a new haptic interface which has the ability to provide force feedback during MIS procedure. These (and other) requirements are obtained by an analysis of the existing literature in real MIS surgery measurement data and existing knowledge in haptic interfaces design. A new device is proposed and its mechatronics design and realization are detailed. Trade-offs in the design procedure, actuators dimensioning, transmission and reduction are discussed. Dynamics and kinematics equations are explicitly made using classical robotic modeling tools. The main characteristics of the prototype such as bandwidth, stiffness, force/torque capabilities, and workspace are presented and compared to other available devices. Experiments are also performed for position and torque control of the assembled prototype, and the obtained performances are discussed.

The third chapter deals with fundamentals in thermal rendering. We present the modeling and identification procedures of thermoelectric modules that we used in thermal displays or as an active artificial finger for probing. In the rest of the chapter, we investigate new thermal rendering methods for telepresence and VR applications. In order to test the efficiency of the developed models, experiments will be conducted using candidate materials that have dissimilar thermal properties. The first developed model is based on the estimation of the temperature in contact for both the finger and the touched object. The estimation uses a combination of a simplified heat transfer model and thermal feedback is provided by a bilateral control between the master (thermal display) and the slave (thermal robotic finger) using local temperature control loops. But the influence of the contact conditions and the finger properties are not negligible. To improve thermal rendering transparency, we propose another approach based on a neural network learning classifier with a model-based control scheme. We also provide a fast analytical method to simulate thermal exchange in VR. All the proposed techniques and models are validated experimentally; the obtained results are discussed in this chapter.

The last chapter is dedicated to the integration of our hardware and methods (including force with thermal feedback) within a interactive simulation software called SOFA. Prior to the integration, we investigate the role of thermal sensation in surgery. Models, based on the Pennes' Bio Heat Transfer Equation (BHTE), are developed and implemented for medical diagnosis and temperature monitoring during heat therapy procedures. In order to allow for thermal rendering, we integrate a thermal display on the surgical-tool handle. The whole interface (Visual/Haptic/Thermal) is mounted according to the general implementation algorithm allowed in the SOFA framework. The results of the conducted experiments are discussed. Finally, concluding remarks and proposition for future works are addressed.

Chapter 2

State-of-the-art in surgery simulators

Contents

2.1 Introduction

The success of flight simulators is a good example of the importance of simulation technology when applied to the teaching of abilities that have an impact on human lives. Just as the flight simulators, the learning of the fundamentals of minimally invasive surgery (MIS) procedures has improved with today's surgical simulators. These simulation devices range from simple, homemade boxes to sophisticated systems mimicking operating tables with plastic manikins or virtual patients. First-generation systems use physical objects (such as cotton string, pegs, latex tubes, and rings) to teach the basic psychomotor coordination actions necessary for MIS procedures. Some of these systems offer electronic metrics. Other members of this group are computer-based and afford virtual images and instruments projected onto monitors/displays. Second-generation devices take advantage of the huge computational advances in graphical representation of tissues and organs. These devices generally include a haptic device for touch sensation, which allows practice of the basic skills, gestures, and instrument-tissue manipulations typically choreographed into surgical procedures. The most advanced of the second-generation systems incorporates virtual 3D models of human anatomy and can support distributed, web-based learning at remote sites.

The aim of this chapter is to provide a state-of-the-art about surgery simulators, especially those used for MIS training. This type of surgery has many advantages for patients and hospitals. However, it is difficult to practice due to some constraints specific to MIS; the major advantages and difficulties are highlighted. Then, we present the different training methods most commonly used to train in MIS. Finally, we provide a description of the surgical simulator systems currently available and offer a set of recent comparison and evaluation works against which to judge their usefulness.

2.2 MIS: History, advantages and difficulties

Minimally invasive surgery, commonly referred to as laparoscopy, differs from opened surgery by the fact that the surgeon works through small incisions (typically, 5 to 12 mm in diameter) and using specific instruments (scalpel, grip, clamp, etc.), (see Figure 2.1)[1]. These instruments, in form of stem, are longer than traditional instruments (between 30 cm and 40 cm) to take into account of outdistance between the point of incision and the body. Several incisions are carried out and equipped each with a trocar, two for the surgical instruments and for the laparoscope (camera), (see Figure 2.2)[2]. Carbon dioxide under pressure is also injected by one of the trocars in order to release more space between the body and the abdominal wall [Liu 2003].

The first practical use of MIS is credited to Hans Christian Jacobäus in Stockholm, who, in 1910, published his findings of endoscopic investigation of the abdom-

[1] www.stryker.com
[2] www.levelfive.com

Figure 2.1: Minimally Invasive Surgery Instruments.

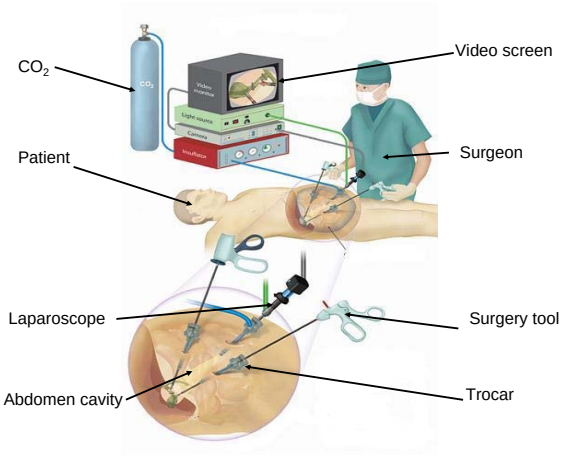

Figure 2.2: Minimally Invasive Surgery Procedure.

inal cavity in 19 patients using air to insufflate [Wayand 2004]. It was Christoph Zollikofer, who used carbon dioxide for the first time to insufflate into the abdominal cavity that made possible electrical coagulation in interventions in the abdominal area. In 1938, the Hungarian physician Janos Veress developed a point in a needle that was named after him and it is still used today to insufflate gas into the abdominal cavity. The further development of endoscopy to video endoscopy, i.e. the transferability of a picture onto a screen, was the prerequisite that resulted in the method finding wide use. However, it was the gynecologists, in particular Kurt Semm, who, through manifold innovations and creative applications, became the pioneers of modern laparoscopic surgery. He performed the first laparoscopic appendectomy in 1981. Erich Mühe carried these ideas to further development by performing the first laparoscopic cholecystectomy in 1985. His operation was restricted, however, to access through the placing of a trocar with a large diameter. It was the French surgeons Philippe Mouret and Francois Dubois who brought the

method to clinical acceptance in France [Wayand 2004].
In June 1989, Jacques Perissat's (Bordeaux) video demonstration of a laparoscopic cholecystectomy was the starting signal for laparoscopic cholecystectomy throughout Europe. Perissat initiated the establishment of an international association for this new form of surgery and convened the initiation meeting of the foundation. In October 1990, the European Association of Endoscopic Surgery (EAES) was founded in Paris. In the course of the following two years, practically all the countries of Europe started to operate laparoscopically. The flagship of MIS was cholecystectomy. The penetration speed was breathtaking: within a few years, almost all cholecystectomy procedures were performed laparoscopically in 60% to 90% of European countries.
In general, since the late of 1980's, MIS has gained widespread acceptance because of its numerous advantages such as faster patient recovery, less damage to healthy tissue and smaller scars, less pain, less need for post-surgical pain medication, and less likelihood for incision complications [Woodrum 2006]. MIS has replaced open surgery for a variety of procedures. In general, surgery procedures such as cholecystectomy, antireflux surgery, bariatric surgery, colon surgery, and knee and shoulder surgery are performed laparoscopically. Laparoscopy is used increasingly for surgical procedures fields of gynecology, cardiac surgery, and urology, leaving patients with only four tiny marks and minimal discomfort. These dramatic patient benefits make laparoscopic surgery the procedure of choice among both surgeons and patients [Schijven 2003].
On the other hand, during MIS, the surgeon interacts primarily through two senses: tactile and visual. As surgical instruments are used to manipulate internal organs and the laparoscope is used to provide a camera view from the inside of the body on a video monitor that displays a two dimensional image, allowing the surgeon to visualize the surgery inside the patient [Upton 2002]. So that, MIS is characterized by an increased need for

- hand-eye-coordination to perform tasks looking at a screen to compensate for not being able to operate under direct vision;

- manual dexterity to compensate for the use of long instruments, which can amplify any error in movement; and fulcrum effect of the body wall, i.e. when the surgeon moves his hand to the patient's right, the operating end of the instrument moves to the patient's left on the monitor [Gallagher 1999];

- handling tissues carefully with limited mobility, limited degree-of-freedom (to compensate for the lack of sensation of touch using hands);

- compensation for the lack of 3-dimensional images and handling of instruments, adding to that the reduced dexterity and the lack of tactile feeling [Xin 2006][Payandeh 1997].

- coordination of the activities of the surgeon who manipulates the instruments and the assistant who handles the scope and positions it, because the scope

and instruments may be incorrectly positioned and there may be trembling of the hands.

For all these reasons, it is clear that MIS operations require much training and skills than those needed for the open surgery [Chiasson 2003].

2.3 Training Methods in MIS

The request for more efficient and effective training facilities is a real medical need. The training methods most commonly used are described and their advantages and disadvantages are given.

2.3.1 Training on patients (apprenticeship model)

Traditionally, residents are trained in the classical apprenticeship with hands-on training in the operating room. However, the specific psychomotor abilities and skills needed for minimally invasive surgery are not easily obtained in the operating room. In addition, training on patients is potentially unsafe. Therefore, it is ethically questionable whether the patient may be used as a learning object for basic skills. Furthermore, the resident is not trained to make the right decisions during critical situations, because the critical part is taken over mostly by the expert. Thus, the resident does not have the opportunity to make mistakes and to learn from the consequences, which is very essential for effective training. The concept that gaining skills from the training on patient is not always the best way to learn, for the sake of the patient as well as for the sake of the surgical trainee, has been effectively described. Reduced working hours for trainees, increased complexity of procedures and ethical considerations force engineers and clinicians to work together and develop training methods without using patients.

2.3.2 Training on cadavers

This method offers realistic anatomy, the appropriate organ colors, the correct surgical environment, as well as a chance to place trocars. However, the property of tissues will have altered, especially if the cadaver has been embalmed and blood will not flow from severed vessels. In addition, this method is expensive since only one of each type of operation can be performed on a single cadaver.

2.3.3 Training on animals

Performing laparoscopic surgery on animals is another method that is used for training trainee surgeons. The use of animals offers the chance for trainee surgeons to practice placing trocars, dissecting tissues and blood vessels, exploring the properties of tissues, and familiarizing themselves with the procedures [Carsten 2002]. However, there are limits to the viability of this method. For reasons of animal rights, this method is illegal in the United Kingdom, parts of Europe and is highly

unpopular in the United States. Also, this method is expensive, puts a student under time pressure (since the animal is anaesthetized), cannot be easily repeated, and does not possess the correct anatomy.

The problems with learning on patients, cadavers and animals are reasons why training methods outside the operating room are becoming more important.

2.3.4 Pelvi-trainers

A Pelvi-trainer is basically just a box, mimicking the abdomen, through which the surgical instruments are inserted (see Figure 2.3[3]). The contents of the box vary from simple objects to animal organs and synthetically produced organs. Force feedback is naturally obtained in a trainer that uses physical (tissue) materials to interact with. The use of physical materials allows for measurements of instrument-tissue interaction that can be used to optimize the training of tissue handling. However, training in Pelvi-trainers is currently not very often used. They are experienced not to be very stimulating, mainly because Pelvi-trainers do not give information about the level of task performance.

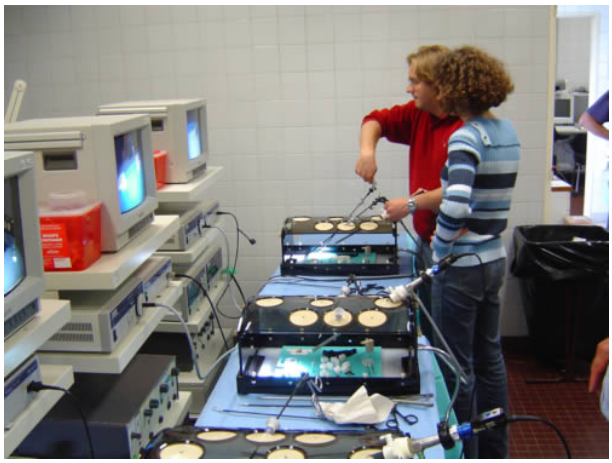

Figure 2.3: Pelvi-trainers.

2.3.5 Virtual Reality simulators

With the continuously increasing power of computers, simulators are now being acquired by hospitals as a means of improving training and reducing the costs of education. Virtual Reality (VR) simulators will increasingly become more eligible as a training aid, particularly due to their extensive range of educational features. In many recent studies, it has been shown that they improved surgeons' performance, thus contributing to patient care.
In VR simulators, abstract environments with objects or tissues and organs are simulated with computer models. Some of the simulators are equipped with force feed-

[3]Image from http://urologie-chu-mondor.aphp.fr

back. The performance feedback properties of VR simulators are stimulating their use and automatic supervision of training sessions is easily implemented. The rapid expansion of MIS has demonstrated that the traditional model of "see one, do one, teach one" is not an optimal approach for training surgical skills [Gallagher 2005] . Due to increasing time constraints, cost, stress, and ethical considerations, the modern operating room is not the ideal learning environment [Stolzenburg 2007]. The MIS revolution has forced the surgical community to rethink how they train residents and adapt to new technologies. This rethinking has driven the search for innovative training solutions. The next section is dedicated to VR Simulators.

2.4 Major characteristics of MIS simulators

2.4.1 Advantages

Over a decade ago, Satava [Satava 1993] proposed early adoption of VR as a training tool. Despite this early vision, VR simulation has only recently begun to be accepted by the surgical community. While the reasons for this delayed acceptance are numerous, the initial lack of robust scientific evidence to support the use of VR for skills training and the lack of knowledge of how to apply effectively simulation to a surgical skills training program are the two most likely reasons for delayed adoption of this technology [Champion 2003][Gallagher 2005]. It took a multidisciplinary team who looked beyond the "prettiness" of the simulator and drew from more than 50 years of sound research on aviation simulation and 100 years of behavioral sciences research to demonstrate the power of simulation for surgical training [Seymour 2002]. Due to the complexity of the MIS procedures, teaching programs must meet the demand for skilled surgeons to conduct those operations. The teaching program should also include a range of teaching devices from low-fidelity to high-fidelity simulators, which vary in degree of similarity with actual clinical procedures [Sternberg 2007]. If executed properly, VR offers inherent advantages over other training systems such as:

2.4.1.1 Training

Those who are involved in evaluating learning theories in surgery have found a very reliable application of the model of Rasmussen [Rasmussen 1983] that indicates that different training simulators need to be developed relating to different behavior levels [Lorenzo 2005]. At the low level (skill-based behavior), simulators are needed for learning basic skills such as using instruments. For higher-level trainers (rule-based behavior and knowledge-based behaviors), training has to be developed using more sophisticated training methods. For example, to enhance patient safety by reducing human errors and critical and unexpected situations (e.g. power failure or instrument breakdown), trainees should be trained at the higher-level. Also, VR simulators need to be developed in which the subjects can be confronted with unexpected complications and where quick decisions have to be made about what

the next step in the procedure should be. These types of crisis trainers should be developed to train surgical residents to make the right decisions while under stress.

2.4.1.2 Safety

Recognition of the importance of errors is now becoming an essential new component in the practice of surgery and new methods and technologies are being used to identify, avoid and reduce errors [Lorenzo 2005]. By using simulators, the novice surgeons can err without any dangerous consequences for the equipment, the public or the patients themselves. Testing and evaluating new instruments will also benefit from the introduction of simulation; new techniques and technologies will be safely tested and mastered, new and complex procedures can be practiced safely on a simulator before proceeding to the patient. In addition, simulators can decouple the student's time dependency so that they can practice on their own schedule. The potential of error reduction can substantially improve the healthcare systems in a similar way flight simulators did in aeronautics in the 1980s, inducing several socioeconomic advantages.

2.4.1.3 Standardization of surgeons' evaluation

The certification of surgeons in recent years has consisted of a written exam and an oral exam. No formal board certification process currently includes a technical skills proficiency examination. Competency is judged subjectively, even though there is a consensus that objective measures are required. Simulators can be used to ensure that minimum standards are met prior to performing the next level of case complexity in the operating room, or progressing to the next level of training. Practice sessions can be stored for later review by the physician. In addition, simulator can be used for certification of skill maintenance, which is considered of greatest importance in the future of surgery, leading to a continuous evaluation of surgeons with the final aim of elevating the standard of care.

2.4.1.4 Reduction of training costs

The economics of medicine has drastically reduced teaching time. Residents also face time constraints; regulations are now being adopted that limit both the number of hours that a resident can work per week, and the number of days that can be worked sequentially. The use of VR simulators reduces the use of the Operating Rooms that decreases the cost of the anesthesia, surgical instruments, and assistant's fees. In addition to that, the costs generated by the acquisition and preservation of cadavers and animals are reduced and ethical problems can be avoided.

In their latter role, VR training systems are designed to measure various facets of performance, such as motion and efficiency characteristics, errors, and time to complete a specified task. The systems also make it possible to record this information in a database from which it can be recovered for analysis. Final goals of the use of simulation would also encompass:

- a dramatic reduction of the training time - therefore reducing residency length and, more importantly, the learning curve for new techniques;
- the selection of residents, predicting those who will never achieve the skills needed for complex surgical procedures; and
- a less stressful-inducing approach to the operating room, considering that the real procedure can be simulated and pre-tested in a safe environment.

2.4.2 The sense of touch in MIS

One of the most important senses for performing varied complex and precise tasks autonomously or remotely is the sense of touch. The touch sensation from the human skin provides a multitude of information, including force, vibration, hardness, texture, temperature, etc. However, during MIS operations, the surgeon has no direct contact with the tissue, but manipulates the tissue via laparoscopic instruments. Therefore, haptic feedback is reduced to force feedback. The feedback of perceptive information is further disturbed because the used instruments have friction in the hinges and there is friction in the trocar. As a consequence, there is limited perception of pinching and pulling forces. Although the force feedback is limited, its role is of special interest because it is used in important decision-making scenarios such as the discrimination of healthy versus abnormal tissues and identification of organs and allows to commit appropriate force control actions for safe tissue manipulation [Puangmali 2008]. However, important properties such as tissue compliance, viscosity and surface texture, which give indications regarding the health of the tissue, cannot easily be assessed since tactile sensing is not present. In addition, high temperatures have a selective casualty effect on cancer cells, while higher temperatures can also harm normal cells. Thermal sensing finds particular utility in detecting and isolating unstable arterial plaque. Consequently, adding a medium for sensing the thermo-physical properties and temperatures of living organs or tissue will help surgeons work out the therapeutic program safely and effectively [Zhang 2000].

Haptic perception can also complement sensory modalities such as vision and therefore, can counterbalance the restricted camera vision in MIS [Feygin 2002]. It can affect the three main metrics of motor functioning (i.e. precision, speed, force) during surgery [Tavakoli 2005]. Therefore, haptic feedback is very important in performing surgical tasks with complex kinematics and can enhance precision in the case of MIS operation. Some studies have been performed to characterize the role of force feedback in MIS operations.

Bholat et al. [Bholat 1999] have shown that surgeons are able to determine shape, texture, and consistency in the absence of visual feedback using direct palpation, conventional instrument, and laparoscopic instrument.

A study done by Arsenault and Ware [Arsenault 2000] concludes that force feedback can improve performance when the perspective is incorrect. This suggests that force feedback may assist the surgeon's adaptation to incorrect viewpoint through

recalibration of the eye-to-hand mapping and, therefore, accelerate the learning process for MIS operations.

A study of the effect of force feedback on performing blunt dissection has shown that force feedback can reduce contact forces, task completion time and number of errors [Wagner 2002]. Moreover, in needle insertion tasks, the ability to detect the puncturing of different tissue layers is improved when users receive haptic feedback [Gerovichev 2002].

Palpation is another procedure frequently used by surgeons to estimate tissue characteristics and locate blood vessels. Without haptic perception and thereby palpation capability, excessive forces may be applied by surgeon causing complications such as accidental puncturing of blood vessels or tissue damage [Hashizume 2002]. In addition, a study performed in [Richards 2000] demonstrates that force and torque magnitudes associated with the tool/tissue interactions provide an objective means of distinguishing novices from skilled surgeons.

In order to restore the surgeon's perceptual capability, methods and technologies of tactile sensing have been applied with attempts to develop instruments that have been used to generate tactile feedback to the MIS surgeon [Matsumoto 1997][Eltaib 2003][Yao 2005][Puangmali 2008]. A detailed state-of-the-art in tactile display technologies can be found in [Benali-Khoudja 2004][Ottermo 2005][Hafez 2007], and particularly in [Puangmali 2008].

2.4.3 Haptic Feedback in MIS Simulators

Full interaction with a virtual environment requires haptic capabilities for manipulating objects and gesturing [Cotin 1999][Toole 1999][Bholat 1999][Cakmak 2000][Basdogan 2001]. The rapid increase in the number of papers on haptics and surgical simulation published in journals and international conference proceedings in the last decade indicates haptics' growing importance [Basdogan 2004]. For example, the study developed by Bell *et al.* in [Bell 2007] suggests that artificial force feedback may be processed differently than real force feedback in laparoscopic surgery simulations. In addition, results indicate that tissue differentiation is made easier by a large difference in compliance between two materials. A large compliance difference appears to be more useful for differentiation than an increase in force feedback alone.

Current VR technology provides very reliable force feedback, and accurate modeling of soft-tissue dynamics such as the mathematical modeling of non-homogeneous, hyper elastic materials, which are current research programs.

A key issue in integrating force feedback devices into a surgical simulation system is the update rate required for high fidelity. Although the visual display can be updated at 30Hz, the haptic interface update rate should be around 1kHz for stability reasons and to obtain a responsive interface (see Figure 2.4). This can be accomplished by a multi-rate simulation with a high-bandwidth force feedback loop [Liu 2003].

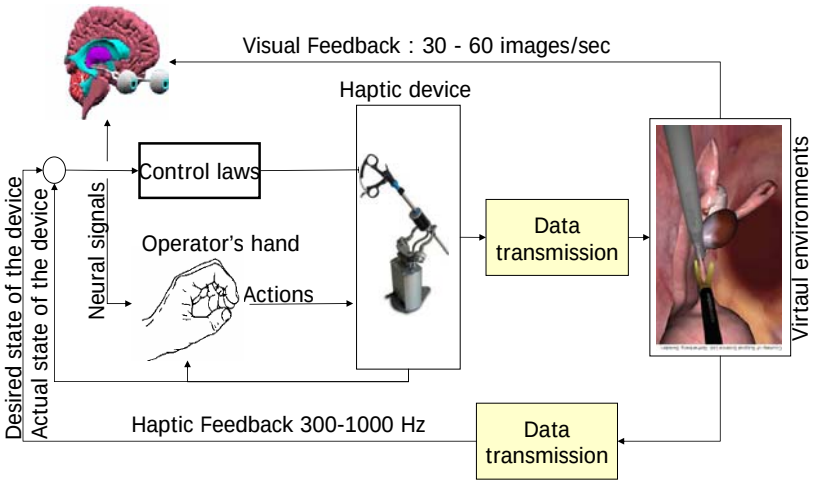

Figure 2.4: Haptic interfacing scheme.

Among the numerous problems in dynamic haptic rendering are the need for novel data structures to encode shape and material properties, the interactive haptic visualization of volumetric data, and the realistic modeling of deformable bodies. In addition, it is computationally extremely expensive to maintain a stable system while displaying smooth and realistic forces and torques because of the required haptic update rates.

Despite ingenious adaptations, haptic devices designed for general use, such as the Phantom, has limited utility for surgical simulation. Surgical procedures require special and more-complex haptic feedback.

However, developing natural haptic interfaces with force feedback and the ability to handle deformable objects remains one of the most difficult challenges in VR research today. Thus, current research has focused on the development of specialized devices for simulating specific classes of procedures, such as laparoscopy. Some attempts to add tactile feedback to MIS simulation systems are described in [Eltaib 2003].

The benefits of using haptic devices in medical training through simulation have already been recognized by several research groups and by many companies working in this area, see section 2.5.

2.5 Current state of MIS simulators

The purpose of this section is to highlight the status of simulation in surgical education, including available laboratory and commercial simulator and to briefly discuss the future of surgical training. One of the main differences between MIS train-

ers is whether haptic feedback is incorporated or not. A comprehensive overview of the major companies in the field of laparoscopic surgical simulation and their simulators is given. Some companies offer complete simulation solutions. Others emphasize either software or hardware development and are often linked in mutual partnerships:

2.5.1 Immersion

Immersion's involvement in medical simulation is somewhat confusing because the company not only markets its own simulators but also provides hardware interface technology to almost every other laparoscopic and endoscopic simulator on the market. So Immersion products consist of haptic devices and simulators.

2.5.1.1 Haptic device from Immersion

Laparoscopic Impulse Engine (LIE) The LIE has five degrees of freedom (DOFs) for motion and tracking with high resolution while providing force feedback in three DOFs (see Figure 2.5)[4]. An application example is the Karlsruhe Endoscopic Surgery Trainer [Cakmak 2000] where a pair of Impulse Engines acting as human-computer interface. Also, the VEST system (from Select-It AG) uses the LIE as its force-feedback interface for simulating laparoscopic surgery interventions.

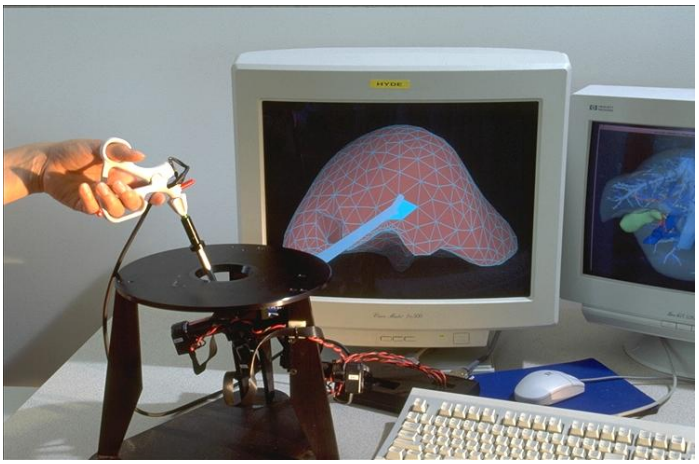

Figure 2.5: The Laparoscopic Impulse Engine from Immersion.

Laparoscopic Surgical Workstation (LSW) This system consists of two laparoscopic tools with interchangeable handles, (Figure 2.6)[5]. Each tool has four haptic DOFs and an additional twist knob that reorients the virtual tool tip. With the standard scissor-type handle there is a fifth haptic degree of freedom that allows

[4] Image from: http://www.cs.uu.nl
[5] www.immersion.com

the simulation of grasp forces associated with operations such as cutting and blunt dissection. The optional pen-type handle tracks the grasp motion. The intertrocar distance of 135mm closely replicates trocar placements used in actual laparoscopic procedures. A large system workspace accommodates a wide variety of procedures and patient geometries. The LSW costs about 28000 Euro.

Figure 2.6: The Laparoscopic Surgical Workstation from Immersion.

Virtual Laparoscopic Interface (VLI) The VLI tracks the motion of a pair of surgical instruments through three-dimensional space (Figure 2.7)[6]. The pitch and yaw motions allow each surgical tool to pivot about its insertion point, resulting in a large range of motion throughout a conical workspace. Insertion and retraction allow tools a third degree of freedom. Each instrument can also spin about its insertion axis, providing a fourth degree of freedom. The open-close motion of the tool handle is also tracked by the system. However, this interface does not generate force feedback and it costs about 6000Euro.

2.5.1.2 Surgical simulators from Immersion

LapVR^{TM} Surgical Simulator The LapVR^{TM} Surgical Simulator provides a platform for VR training. The system's hardware and software interface simulates laparoscopic surgery and provides VR training in the essential skills required of laparoscopic procedures (Figure 2.8)[7]. The LapVR^{TM} recorded performance, precision, and error metrics allow medical institutions to assess individual and team performance. This simulator supports three fully instrumented tools, two trocars with interchangeable simulated tool tips and an endoscopic camera with 0, 30, and 45 degree lenses and high-speed optical tracking technology to monitor accurately tool motion. The LapVR^{TM} enables developers, researchers, and educators to supply realistic VR training of laparoscopic abdominal procedures and skills.

[6] www.immersion.com
[7] www.immersion.com

Figure 2.7: The Virtual Laparoscopic Interface from Immersion.

Figure 2.8: LapVR system overview.

AccuTouch Endoscopy Simulator The AccuTouch Endoscopic Simulator is actually a suite of simulations covering bronchoscopy, sigmoidoscopy and colonoscopy using a flexible endoscope. Each type of endoscopy has didactic content, introductory cases and various procedures available. Haptic feedback is used to create the feeling of tissue and anatomic landmarks.

AccuTouch Endovascular Simulator Several endovascular fluoroscopic techniques are simulated in this trainer, including balloon angioplasty and pacemaker placement. Incorporation of realistic devices allows a user to become accustomed to the tools and environment as well as the procedure itself. Realism is enhanced by the addition of haptic feedback.

CathSim Intravenous Training System CathSim is a VR system which is used to instruct phlebotomy as well as catheter placement in adult, geriatric and

pediatric arms, with or without complications. It incorporates haptic feedback to allow the user to feel anatomic landmarks as the catheter is advanced through the skin and soft tissue to the blood vessel lumen.

2.5.2 Simbionix Ltd.

Simbionix was formed in 1997 in Lod, Israel. The company's first efforts concentrated on gastrointestinal flexible endoscopy, leading to the launch of its first product in 1998, the GI Mentor. Later, Simbionix moved its headquarters to Cleveland, Ohio. Simbionix incorporates haptics into all its simulators to mimic the feel of touch in surgery. Simbionix collaborated with Xitact, a Swiss company, to build its laparoscopic surgery simulator, the LapMentor platform with haptics. The LapMentor is introduced in October 2003 (see Figure 2.9)[8]. The simulator offers a Basic Tasks Module, a Procedural Tasks Module, and a Virtual Patients Module. The Basic Tasks Module simulates fundamental tasks in laparoscopic surgery in a game-type environment. It makes it possible to practice camera manipulation, hand-eye coordination, two-handed maneuvers, clip applying, and translocation of objects. There are 17 studies published between 2002 and 2008, reporting use of the LapMentor. Most of these studies provide evidence that LapMentor training may lead to improved operating room performance. The LapMentor lists at around 90000 dollars. Simbionix has also designed the GI Mentor, the PERC Mentor and

Figure 2.9: The LapMentor surgical simulator from Simbionix Ltd.

the Uro Mentor for virtual trainer in upper and lower gastrointestinal endoscopy, urology and radiology. Customized scopes are realistic, thus allowing training of the equipment in addition to diagnosis and procedure implementation. Some of the modules use realistic computer-generated images. Others focus on honing isolated skills and do not use anatomic images.

[8] www.simbionix.com

2.5.3 Xitact SA

Xitact SA was founded in 2000 in Morges, Switzerland, as spin-off from the Swiss Federal Institute of Technology Lausanne (EPFL). Its product, the Xitact LS500 laparoscopy trainer platform, was developed by independent expert laparoscopic surgeons and technical hardware and software engineers. The Xitact LS500 (Figure 2.10) is a laparoscopy simulator providing a modular training environment for the education and assessment of laparoscopic procedural surgical skill and it uses the Xitact haptic device.

Figure 2.10: The Xitact LS500 surgery simulator.

The Xitact IHP which is a 4-DOF force-feedback manipulator is based on a spherical remote-center-of motion mechanical structure and was originally designed for VR based MIS simulation, (see Figure 2.11)[9]. It features high-output force capability, low friction, zero backlash and a large, singularity-free workspace. The Xitact LS500 costs about 110000Euros.

2.5.4 SimSurgery A/S

SimSurgery has since 1999 been developing products for surgical simulation and solutions for virtual training and robotic surgery. SimSurgery A/S, is based in Oslo, Norway. Its products are based on the SimSurgery Educational Platform - SEP (Figure 2.12[10]). SEP is a training and educational platform for laparoscopic and robotic surgery.

Basically, their software can be adapted to any surgical simulator or any other system requiring real-time three-dimensional capacity.

[9] www.mentice.com
[10] www.simsurgery.com

Figure 2.11: The Xitact IHP Haptic Device.

Figure 2.12: The SimSurgery Educational Platform (SEP).

2.5.5 Mentice

Mentice SA, the Mentice office in Morges, Switzerland, was originally founded as Xitact SA. In August 2005, Xitact was acquired by Mentice. Its most well-known product is the MIST-VR (Minimally Invasive Surgical Trainer-Virtual Reality). The original MIST-VR system is among the most extensively tested virtual-reality testing systems on the market. The MIST-VR module has evolved into Procedicus MIST (Figure 2.13)[11] and has expanded to contain Core Skills 1 and 2, with 12 different tasks. Procedicus is a platform that allows the modular addition of each of the Mentice modules with the option of running each with haptic feedback. The technology for the haptics is provided in collaboration with Immersion. In February 2009, a search of the literature revealed more than 83 articles in print. Many of these articles confirm construct validity. Mentice has designed the Vascular Intervention

[11] www.mentice.com

Figure 2.13: The Procedicus MIST from Mentice SA.

System Training (VIST) to introduce users to endovascular interventions. A haptic feedback device is coupled to a program that produces patient interaction via real time fluoroscopic images and vital signs. Contrast media mixing and hemodynamic factors have been incorporated to increase the realism. Up to February 2009, 29 articles about the VIST were published those confirm its validity.
More recently, Mentice has collaborated with SimSurgery A/S to develop a Key Surgical Actvities (KSA) module and a MIST Suture Module. The KSA module is designed for more advanced laparoscopic training and includes tasks such as camera navigation, instrument handling, pick and place, pick and pass, cutting, suturing, needle passing, and the use of diathermy. The results presented in [Strom 2003] show that the use of surgical simulators such as the Procedicus KSA and MIST as pedagogical tools in medical student training is successful and that it provides students with experience using endoscopic tools and it will presumably reduce medical errors.
Procedicus MIST, the KSA module, and the MIST Suture Module are now all run on the Procedicus platform, which costs between 16000 and 25000US depending on the modules and features desired.

2.5.6 Haptica

Haptica was established in 2000. The company is headquartered in Dublin, Ireland. Haptica works closely with world-leading surgeons and practitioners to develop products like ProMIS shown in Figure 2.14[12]. ProMIS is designed to train surgeons in basic skills of MIS procedures. It comprises a number of modules designed to develop and evaluate surgical proficiency. ProMIS is a hybrid simulator; it uses augmented and virtual reality. Depending on the objectives of the session, the trainee works either in a real physical world on task trainer models or in a virtual world. Teaching

[12] www.haptica.com

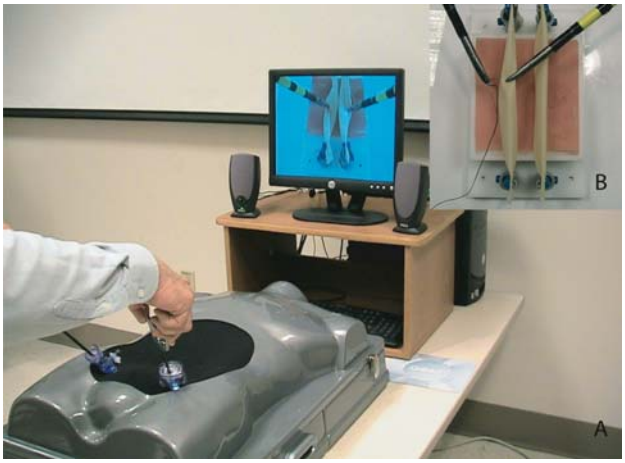

Figure 2.14: The ProMIS surgical simulator from Haptica.

points such as trocar placement, equipment in-service, or camera movement are done using the task trainer features. When moving to skills such as motion smoothness or diathermy use, the virtual world is used. Both physical and virtual training have haptic feedback. To date, more than 25 studies have been published on ProMIS. All are positive about the applicability and benefits of ProMIS in surgical training and research.

2.5.7 Verefi Technologies, Inc.

Verefi Technologies, Inc. develops software and hardware products for training medical personnel worldwide in key medical and surgical skills. Its products are surgical simulators or VR trainers. Its initial product offerings are simulation software for training in MIS such as the RapidFire which is a minimally invasive skills training program that runs with the VLI interface from Immersion. The program allows users to acquire a range of skills, from a basic understanding of the physical environment (equipment fulcrum effect, lack of depth perception, etc.) to more complex tasks such as transferring objects between hands and placing objects accurately in space.
Verefi has also developed the SmartTutor, which is incorporated into RapidFire in order to adapt the task difficulty to the user's metrics, while the Endotower is designed to introduce users to the skills needed to drive an angled laparoscopic camera / lens combination. The virtual model is abstract, meaning there are no simulated tissues, in order to increase the application to multiple specialties, including laparoscopy, arthroscopy, urology, and gynecology.

2.5.8 Surgical Science AB

Surgical Science AB was founded in 1999 in Göteborg, Sweden. In April 2002, the company formed a strategic partnership with Immersion Medical to bundle the Sur-

gical Science LapSim Basic Skills software with Immersion's VLI. More recently, Immersion's LSW was added to the platform, allowing for haptics (see Figure 2.15)[13]. Surgical Science AB currently offers three products. The first is LapSim Basic Skills 2.0 released. It offers nine basic laparoscopic surgical tasks at three different levels of difficulty. Haptics are not available for the Basic Skills module. The LapSim Dissection is an expansion module to LapSim Basic and simulates the dissection and subsequent clipping and cutting of the cystic duct and artery as done during a laparoscopic cholecystectomy. It requires two-handed manipulation of the infundibulum during dissection. A number of different instruments are available. LapSim Gyn is also an expansion module of the LapSim Basic. Haptics are available for the LapSim Gyn module as well.

Figure 2.15: The LapSim surgical simulator from Surgical Science AB

LapSim Basic Skills 2.0 has a list price around 39000$. The LapSim Dissection and LapSim Gyn modules require the LapSim Basic Skills. Each of the expansion modules costs 16000$. A steadily increasing number of papers have clearly demonstrated the beneficial effects of both short-term and long-term systematic training with LapSim (In July 2008, 30 studies). The vast majority of these papers are well-designed studies based on sound scientific principles. For example, Sherman et al. in [Sherman 2005] have developed summary metrics for the LapSim that differentiate among levels of laparoscopic experience. These metrics included the formulation of both a global efficiency score (time-error) and an economy of motion score (motion). The study also provides evidence of construct validity for the LapSim. While in [Panait 2008], the authors used the LapSim to improve basic skills in their residents developing and instituting a laparoscopic skills curriculum.

[13] www.surgical-science.com

2.5.9 Select IT VEST Systems AG

The Select IT VEST Systems company was founded in 2000 and has its headquarters in Bremen, Germany. It offers the Virtual Endoscopic Surgery Training (VEST) system, which includes a Basic Task Training Set (BTT) and a Surgical Procedure Training Set (SPT). The BTT set simulates camera navigation and develops hand-eye coordination and dexterity in a game environment. The SPT set simulates suturing, knot tying, dissection, clipping, and cutting. Two clinical modules are available to be added to the platform: VSOne Cho simulates a laparoscopic cholecystectomy including two-handed manipulation of the cystic duct and artery, clipping, and division. VSOne Gyn simulates two-handed manipulation of the uterus and fallopian tubes with clip application and cutting. Force feedback is available for both VSOne Cho and VSOne Gyn. Some facts about the new VEST System VSOne (see Figure 2.16) [14]:

- new compact design with electrically driven trainer input box,
- 3 haptic devices as mock-up endoscopic instruments,
- 1 virtual endoscopic camera.

Figure 2.16: The VSOne surgical simulator from Select IT VEST Systems AG.

2.5.10 Reachin Technologies AB

Reachin Technologies AB was founded in 1997 as a result of collaboration among research institutions in Australia, Singapore, and Sweden. The company focuses on human-computer interfaces and offers products for engineering and design, oil and gas, medicine, research, and education. In September 2002 Reachin launched its first

[14] www.select-it.de

surgical simulator, the Reachin Laparoscopic Trainer (RLT) (see Figure 2.17[15]). In January 2004, Reachin AB entered into cooperation with Mentice AB to integrate the RLT platform into Procedicus MIST.

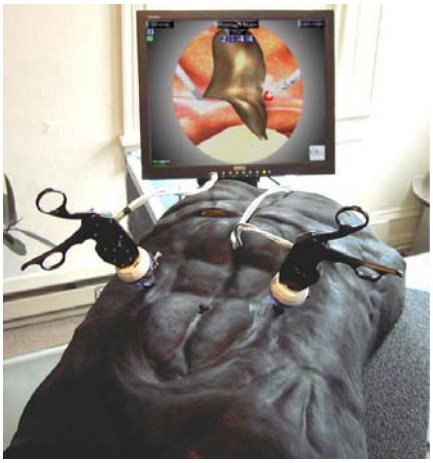

Figure 2.17: The Reachin Laparoscopic Trainer.

The RLT is designed for training of basic laparoscopic dexterous skills and a specific laparoscopic procedure, Cholecystectomy. There are two RLT modules-RLT Basic Skills (RLT-B) and RLT Basic and Laparoscopic Cholecystectomy (RLT-BC). In their original format, RLT-B offered simulation in basic laparoscopic skills only, and RLT-BC added full simulation of laparoscopic cholecystectomy. Unique features of the RLT system included the option for haptics using Immersion's technology and a full haptic guide called Forceback. Forceback puts the instruments through the paces of a laparoscopic cholecystectomy as performed by an expert while the trainee simply rests his or her hands on the instruments during the procedure to get the feel of what an expert is doing.

2.5.11 EXOS Inc.

EXOS Inc. was founded in November 1988 in Boston. In April 15, 1996 Microsoft Corp. announced the acquisition of EXOS Inc. EXOS Inc. has designed the EXOS haptic device for medical simulations. EXOS provides force feedback in 4DOFs. Feedback is provided via a handle connected to a larger tool shaft, which is pivoted at one point with an active 3DOF gimbals. The fourth DOF is provided by a linear sliding module, allowing the tool to be translated (heaved) along the shaft of the tool. MIS simulation is one possible application of this device.

2.5.12 Other simulators

These simulators are generally developed for laboratory experimentation and for specific use. We cite the LTS 2000-ISM60 (LTS; Realsim Systems, Albuquerque,

[15] www.reachin.se

NM, USA) which is a computer-enhanced video-laparoscopic training system, this simulator costs about 18800 dollars [Hasson 2001]. VESTA, is another laparoscopic simulator developed for understanding, training, and assessing surgical skills [Tendick 2000]. VESTA provided force feedback using modified Phantom haptic interface devices. Figure 2.18 shows some other devices developed in several universities .

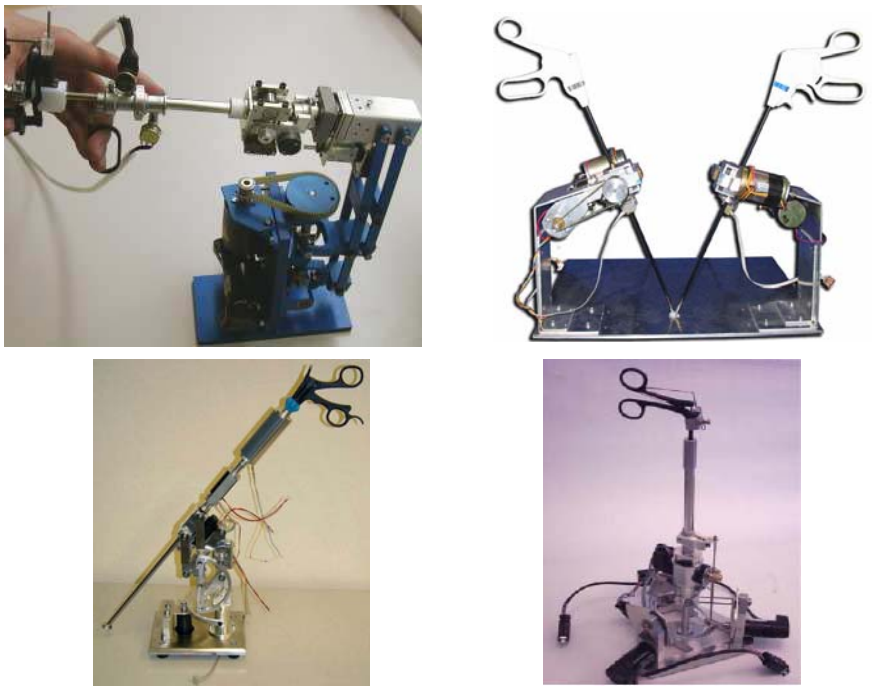

Figure 2.18: Force feedback device prototypes for MIS simulation: (Top-right) Monash University, Australia [McColl 2006]; (Top-left) Federal Polytechnic School of Lausanne, Switzerland [Spaelter 2007]; (Bottom-right) Simon Fraser University, Canada [Li 2006]; (Bottom-left) University of Leipzig, Germany [Kühnapfel 2004].

2.6 Recent comparison and validation studies

2.6.1 Comparison studies of laparoscopic simulators

All the available simulators are designed to train laparoscopic skills, but they use different didactic resources. The Work Group for Evaluation and Implementation of Simulators and Skills Training Programmes of the European Association of Endoscopic Surgeons (EAES), has undertaken the first consensus review procedure for validation of surgical simulators [Carter 2005]. A total of 32 documents concerning systems produced by five different simulation companies were examined for their level of evidence for validity. For simulation of flexible endoscopy, the highest level of recommendation is provided for Accutouch Colonoscopy and GIMentor Gastroscopy. The lowest level of recommendation was for Accutouch Upper GI modules

and GIMentor Colonoscopy. Among laparoscopic simulators, the highest level of recommendation has been given for Procedicus MIST. Whereas a study by Lamata *et al.* in [Lamata 2006] compares the principal VR simulators and propose a taxonomy to study their differences. Their study considered the following VR simulators: (1) Mentice MIST-VR Basic Skills package and Suture 3.0; (2) Surgical Science's LapSim Basic Skills 2.0 package and Dissection and Gynecologic modules, (3) Haptica's ProMis, (4) ReachIn's Laparoscopic Trainer, (5) Simbionix' LapMentor.

In addition, the study evaluates two generic box trainers, (6) one with physical objects and (7) the other with ex vivo organs. The proposed taxonomy distinguishes between a simulator's ability to emulate reality (fidelity resources: such as surgical setting, mechanical interaction and physiopathological behavior.), to exploit computer capabilities, such as offering new ways of interaction and guidance (teaching resources), and to measure performance and deliver feedback (assessment resources). Figure 2.19 outlines the main results of the comparison.

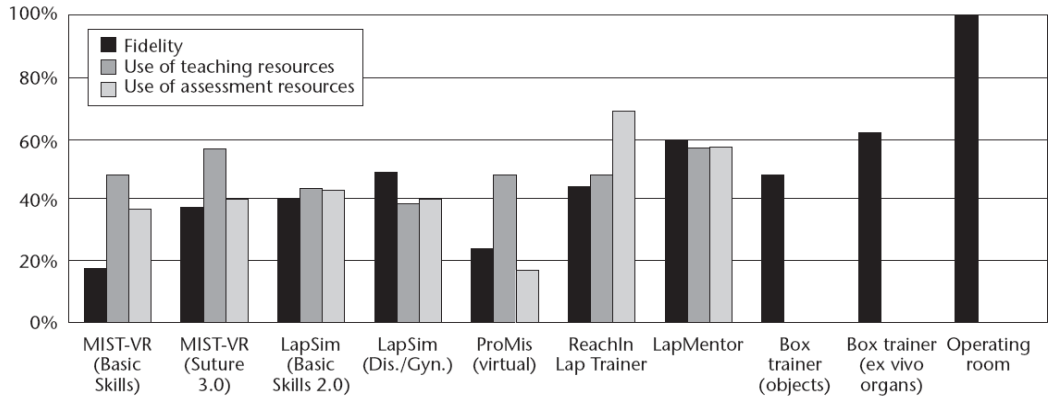

Figure 2.19: MIS trainers comparison according to [Lamata 2006].

In term of haptic feedback, the same study shows MIST-VR's Suture 3.0 provides some force feedback whereas LapSim's Basic Skills 2.0 simulates some bleeding effects. The haptic device used in ReachIn's Lap Trainer introduces frictions and inertias (lower handling fidelity). However, it provides better mechanical interactivity, some bleeding effects, and a complete anatomy in cholecystectomy tasks. Lapsim's modules and LapMentor increase psychopathological fidelity with pathological conditions in some tasks and present fairly good surgical setting realism with the anatomy of different procedures. LapMentor has the highest fidelity in almost every category whereas box trainers do not have any physiopathological feature although they have perfect handling and illumination.

2.6.2 Recent validation studies of laparoscopic simulators

Recent investigations have shown that a VR simulator (MIST-VR) is a reliable tool for the assessment of laparoscopic psychomotor skills and that it improves the au-

tomation of the so-called fulcrum effect [Gallagher 1999]. A number of studies have been undertaken to demonstrate that skills acquired during VR training transfer to the operating room [Sternberg 2007][Seymour 2008]. The authors in [Pham 2005] demonstrate that the RapidFire with Smart Tutor adaptive environment provides less frustrating learning environment, which may enhance acquisition of laparoscopic skills for novice users.

The objective of the study presented in [McClusky 2005] was to analyze whether perceptual, visuo-spatial, or psychomotor aptitude are related to the amount of training required to reach specific performance-based goals on a VR surgical simulator. Training was performed on a custom designed MIST-VR manipulation-diathermy task (Mentice AB). The study demonstrates that the number of trials required to train subjects to reach criterion-based performance goals on the MIST-VR manipulation diathermy task is significantly related to perceptual and psychomotor ability. However, visuo-spatial ability did not significantly correlate with training duration.

A very recent study developed by Gurusamy et al. in [Gurusamy 2009] included 23 experiments with 612 participants. The experiments compared VR versus video trainer training, no training or standard laparoscopic training. The authors concluded that VR training can supplement standard laparoscopic surgical training of apprenticeship and is at least as effective as video trainer training in supplementing standard laparoscopic training. The experiments performed by Tholey *et al.* in [Tholey 2004] and Morris *et al.* in [Morris 2007] confirmed that providing both vision and force feedback leads to better tissue characterization than visual feedback or force feedback alone.

According to [Wentink 2003] and [Mettler 2006], skill-based behavior does not necessarily require a highly sophisticated means of training; a simple Pelvi-Trainer already suffices. However, in order to train knowledge-based behavior outside the operating room and without using living animal models, a high-fidelity laparoscopic simulator that accurately imitates the surgical environment is needed.

A study by [Domuracki 2008] showed that a short training session using a high fidelity simulator with force feedback significantly improved performance of cricoids pressure skills during the resuscitation.

Berry in [Berry 2007] performed a study to compare VR simulator training with porcine training in endovascular novices. Subjective and objective analysis has shown that the skills were improved for all participants regardless of which training method they used. In spite of the fact that most users felt VR to be a good training tool, they did not think that it could replace the porcine training laboratory.

Boyd *et al.* [Boyd 2006] from the University of Mississippi Medical Center, found that residents, especially junior ones, seem to agree with the use of simulation in assessing skills and feel that there needs to be a progression to the operating room only after completion of assigned tasks on simulators. However, the great majority of surgery residents do not believe that a surgeon's competency should be assessed on a simulator before granting operating privileges.

The aim of the study performed by Aggarwal *et al.* in [Aggarwal 2008] was to

investigate the perceptions of senior and junior surgeons to VR simulation within the context of current training opportunities for basic laparoscopic procedures. The results show the existence of a lack of experience in index laparoscopic cases of junior, and that laparoscopic VR simulation is recognized as a useful mode of practice to acquire technical skills that should encourage surgical program directors to drive the integration of simulation-based training into the surgical education.

The study in [Chopra 2008] shows the increasing awareness amongst a group of trainees for VR simulators and that over 95% of them believe it to be a useful tool for acquisition of basic laparoscopic skills.

The authors in [Hogle 2008] investigated approaches for difficult training exercises using the LapSim and the ProMis systems that use real instruments. The experience concerned experienced video gamers and non-gamers residents. The results showed that although experienced video gamers achieve competency faster than non-gamers on the simulator, that skill set does not translate into improved clinical performance and according to [Ahlberg 2002], MIST-VR did not improve the surgical skills of the subjects, but it predicted surgical outcome. So, there is still much effort needed to implement these complex systems with a more effective realistic simulation of tissue properties and haptic feedback. Actually, many research groups are investigating related issues and much research work is currently undertaken for restoring the tactile capability to MIS surgeons by artificial means that would bring immense benefits in patient welfare and safety [Puangmali 2008]. However, no research, simulator or device developed so far is able to provide thermal sensation combined or not with force or tactile feedbacks. If thermal sensation appear to be of some interest in MIS, issues concerning hardware design, signal processing, thermal modeling, integration, and human-machine interface must be tackled.

Challenges for the future include not only overcoming obstacles to implementation of VR training but also the development of more sophisticated procedural simulation devices and teaching systems and the extension of accomplishments in VR for laparoscopic surgery to the area of open surgical procedures [Seymour 2005]. High-fidelity VR simulations will confer the greatest skills transfer to the in real surgical situation, but less expensive VR trainers will also lead to considerably improved skills generalizations that should increases the important role for VR simulator training to allow trainees to develop basic proficiency skills as a part of their training curricula [Chopra 2008].

2.7 Conclusion

The difficulties encountering for skills acquisition in MIS procedures training make VR simulation an outstanding training means. However, to obtain good performances a full interaction with VR systems requires integration of multimodal interfaces. The objective of integrating multi-cues haptic feedback is to improve the immersion and realism of these simulators. Since dexterous manipulation and haptic

sensation are especially interrelated in surgery, it is required to meet the different challenges in order to interface successfully haptic feedback with the typical environmental characteristics found in surgery. The state-of-the-art in surgery simulators developed for MIS training shows that a variety of devices and software exist both in commerce and laboratories although there are until today some difficulties to be overcome. We previously noted that tactile and thermal sensations are not used in conventional MIS procedures although they might bring additional functionality or enrich the feedback (through direct replication or sensory substation) for interaction with the human organs. Therefore, some researches have been conducted in order to add these sensations to the new generation of surgery instruments.

In order to provide a contribution in this area, we will investigate the thermal rendering fundamentals for the general purpose of telepresence and VR applications. Prior to that, we will develop our proper haptic device inspired from real forces and motions of the tool during practical use in real procedures. Our aim is also to master the technology for reducing the costs of accessing such technologies which are still very expensive for developing countries. The two modalities (haptic and thermal) will be integrated in an interactive VR system (SOFA) for evaluation in the last chapter.

Chapter 3

Mechatronics Design, Control and Evaluation of the Haptic Interface

Contents

3.1 Introduction

Design of high performance haptic devices for surgery simulation requires a multi-disciplinary approach and collaborative teams, since haptic devices include several mechanical and electronic parts able at the same time to track the user's intended actions through hand/device interaction, and to produce, as a feedback, the resulting user's arm's motions constraints if any. Therefore, it is important to examine closely the human sense of touch and the application constraints when constructing these devices. Especially for MIS simulation applications, the role of the haptic device is to replicate the holding of the surgery tool in a natural manner i.e. keeping the same DOF and the same workspace as the real surgical tool during its effective use by the surgeon [Baumann 1998]; the haptic device should also provide sufficient forces and torques feedback for the user. So that, the usual methodology followed when designing haptic devices for surgery simulation is to keep part of the surgical tool like a grasper between the operator and the motorized part of the haptic interface [Hayward 1998]. In this case, different tools can be interchanged so that identical visual and functional aspects are maintained between the haptic interface and the surgical tool usually used [Hayward 1998].

The aim of this chapter is to present and discuss the mechatronics design of a new 4-DOF haptic interface that has the ability of providing force feedback in all DOF available during MIS procedure. There are many engineering challenges that will be addressed in order to integrate successfully haptics with the environmental characteristics found in surgery. The general specifications of haptic devices will be adapted to the MIS procedure characteristics. We present a procedure that is designed to meet these challenges by analyzing the task, the haptic, and the hardware constraints of surgery interactive simulation.

3.2 Design issues

3.2.1 General requirements for haptic devices

The most important characteristics that have repeatedly been stated in the literature are presented in this section.

3.2.1.1 Back-drivability

This requirement is of prime importance [Ellis 1996]. Back-drivability can be presented as the ability to move the end-effector of the haptic device in the workspace without opposition. The device should ideally produce no forces on the user's hand when there is no interaction with an object in the virtual world. The use of gears and the presence of friction in the motors and their transmissions reduce back-drivability since they increase the back-drive friction.

3.2.1.2 Friction

All haptic interfaces exert a resistance to the user's voluntary motion, even when no resistance is desired. The term friction is used to include all contributions to this resistance, which may come from Coulomb friction, viscous and inertial forces, and mechanical imperfections [Lawrence 1998]. In order to increase the transparency of the haptic device, it is necessary to decrease the friction in the various joints. This is usually obtained using precision machined parts, bearings, cable transmissions, and other lower friction options for the actuators and joints can help reduce friction [Tholey 2006]. However, estimation of accurate friction in a haptic device is necessary for improving the overall performance of the device [Tholey 2006]. The mechanism must also have an internal friction level of at most 5% of the peak force [Adelstein 1992][Ellis 1996].

3.2.1.3 Stiffness

This criterion can be interpreted as the ability of the interface to mimic a solid virtual wall. The minimum stiffness required to simulate a hard wall is about $24200 N/m$ [Tan 1994]. Stiffness can be decomposed into a transmission stiffness and structural stiffness, which is due to the inherent flexibility of mechanical structure [Gosselin 2005]. The structural stiffness should be maximized in order to reduce as much as possible the undesired deformation at the endpoint (operational point), which is affected by linkages, joints and backlash. The structural stiffness can be analyzed during the CAD design process using usual analysis software.

3.2.1.4 Bandwidth

There are two principal considerations for bandwidth requirement: at what frequency can the human wrist move (motor bandwidth), and at what frequency can the human hand perceive vibration (sensory bandwidth)?
The first is dominated by human motion studies, and the second is dominated by psychophysics of touch. The human wrist easily exceeds 12 Hz, and can reach 25 Hz for fingers [Fischer 1990][Ellis 1996][Gosselin 2005], while the human can perceive force and vibration well above $300 Hz$ [Hayward 1994][Tan 1994]. However, the force control and perceptual bandwidths of a human operator are quite different.

3.2.1.5 Inertia

The haptic device must have the lowest inertia possible. In addition, its inertia must be well mastered everywhere inside the workspace [Hayward 1995] in order to increase the transparency of the device. In other words, a haptic device needs to communicate between the real and virtual world without introducing any inertial effects. According to [Fischer 1990], the maximum inertial load induced by the haptic device must not exceed $0.1 Kg$.

3.2.1.6 Maximum velocity and acceleration capabilities

The device should allow the operator to exert a natural movement with natural speed and acceleration. According to [Fischer 1990], a maximum velocity of 1 m/s and an acceleration of 1 g are needed in order to achieve this capability. If these conditions are not satisfied, the operator wil feel a resistance.

3.2.1.7 Position resolution

Position resolution represents the smallest amount of movement over which the sensors are able to perceive a change of position [Hayward 1996]. Good position resolution is one factor in displaying stiff virtual walls without vibration [Wang 2004] and it influences considerably the stability of the system. However, it is not required to adopt too high a position resolution at given operating speed [Wang 2004].

3.2.1.8 Workspace

With haptic devices, workspace should be taken into consideration without sacrificing performances. Researcher's experiences show that high DOF haptic devices are suitable for the applications where it is necessary to reach larger workspace [Laycock 2003]. A designer can reach larger workspace in two ways. The first is to increase link lengths and the other is to increase degrees of freedom using same link lengths. However, the increase in link lengths affects inertia, stiffness and dynamic performance badly. The workspace must be free of intrusion by linkages, strings [Hayward 1995] without kinematics singularities or coupled motion.

3.2.1.9 Human motor system

Sensory information from the kinesthetic receptors combines with available information from the motor and cognitive systems to produce perceived limb position. However, the ability to detect a change in position differs in each joint. It depends on the joint moving, the velocity, and the contractile state of the muscles controlling the joint. The Just-Noticeable Difference (JND)[1] for the finger joints is 2.5° whereas the wrist and elbow can detect 2° and the shoulder 0.8° [Tan 1994][Hale 2004]. This would mean that the finger tip can detect 0.4mm (assuming a fingertip length of 10 mm) while the JND in distance between the thumb and forefinger in a pinching motion has been reported to be 1mm [Tan 1992]. Therefore, at a minimum, the position resolution of the haptic device needs to be 0.4mm for human capabilities, but in fact should try to exceed that by a factor of 4. It means that we need a minimum resolution of 0.2 to 0.5° in rotation and 0.25mm in translation) [Burdea 1996].

[1] The JND or the difference threshold, is the minimum amount by which stimulus intensity must be changed in order to produce a noticeable variation in human sensory experience.

3.2.1.10 Backlash

The backlash in the system is another critical issue [Ellis 1996]. It is a function of many other variables and hence is not constant over the working envelope, configuration and many other variables of the system. Few measures, taken to reduce backlash, such as the use of anti-backlash gears and high precision bearing tend to increase the friction levels in the mechanism. However, cable driven transmission technique helps overcome undesired backlash.

3.2.2 MIS procedures specifications

In addition to the general design requirements presented above, some considerations are directly imposed by the MIS procedure specifications. This includes the required workspace and related range of motion, forces and torques.

3.2.2.1 Workspace

For the fixed objective, the kinematics motion can be defined to achieve 4 DOF, three rotational DOF: yaw, pitch and roll (twist) and one translational (linear) DOF with respect to the incision point, see Figure 3.1. According to [Li 2006], the critical design requirements includes:

- The yaw motion (rotation around the X axe) can reach 45° in both sides (55° according to [Spaelter 2007]).
- The pitch motion (rotation around the Y axe) can reach 45° in both sides (55° according to [Spaelter 2007]).
- The twist motion (rotation around the Z axe) can reach 70° in both sides (∞ according to [Spaelter 2007]).
- The linear movement stroke (insertion) is able to reach 150mm along the Z axe (200mm according to [Spaelter 2007]).
- The mechanism must move with respect to the incision point without any interference.

The workspace optimization is also performed in accordance with the data collected *in-vivo* during MIS procedures [Rosen 2005]. The study provided by Rosen *et al.* is focused on developing a new class of surgical robotic arms while maximizing their performance and minimizing their size. The required dexterous workspace (DWS) is defined as the region in which 95% of the tool motions are contained based on *in-vivo* measurements. The extended dexterous workspace (EDWS) is defined as the entire abdominal cavity reachable by a MIS instrument. The DWS is defined by a circular cone with a vertex angle of 60° and the EDWS is defined by a cone with an elliptical cross section by two orthogonal vertex angles of 60° and 90° [Rosen 2005]. So that, a spherical mechanism, which is a rotational manipulator with all axes

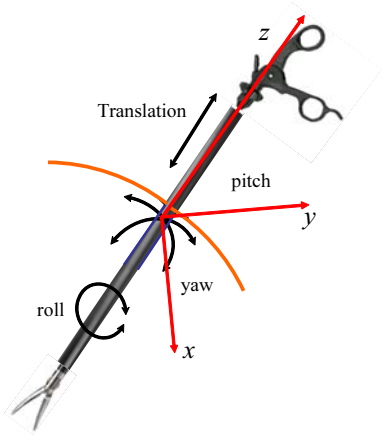

Figure 3.1: MIS tool motions.

intersecting at the center of a sphere, is a suitable candidate for the first two links of a haptic device for MIS.

3.2.2.2 Force/torque requirements

The dimensioning procedure is performed using a database of forces and torques applied by the surgeons on their instruments during MIS procedures. This database is provided by a study performed at the University of Washington [Rosen 1999][Rosen 2000][Rosen 2002] using an instrumented laparoscopic grasper equipped with a three-axes force/torque sensor to measure the forces/torques applied by the surgeons during *in-vivo* MIS. This database can be used also to evaluate haptic virtual reality surgical simulators for improving realism in surgical education [Richards 2000][Lamata 2008]. By analyzing the database in [Rosen 1999], we deduce that the forces along the Z axe ($\approx$ 50N) were higher compared to the forces in the XY plane ($\approx$ 5N). On the other hand, torques developed by rotating the tool around the Z axis ($\leq$ 0.5Nm) were particularly low compared to the torques generated while rotating the tool along the X and Y axes ($\approx$ 2Nm) while sweeping the tissue or performing lateral retraction. Similar trends in terms of the force/torque magnitude ratios between the X, Y, and Z axes were found in the data measured in other MIS tasks as in [Rosen 2000] while dissecting the gallbladder fossa during laparoscopic cholecystectomy. In this case 95% of the forces are $\leq$ 20N for the Z axe and the torques are $\leq$ 0.5Nm for the X and Y axes.

3.3 Mechanical Design Methodology

3.3.1 Hybrid mechanical structure

When considering the construction of a force feedback device, there is a choice between serial and parallel mechanisms. The key difference between serial mechanisms and parallel mechanisms is in their kinematics structures. Parallel mecha-

nisms are composed of, at least, two closed chains that connect a moving platform to a fixed base thus allowing the actuator to be away from the moving platform. For a relatively similar size of the linkages, a serial mechanism presents a larger workspace volume than a parallel mechanism. For parallel mechanism, workspace is compromised by the constraints of all links that connect the end-effector. For serial mechanism, every actuator has to exert enough torque and power to move all distal links and overhead actuators. However, the actuators of a parallel mechanism can be placed on ground to support stronger payload than a serial mechanism does. It can be made so for serial mechanisms, but at the cost of complex transmission mechanisms and this is not always possible for all the links. For parallel mechanism, the geometrical errors are not accumulated, as all the braches are connected to the end-effector. The dimension accuracy of each link must be high so that the position and orientation of the end effector is more accurate than a serial mechanism. For serial mechanism, the geometrical errors are accumulated for each link. Therefore, the end effector will have lower position accuracy [Li 2006]. For serial mechanism [Laycock 2003], each chain increases the total inertia while it decreases the total stiffness. Parallel mechanisms do not exhibit the above problem and have a much higher stiffness [Birglen 2002]. The disadvantage over serial mechanisms is that the mechanism's elements can physically interfere. The advantages of both mechanisms are incorporated by combining them in a hybrid configuration [Baser 2006] that includes both parallel and serial linkages. By using hybrid configurations, the stiffness remains relatively high and a large workspace can be achieved.

Our design contains 4 DOF: there is 2 DOF parallel mechanism inspired by the 2 DOF agile eye developed at the University of Laval [Caron 1997], which insures the movement around pitch and yaw axes. This parallel mechanism consists in two legs (chains), each being regarded as a serial manipulator. The first chain constitutes a two-axes serial manipulator and the second chain constitutes a three-axes serial manipulator. These two chains are coupled through a moving part that supports a third 2 DOF serial chain. The first DOF of this chain is a rotation around the roll axe that results in three intersecting planes. The second DOF is a translation along the same axe that would hold the surgery tool. The transformation of the motor rotation into a translation is designed based on two parallel beams with precision linear rotary ball splines. Three pulleys are also used in order to insure the cable rotation, see Figure 3.2. The design of our device was performed and validated under the SolidWorks software.

3.3.2 Actuation, transmission and reduction

The actuation, the reduction and the transmission are closely coupled and must be designed together. They are selected according to the requirements specified in the last subsection. The type of the incorporated actuators affects the overall weight of the device. In most cases, a good actuator should be compact and light as well as capable of producing the necessary power to deliver necessary forces. There are

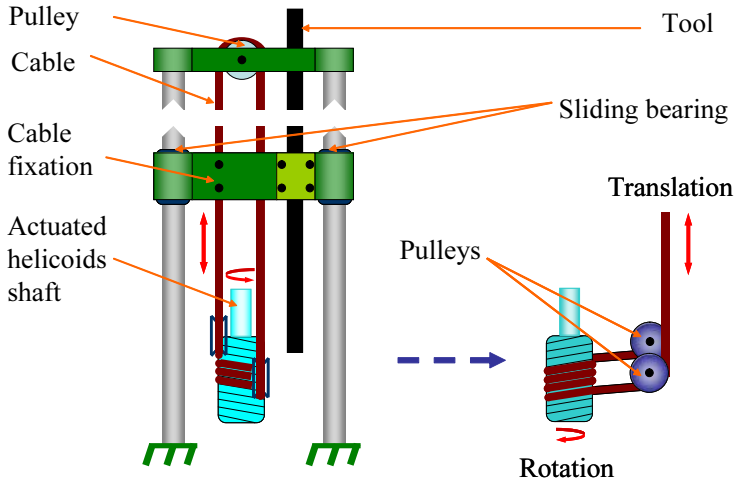

Figure 3.2: Rotation to translation transmission mechanism.

tradeoffs between power, volume and weight since actuators capable of producing large forces are generally heavier and are larger in size than those actuators capable of smaller forces. The dimensioning procedure of the actuator was performed under MotionWorks plug-in of Solidworks, by applying dynamic forces on the handle of the surgical tool and then obtaining the required actuator torques. We select brushed Maxon DC motors with a low inertia and low friction [Tavakoli 2004], which are suitable for haptic devices. Maxon RE40 is used for the yaw and the pitch axes and RE25 for the roll and the translational axes. The actuators features are presented in table 3.1.

Table 3.1: Motor's specifications

Motor	RE40	RE25
Nominal current (A)	6	1.26
Speed constant $(tr/min/V)$	581	406
Torque constant (mNm/A)	16.4	23.5
Inertia (gcm^2)	139	10.7
Axial Backlash (mm)	0.05-0.15	0.05-0.15
Radial Backlash (mm)	0.025	0.025
Efficiency(%)	88	87
Weight (Kg)	480	130

In order to provide the highest amount of fidelity, direct drive (absence of transmission of reduction) is likely to be the best solution. However, this solution does not provide adequate forces/torques needed for our application, which we saw earlier is critical. Among the other transmission and reduction techniques such as the

use of linkages, cables, steel belts, shafts plus gears, this last one gives the worst case [Hayward 1995] since it causes high backlash and high back-drive friction due to the gear gaps and gear friction. Back-drive friction and backlash can be reduced by using cable driven transmission systems. Therefore, cable driven transmission technique (capstan) was used in our design. We take a factor of 20 for the yaw and the pitch axes and a factor of 10 for the roll axe. This gives us the possibility to create continuous torques of about 1Nm for the yaw and the pitch axes and about 0.7Nm for the roll axe and about 18N for the translational axe. A second solution consists of using a combined reduction (Planetary gear/capstan) in order to increase the torques developed by the actuators driving the yaw and the pitch axes. We use planetary gears reduction because it has fewer backlashes and less friction, especially when the reduction ratio is small (the reduction ratio is 4 in this case). So that the torques provided by the yaw and pitch axes are multiplied by a factor of 4. This means 4Nm, without additional weight since the actuators are placed in the base. This solution is able to provide additional torque to compensate for gravity and friction.

As it was presented in section 3.2, the haptic device should include low inertia, no backlash, light weight and negligible friction [Laycock 2003][Astley 2000]. Therefore, a compromise has to be reached between the various design goals. Obtaining negligible friction can be a problem, particularly when high stiffness is required. High stiffness implies a stiff mechanical interface which needs to be constructed from metal which increase the friction and the overall weight of the device. This provides a conflict between obtaining high stiffness while keeping low friction [Baser 2006][Laycock 2003]. So that, the materials used to construct such devices need to be considered with additional costs. Another design consideration is to ensure that the device is statically balanced [Laycock 2003]. In our design:

- Aluminum was used in order to minimize the deflection due to the stiffness of the linkages.
- Cable driven transmission technique was used in order to overcome backlash deflection.
- Stainless steel ball bearings and high precision manufacturing methods were used in order to overcome joint deflections.
- The entire mass of the mobile part remains concentrated in the neighborhood of the centre of rotation. However, for ensuring the total stativity, active compensation will be needed.

The Computer Aided Design (CAD) model of the device is shown in Figure 3.3 and table 3.2, more details about the different designed parts are given in Appendix B.

3.3.3 Stress and deflection analysis

After the completion of the preliminary mechanical design procedure, links shape and thickness must be optimized to satisfy the design requirements mentioned be-

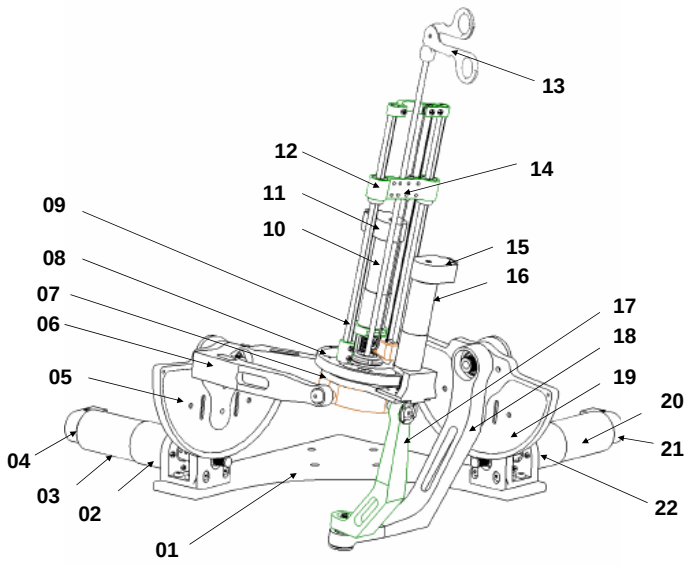

Figure 3.3: CAD Model of the haptic device.

Table 3.2: Parts designation for the CAD model

Part Number	Designation	Part Number	Designation
01	Fixed base	12	Body 6
02	Planetary reduction (GP42)	13	MIS Tool
03	Motor 1 (RE40)	14	Tool holder
04	Encoder 1 (HEDS 5540)	15	Encoder 3 (HEDS 5540)
05	Capstan 1 (20:1)	16	Motor 3 (RE25)
06	Body 1	17	Body 5
07	Body 2	18	Body 4
08	Capstan 3 (10:1)	19	Capstan 1 (20:1)
09	Body 3	20	Motor 4 (RE40)
10	Motor 4 (RE25)	21	Encoder 4 (HEDS 5540)
11	Encoder 4 (HEDS 5540)	22	Planetary reduction (GP42)

fore, such as the reduction of the inertia of the device and the maximization of the stiffness. For this structure, the links stress analysis is carried out using COSMOSXpress plug-in of Solidworks. Static analysis of the mechanical design would be sufficient because the device will be used with low speeds. The links shape and weights are computed for aluminum with a Young modulus of 69000 MPa and a mass density of 2700 kg/m^3 as construction material. This material is used because of its high yield strength over weight ratio [Kabadayi 2006]. According to the analy-

sis results, the shape and the thickness of the links should be modified in iterations. The weight values of the motors, reductors and links starting from the tool tip and moving to the base of the robot are used to determine the static load on the robot links.

In Figures 3.4 and 3.5, an example of deformation and distribution of von-Mises stresses are illustrated for two links of the manipulator. Contour diagram and maximum stress points are shown in the figures. Legend on the right side of the figure shows the distribution of contour diagram. Legend on the right hand side of the figure shows the distribution of contour diagram. In this analysis, deformation in the translational movement direction is studied under static loading of 50 N, which corresponds to the maximum force that shall be applied during MIS procedures. Naturally, maximum deflection occurs at the end of the links. The maximum and minimum deformation points are shown in the figure. It has been observed that the link 1 and 3 (parts 06 and 17 in table 3.2) are the most critical links since they are exposed to maximum stress in any condition. The shape and thickness of the links are optimized according to the maximum deflection values obtained from the analysis.

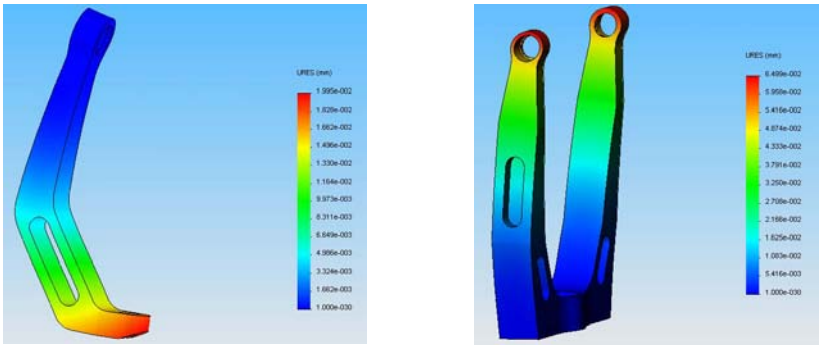

Figure 3.4: Deflection analysis of links 1 (left) and 3 (right).

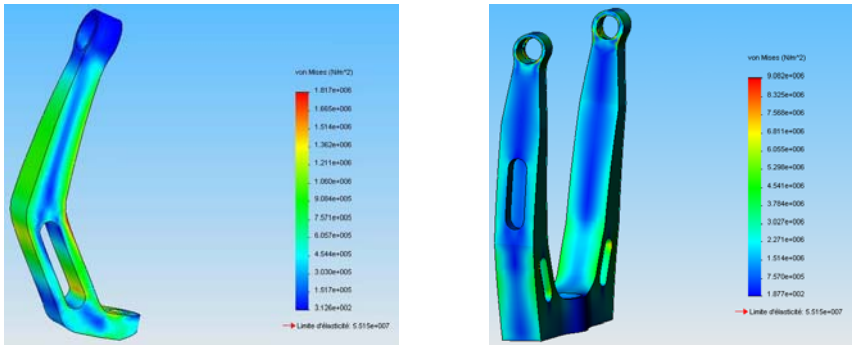

Figure 3.5: Von-Mises Stress analysis of links 1 (left) and 3 (right).

3.4 Sensors and Electronics interface

3.4.1 Position sensing

The angular positions of the four active joints are measured thanks to four incremental encoders type HEDS 5540 from Maxon. These encoders are placed in the rear of the motors and provide 500 pulsations per revolution of the motor axe. Thus, the position measurement resolution is computed by taking into account, the reduction ratios for the rotational axes and the helicoids shaft diameter for the translational axe. It means that the resolution of the yaw and the pitch axes is $((360/500)/80 = 0.009°)$ while it is $((360/500)/10 = 0.072°)$ for the roll axe and $((2 \times \pi/500) \times 4 = 0.05mm)$ for the translational axe where 4 mm is the radius of the helicoids shaft.

3.4.2 Force sensing

3.4.2.1 Force transducer principle

The most popular electrical elements used in force measurements include the resistance strain gage, the semiconductor strain gage, and piezoelectric transducers. The strain gage measures force indirectly by measuring the deflection it produces in a calibrated carrier. In our experiment, four strain gages (type 120LY13 from Hottinger Baldwin Messtechnik (HBM)) are used to measure the deflection of the handle according to the Z axe, two on the top side, and two on the bottom side glued to a cantilever beam (see Figure 3.6). Precise alignment was maintained to prevent bending moments, which can severely degrade the accuracy of the measurements. The gages are connected in a Wheatstone bridge configuration, which gives maximum sensitivity and is inherently linear. This configuration also offers first-order correction for temperature drift in the individual strain gages. In addition, the differential placement of the gauges guaranties the independence between the measured force and the tip of its application.

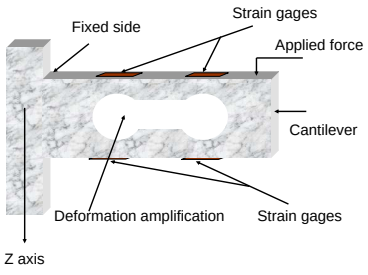

Figure 3.6: Force sensing based on four strain gages.

3.4.2.2 Signal conditioning electronics and calibration

Strain gages are low-impedance devices; they require significant excitation power to obtain reasonable levels of output voltage. The strain-gages used in this experiment have a 120Ω impedance and are specified as having a sensitivity in terms of mV full scale per volt of excitation. We have carried out an electronics unit that convert the small mV changes in Wheatstone bridge output to a range of $[-10\ +10]$V, which is proportional to the applied load or tension. This electronics unit consists of an instrumentation amplifier, a differential amplifier and an ordinary amplifier, see Figure 3.7. The total amplification gain is undertaken so that a maximum force of ±50N can be measured. The linear relation ($F = \alpha V + \beta$), between the applied force and the output voltage, is determined by calibration using troy weights as it is shown in Figure 3.8.

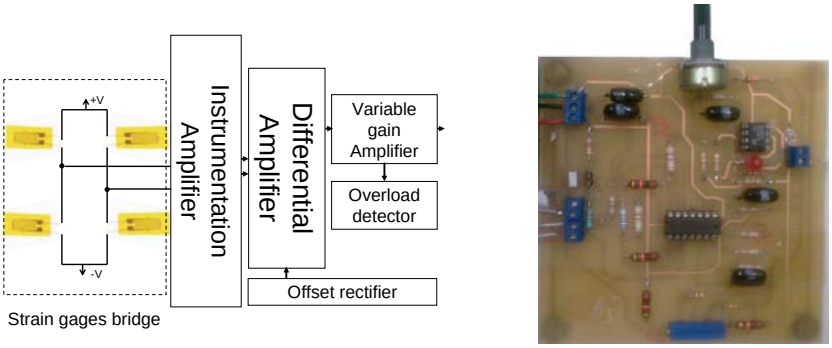

Figure 3.7: Force sensor conditioning electronics .

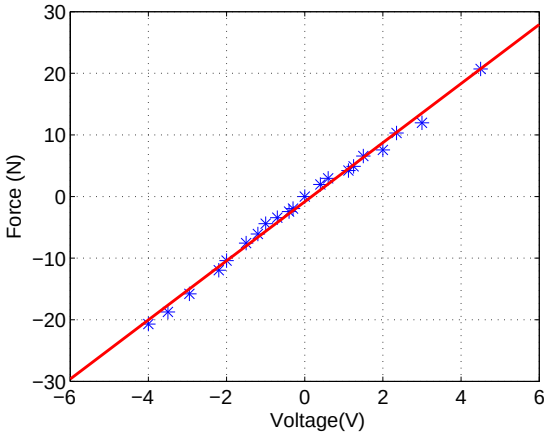

Figure 3.8: Force sensor calibration.

3.4.3 Torque sensing

3.4.3.1 Torque calculation principle

For the rotational axe, torque need to be computed. The motor torque τ can be estimated based on actuator commands since the motor torque is directly proportional to motor current I as follows.

$$\tau = K_\tau I \tag{3.1}$$

where K_τ is the torque constant of the motor. From the motor torque, we can compute forces F based on the Jacobian matrix J.

$$F = (J^T)^\# \tau \tag{3.2}$$

where $(J^T)^\#$ is the pseudo-inverse of the transpose Jacobian.

Many applications use this relationship and a measurement of current to approximate the torque applied to a link. Although this method is imprecise since it does not take into account the complexities of the reduction mechanism, friction, and backlash, which contribute to loss of torque from the motor to the link, the results presented in [Walker 2008] show that such low-cost, force sensors perform just as well as highly accurate sensors. Currents are measured thanks to the Hall-Effect sensors (type LF306-S from LEM Transducer) that offer high frequency response (100KHz).

3.4.3.2 Signal conditioning electronics and calibration

Since the Hall voltage is a low-level signal, it requires an amplifier with low noise, high input impedance and moderate gain. In order to get an accurate calculation of the torque, we perform two sets of calibration experiments. The aim of the first set is to determine the relationship between the motor current and the output voltage of the conditioning electronics, while the second set tries to find the relationship that laid the current to the real torque (see Figures 3.10, 3.11 and 3.12).

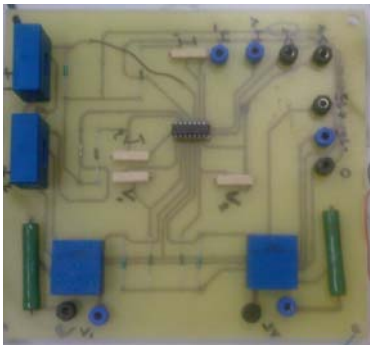

Figure 3.9: Current sensors conditioning electronics.

This figures show that the relation between the measured current and the output voltage is linear ($V = \alpha I + \beta$) for all sensors. When comparing the estimated

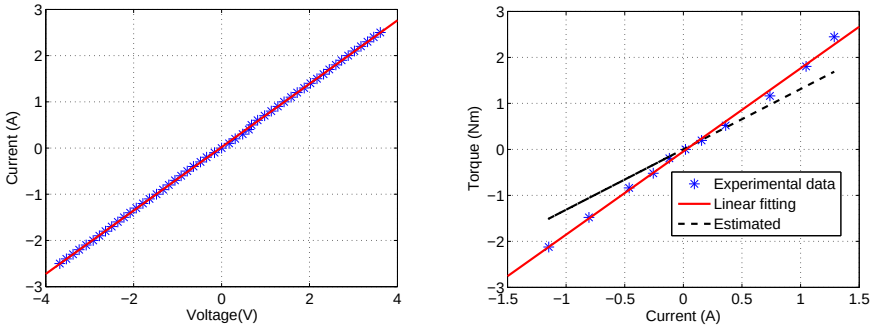

Figure 3.10: Current calibration (right) and torque estimation (left) for yaw axe.

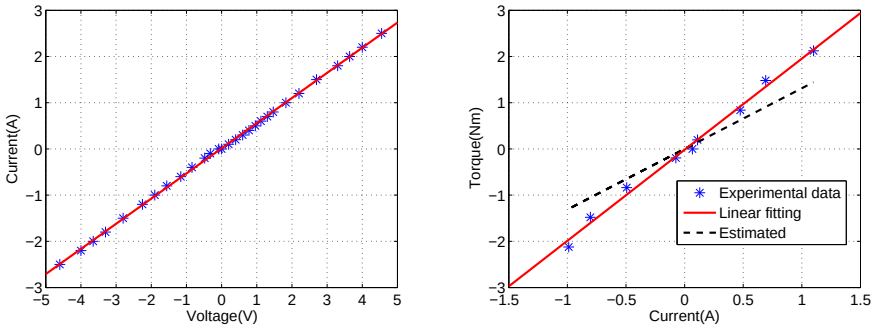

Figure 3.11: Current calibration (right) and torque estimation (left) for the pitch axe.

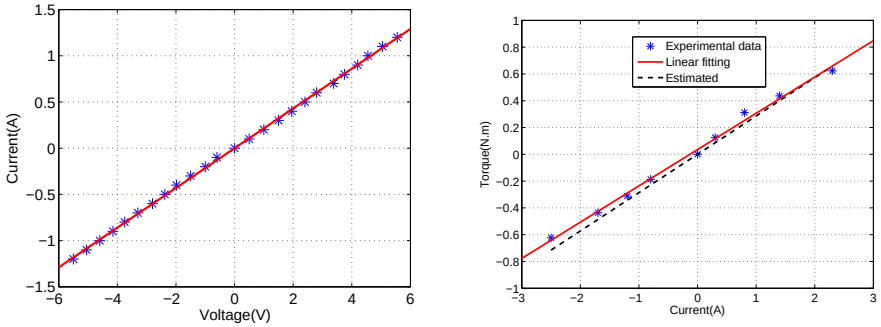

Figure 3.12: Current calibration (right) and torque estimation (left) for the roll axe.

torques based on (3.1) with the real torques, one can remarks the presence of a divergence. This is probably due to the complexity of the reduction mechanism, inertia and possible existing friction. We note that this divergence is small in the case of the roll axe were the low inertia is supported (Figure 3.12). Therefore, in our experiments, torques will be estimated based on the linear fitting of the calibration relation($\tau = \eta I + \gamma$). The calibration parameters of the linear fit are given in Table 3.3.

Table 3.3: Fitting parameters for calibration.

	α	β	η	γ
Axis 1	0.686	0.018	1.994	-0.035
Axis 2	0.544	0.012	1.953	-0.027
Axis 3	0.21498	0	0.270	0.035
Axis 4	4.793	-0.849	/	/

3.4.4 Electronics interface

Figure 3.13 represents the control setup. It consists of a Quanser's Q8 Hardware-in-the-Loop (H.I.L.) Control Board, which is a versatile and powerful real-time measurement and control board. The power electronics module consists of a linear stages designed and realized based on the OPA541 and OPA548 operational power amplifiers from Burr-Brown, which are able to provide a current about 10A and 3A, respectively. Two OPA541 are used for driving the yaw and the pitch motors and two OPA548 are used for driving the roll and the translational motors where less torques are needed.

3.5 Modeling

3.5.1 Forward Kinematics

Figures 3.14 and 3.15 show the position of the frames attachments. All the frames intersect at one point named 'O' situated at the center of the moving platform that connects the two parallel chains to each other, thus simplifies the kinematics modeling. For each chain, the kinematics model is obtained by using the modified method of Denavit and Hartenberg [Khalil 1999], where ${}^{i-1}R_i$ represents the rotation matrix from the frame $F_{i-1}(x_{i-1}, y_{i-1}, z_{i-1})$ to the frame $F_i(x_i, y_i, z_i)$.

$$ {}^{i-1}R_i = \begin{bmatrix} \cos(\theta_i) & -\sin(\theta_i) & 0 \\ \cos(\alpha_i)\sin(\theta_i) & \cos(\alpha_i)\cos(\theta_i) & -\sin(\alpha_i) \\ \sin(\alpha_i)\sin(\theta_i) & \sin(\alpha_i)\cos(\theta_i) & \cos(\alpha_i) \end{bmatrix} \tag{3.3} $$

Kinematics parameters are defined in tables 3.4 and 3.5, where α_j represents the joint offsets, r_j and l_j the link lengths and θ_j the joint variables. For symmetry reason, we replace θ_1, θ_2 and θ_5 by $\theta_1 - \frac{\pi}{2}$, $\theta_2 - \frac{\pi}{2}$ and $\theta_5 - \frac{\pi}{2}$, respectively.

For Chain 1, the rotation matrix from the original frame F_0 to the frame F_2 is computed as follows:

$$ {}^0R_2 = {}^0R_1 {}^1R_2 \tag{3.4} $$

and for Chain 2, the rotation matrix from the original frame F_0 to the frame F_6 is

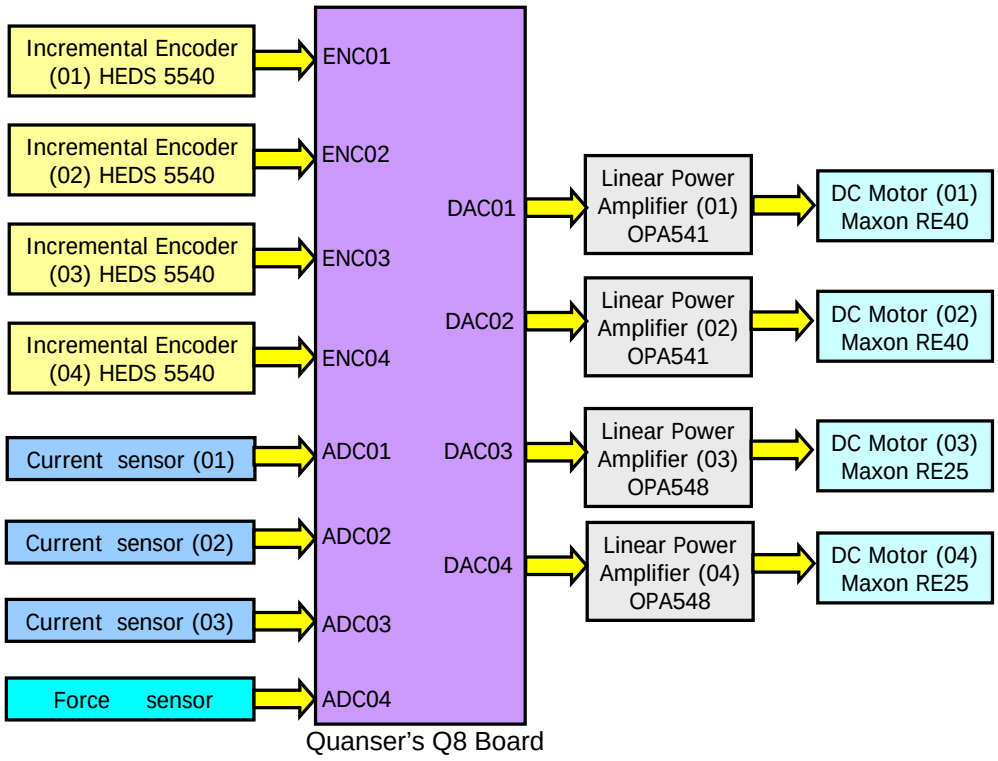

Figure 3.13: Overview of the electronics interface.

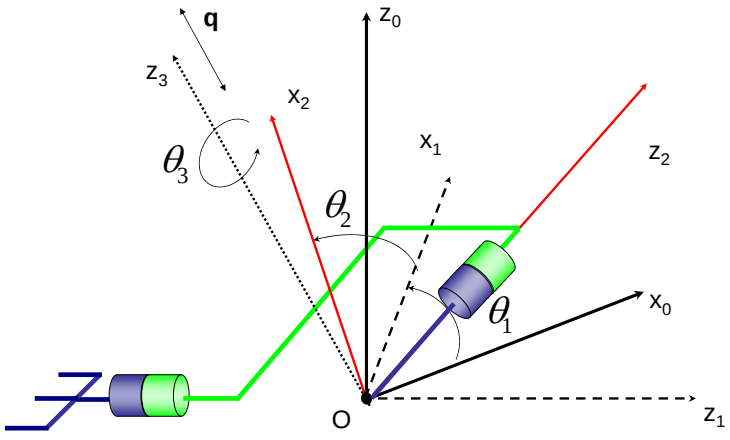

Figure 3.14: Kinematics of Chain 1.

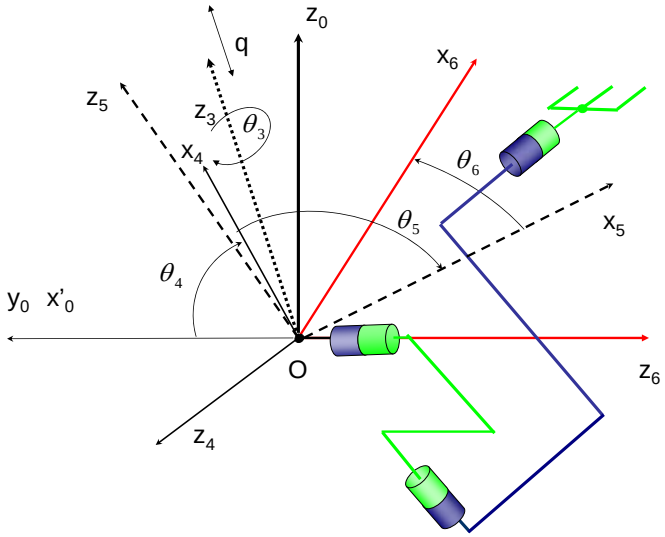

Figure 3.15: Kinematics of Chain 2.

Table 3.4: DH kinematics parameters of Chain 1.

Joint j	α_j	r_j	l_j	θ_j
1	$\pi/2$	0	0	θ_1
2	$\pi/2$	0	0	θ_2
3	$\pi/2$	0	0	θ_3

Table 3.5: DH kinematics parameters of Chain 2.

Joint j	α_j	r_j	l_j	θ_j
4	$-\pi/2$	0	0	θ_4
5	$-\pi/2$	0	0	θ_5
6	$\pi/2$	0	0	θ_6

computed as follows:

$$ {}^{0}R_6 = {}^{0}R_{0'}\,{}^{0'}R_4\,{}^{4}R_5\,{}^{5}R_6 \tag{3.5} $$

where:

$$ {}^{0}R_{0'} = \begin{bmatrix} 0 & -1 & 0 \\ 1 & 0 & 0 \\ 0 & 0 & 1 \end{bmatrix} $$

The moving platform is a body of both Chain 1 and Chain 2. In Chain 1, it is referenced by the frame F_2 and in chain 2 by F_6. So that, the kinematics constraints representing the closure condition of the parallel structure formed by Chain 1 and

Chain 2 are then:

$$\begin{cases} {}^0\vec{x}_2 = {}^0\vec{z}_6 \\ {}^0\vec{y}_2 = {}^0\vec{y}_6 \\ {}^0\vec{z}_2 = -{}^0\vec{x}_6 \end{cases} \tag{3.6}$$

that is equivalent to write:

$${}^0R_2 = {}^0R_6 {}^6R_2 \tag{3.7}$$

where:

$${}^0R_2 = \begin{bmatrix} S1\,S2 & S1\,C2 & -C1 \\ C2 & -S2 & 0 \\ -C1\,S2 & -C1\,C2 & -S1 \end{bmatrix}$$

$${}^6R_2 = \begin{bmatrix} 0 & 0 & 1 \\ 0 & 1 & 0 \\ -1 & 0 & 0 \end{bmatrix}$$

$${}^0R_6 = \begin{bmatrix} -C5\,C6 & C5\,S6 & -S5 \\ C4\,S5\,C6 - S4\,S6 & -C4\,S5\,S6 - S4\,C6 & -C4\,C5 \\ -S4\,S5\,C6 - C4\,S6 & S4\,S5\,S6 - C4\,C6 & S4\,C5 \end{bmatrix}$$

Where Ci and Si stand for $\cos(\theta_i)$ and $\sin(\theta_i)$, respectively.

The solution of (3.7) gives:

$$\theta_2 = \arctan\left(\tan\left(\theta_4\right)/C1\right) \tag{3.8}$$

and

$$\begin{cases} \theta_5 = \arctan 2\left(\left(S1\,S2\right), \pm\sqrt{1-\left(S1\,S2\right)^2}\right) \\ \theta_4 = \arctan 2\left(\left(C1\,S2/C5\right), \left(C2/C5\right)\right) \\ \theta_6 = \arctan 2\left(\left(S1\,C2/C5\right), \left(C1/C5\right)\right) \end{cases} \tag{3.9}$$

The angular positions of the passive joints θ_2, θ_5 and θ_6 are computed based on the angular positions of the active joints θ_1 and θ_4. Expressions (3.8) and (3.9) are not defined for $\theta_1 = \pm\frac{\pi}{2}$ and $\theta_2 = \pm\frac{\pi}{2}$. Fortunately, all these configurations are outside the reachable workspace.

The orientation in (3.10) and position in (3.11) of the end-effector is determined by taking the joint angles of the linkages and using the forward kinematics calculation as follows.

$$R = \begin{bmatrix} S1\,S2\,C3 - C1\,S3 & -S1\,S2\,S3 - C1\,C3 & -S1\,C2 \\ C2\,C3 & -C2\,S3 & S2 \\ -C1\,S2\,C3 - S1\,S3 & C1\,S2\,S3 - S1\,C3 & C1\,C2 \end{bmatrix} \tag{3.10}$$

and

$$\begin{cases} {}^0p_x = q\,S1\,C2 \\ {}^0p_y = -q\,S2 \\ {}^0p_z = -q\,C1\,C2 \end{cases} \tag{3.11}$$

where q represents the translation movement of the tool along the z_3 axe, θ_3 represents the rotation movement around the same axe and $({}^0p_x, {}^0p_y, {}^0p_z)$ represents the position of the handle defined in the frame ${}^0F$.

3.5.2 Inverse Kinematics

In order to determine the inverse kinematics, we need to express $\theta_i \quad i \in [1, \cdots, 6]$ and q as a function of ${}^0p_x$, ${}^0p_y$, and ${}^0p_z$ and the pitch θ, yaw ψ and roll ϕ angles used to describe the orientation of the handle, where:

- θ is the rotation around the y_0 axe.
- ψ is the rotation around the x_0 axe.
- ϕ is the rotation around the z_0 axe.

From (3.11)

$$\begin{cases} \theta_1 = -\arctan\left(p_x/p_z\right) \\ \theta_2 = \pm \arctan 2\left(p_y, \sqrt{p_x^2 + p_z^2}\right) \\ q = -p_z/(C1\,C2) \end{cases} \tag{3.12}$$

However, only 4 DOFs are available in our device, so that we can specify only the roll angle which is independent of θ_1 and θ_2. By identification, we can easily find that:

$$\theta_3 = \phi \tag{3.13}$$

On the other hand, we get:

$$\begin{cases} \theta = \theta_1 \\ \psi = \theta_2 \end{cases} \tag{3.14}$$

In order to compute the singularity points, we need to express the Jacobian matrix J of the device. Since the orientation on the end-effector is derived directely from the joint angles, we consider only the jacobian matrix resulting from position derivation :

$$J = \begin{bmatrix} q\,C1\,C2 & -q\,S1\,S2 & S1\,C2 \\ 0 & -q\,C2 & S2 \\ q\,S1\,C2 & q\,C1\,S2 & -C1\;C2 \end{bmatrix} \tag{3.15}$$

so

$$|J| = 2\,q^2\,C2$$

The singularity points are defined for $|J| = 0$, that is:

$$\begin{cases} \theta_2 = \pm\frac{\pi}{2} \\ q = 0 \end{cases}$$

The singularity $\theta_2 = \pm\frac{\pi}{2}$ is not reachable and the singularity $q = 0$ can be avoided by taking a start point just under the point 'O'.
From 3.8:

$$\begin{cases} C2 = \frac{1}{\sqrt{1+\left(\frac{tg4}{C1}\right)^2}} \\ S2 = \frac{tg4}{C1}\frac{1}{\sqrt{1+\left(\frac{tg4}{C1}\right)^2}} \end{cases} \tag{3.16}$$

So that, the Jacobian matrix J_a with respect to the actuated joints, is then:

$$J_a = \begin{bmatrix} \left(C1 - tg1\ S1\ S2^2\right) C2 & \frac{-tg1\ S2\ C2^2}{C4^2} & S1\ C2 \\ S2^3 S1 & -\frac{C2^3}{C4^2} & -S2 \\ C2S1\left(1 + S2^2\right) & \frac{S2\ C2^2}{C4^2} & -C1\ C2 \end{bmatrix} \tag{3.17}$$

3.5.3 Dynamic equations

The kinetic energy E_{K_i} and potential energy E_{P_i} of each moving part i ($i = 1, \cdots, 6$) constituting the device can be obtained as:

$$E_{K_i} = \frac{1}{2} m_i \overrightarrow{v}_{G_i}^2 + \frac{1}{2} \overrightarrow{w}_i^T I_{/G_i} \overrightarrow{w}_i \tag{3.18}$$

$$E_{P_i} = -m_i g^T \overrightarrow{OG_i} \tag{3.19}$$

where m_i is its mass, $I_{/G_i}$ is its inertial matrix (given in Appendix B), $\overrightarrow{OG_i}$ and $\overrightarrow{v}_{G_i}$ are, respectively, the position and the linear velocity of its center of gravity, $\overrightarrow{w}_i$ is the angular velocity and g is the gravity constant.
For part 1, we have:

$$\vec{w}_1 = \begin{bmatrix} 0 & 0 & \dot{\theta}_1 \end{bmatrix} \tag{3.20}$$

so, the kinetic energy is given as:

$$E_{K_1} = \frac{1}{2} \left(I_{zz_1} + m_1 y_{G_1}^2 \right) \dot{\theta}_1^2 \tag{3.21}$$

and the potential energy is:

$$E_{P_1} = -m_1 g y_{G_1} \cos\left(\theta_1\right) \tag{3.22}$$

For part 2, we have:

$$\vec{w}_2 = \begin{pmatrix} -\dot{\theta}_1 C2 & \dot{\theta}_1 S2 & \dot{\theta}_2 \end{pmatrix}^T \tag{3.23}$$

$$\vec{v}_{G_2} = \begin{pmatrix} \dot{\theta}_1 C1\left(x_{G_2} S2 + y_{G_2} C2\right) + \dot{\theta}_2 S1\left(x_{G_2} C2 - y_{G_2} S2\right) \\ -\dot{\theta}_2\left(x_{G_2} S2 + y_{G_2} C2\right) \\ \dot{\theta}_1 S1\left(x_{G_2} S2 + y_{G_2} C2\right) - \dot{\theta}_2 C1\left(x_{G_2} C2 - y_{G_2} S2\right) \end{pmatrix} \tag{3.24}$$

$$\overrightarrow{OG}_2 = \begin{pmatrix} S1\left(x_{G_2} S2 + y_{G_2} C2\right) \\ x_{G_2} C2 - y_{G_2} S2 \\ -C1\left(x_{G_2} S2 + y_{G_2} C2\right) \end{pmatrix} \tag{3.25}$$

For part 3, we have:

$$\vec{w}_3 = \begin{pmatrix} -\dot{\theta}_1 C2C3 + \dot{\theta}_2 S3 & \dot{\theta}_1 C2S3 + \dot{\theta}_2 C3 & \dot{\theta}_3 - \dot{\theta}_1 S2 \end{pmatrix}^T \tag{3.26}$$

$$\overrightarrow{OG}_3 = \begin{pmatrix} S1S2\left(x_{G_3}C3 - y_{G_3}S3\right) - C1\left(x_{G_3}C3 + y_{G_3}C3\right) - S1C2z_{G_3} \\ x_{G_3}C2C3 - y_{G_3}C2S3 + S2z_{G_3} \\ C1S2\left(x_{G_3}C3 - y_{G_3}S3\right) + S1\left(x_{G_3}C3 + y_{G_3}C3\right) - C1C2z_{G_3} \end{pmatrix} \tag{3.27}$$

$$\vec{v}_{G_3} = \begin{pmatrix} \dot{\theta}_1\left(C1S2\left(x_{G_3}C3 - y_{G_3}S3\right) + S1\left(x_{G_3}S3 + y_{G_3}C3\right) - C1C2z_{G_3}\right) \\ +\dot{\theta}_2 S1\left(C2\left(x_{G_3}C3 - y_{G_3}S3\right) + S2z_{G_3}\right) \\ -\dot{\theta}_3\left(S1S2\left(x_{G_3}S3 + y_{G_3}C3\right) - C1\left(x_{G_3}C3 - y_{G_3}S3\right)\right) \\ \\ -\dot{\theta}_2 C3S2x_{G_3} - \dot{\theta}_3 S3C2x_{G_3} + \dot{\theta}_2 S3S2y_{G_3} - \dot{\theta}_3 C3C2y_{G_3} + \dot{\theta}_2 C2z_{G_3} \\ \\ \dot{\theta}_1\left(-S1S2\left(x_{G_3}C3 - y_{G_3}S3\right) + C1\left(x_{G_3}S3 + y_{G_3}C3\right) + S1C2z_{G_3}\right) \\ +\dot{\theta}_2 C1\left(C2\left(x_{G_3}C3 - y_{G_3}S3\right) + S2z_{G_3}\right) \\ -\dot{\theta}_3\left(C1S2\left(x_{G_3}S3 + y_{G_3}C3\right) - S1\left(x_{G_3}C3 - y_{G_3}S3\right)\right) \end{pmatrix} \tag{3.28}$$

For part 4, we have:

$$E_{K_4} = \frac{1}{2}\left(I_{zz_4} + m_4 y_{G_4}^2\right)\dot{\theta}_4^2 \tag{3.29}$$

$$E_{P_4} = -m_4 g y_{G_4} C4 \tag{3.30}$$

For part 5, we have:

$$\vec{w}_5 = \begin{pmatrix} \dot{\theta}_4 S5 & \dot{\theta}_4 C5 & \dot{\theta}_5 \end{pmatrix}^T \tag{3.31}$$

and

$$\overrightarrow{OG}_5 = \begin{pmatrix} -x_{G_5}C5 \\ x_{G_5}C4S5 - z_{G_5}S4 \\ -x_{G_5}S4S5 - z_{G_5}C4 \end{pmatrix} \tag{3.32}$$

after derivation, we get:

$$\vec{v}_{G_5} = \begin{pmatrix} x_{G_5}\dot{\theta}_5 S5 \\ -x_{G_5}\dot{\theta}_4 S4S5 + x_{G_5}\dot{\theta}_5 C4C5 - z_{G_5}\dot{\theta}_4 C4 \\ -x_{G_5}\dot{\theta}_4 C4S5 - x_{G_5}\dot{\theta}_5 S4C5 + z_{G_5}\dot{\theta}_4 S4 \end{pmatrix} \tag{3.33}$$

Finally, for part 6, we have:

$$\vec{v}_{G_6} = \begin{pmatrix} -\dot{q}S1C2 & \dot{q}S2 & \dot{q}C1C2 \end{pmatrix}^T \tag{3.34}$$

and

$$\vec{w}_6 = 0 \tag{3.35}$$

The total energies of the device are given as:

$$E_K = \sum_{i=1}^{6} E_{K_i} \tag{3.36}$$

and

$$E_P = \sum_{i=1}^{6} E_{P_i} \tag{3.37}$$

Using the Lagrange's equation, the dynamic equations can be obtained with the kinetic energy and the potential energy obtained in the above.

$$\tau_i = \frac{d}{dt}\left(\frac{\partial L}{\partial \dot{\theta}_i}\right) - \frac{\partial L}{\partial \theta_i} + \lambda^T \frac{\partial \Phi(\theta)}{\partial \theta_i} \tag{3.38}$$

where τ_i is the generalized torque associated with the i^{th} body, λ is the Lagrangian multiplier(s), L is the Lagrangian operator defined as :

$$L = E_K - E_P$$

and $\Phi(\theta)$ denotes the constraint function from (3.6). The final form of the dynamic model would be formulated as :

$$\tau = M(\theta)\ddot{\theta} + B(\theta)\left[\dot{\theta}\right] + C(\theta)\dot{\theta}^2 + G(\theta) + F(\theta) \tag{3.39}$$

where M is the inertia matrix, B the Coriolis matrix, C the centrifugal coefficient matrix, G the gravity vector and F a vector that gathers friction and external forces.

3.6 Evaluation experiments

3.6.1 Reachable workspace determination

In this study, we targeted an elliptical cone with 90° angle around the yaw and the pitch axes, in accordance with what we had mentioned in the design constraints. The evaluation of the workspace of this 4-DOF haptic device is performed by comparing it with the required workspace. The obtained ranges of rotations and translation are presented in Table 3.6. The reachable workspace is totally free from the linkages intrusion and it approximately constitutes a half sphere with $20cm$ radius, see Figure 3.16. However, the self-rotation of the tool is limited to 210°, which proved to be sufficient for our target applications. Therefore, the designed haptic device has enough workspace inside which one can operate in a natural and friendly way. Moreover, the designed device provides an additional workspace of approximately 50%, compared to the required volume.

3.6.2 Performance measurement and evaluation

3.6.2.1 Frequency analysis

The objective of the frequency analysis experiments is to characterize the mechanical bandwidth of the device in position and force. For position's bandwidth determination, sinusoidal signal inputs have been applied independently to each axis. The

Table 3.6: Workspace boundaries.

	Workspace boundaries
Axis 1 (Yaw)	$[-70, \ +70]^{\circ}$
Axis 2 (Pitch)	$[-70, \ +70]^{\circ}$
Axis 3 (Roll)	$[-100, \ 100]^{\circ}$
Axis 4 (Translation)	$200mm$

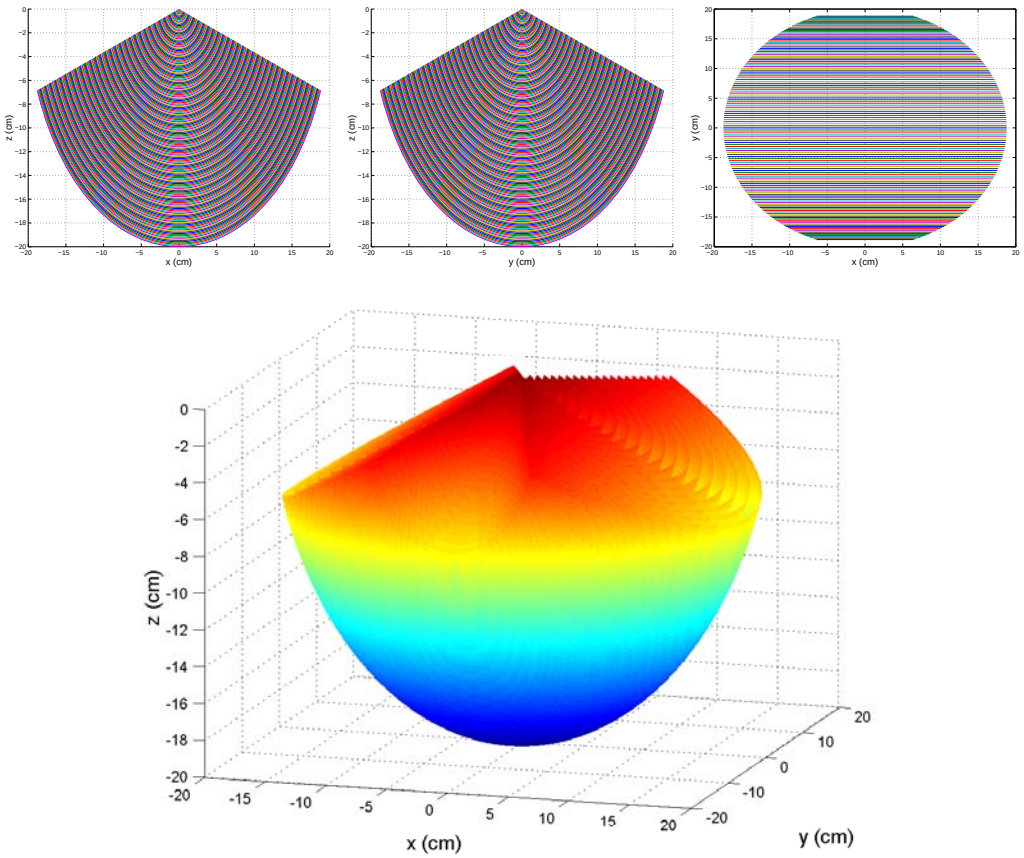

Figure 3.16: Workspace of the Designed 4-DOF Haptic Device.

frequency of the sinusoid has been modified ranging from $2Hz$ up to $40Hz$ for the translational and the roll axes, and up to $30Hz$ for the pitch and yaw axes. The amplitude and the phase of the output velocity (sinusoidal signal also) have been noted for each frequency value. Figure 3.17 shows that all axes exhibit a similar behavior with a low frequency constant gain and -3dB cut-off frequency of nearly $13Hz$, $15Hz$, $25Hz$ and $28Hz$ for the yaw, pitch, roll and translational axes, respectively. Note that, at these frequencies, the phase is about -45°, which is very close to the theoretical phase of a first-order system. By observing these values

(presented in Table 3.7), one can see that the mechanical bandwidths of both the roll and the translational axes are twice greater than those of the pitch and the yaw axes. This is due to the fact that the pitch and yaw axes support more inertia than do the other two. Although the obtained bandwidths are sufficient for the operators, as has been shown in the previous chapter, friction compensation can increase the system bandwidth by reducing its damping effect.

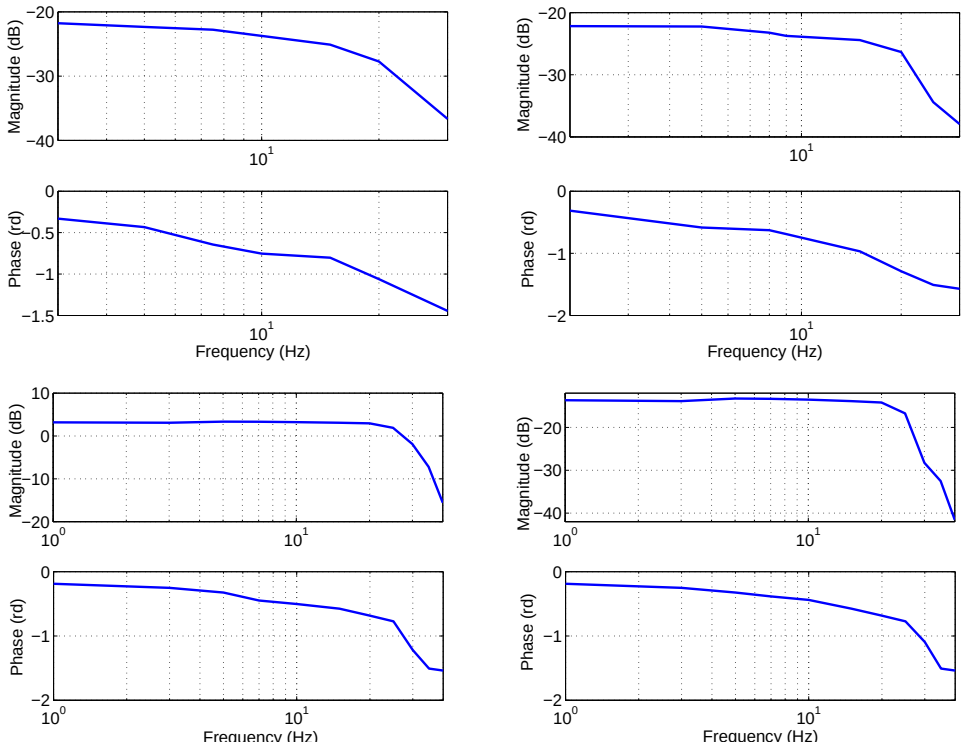

Figure 3.17: Bode plot: magnitude and phase for position evolution as a function of frequency: (Top-right) yaw; (Top-left) pitch; (Bottom-right) roll; (Bottom left) translation.

In order to establish the force bandwidth, an open-loop excitation is applied to each axes using a PRBS signal approximating a white noise signal sampled at 0.002 *sec*. During this experiment, the device is maintained in contact. The electric current provided to the actuators is measured before being converted to torque. Figure 3.18 represents the power spectral density estimation based on the Welch method. The frequency responses for the yaw and pitch axes are approximately flat for frequencies $< 250Hz$. However, we note the existence of an attenuation of $\approx -4dB$ at $39Hz$ for the yaw axes and $21Hz$ for the pitch. A relatively high bandwidth is observed for the roll axe ($> 250Hz$) and the translation axe ($150Hz$).

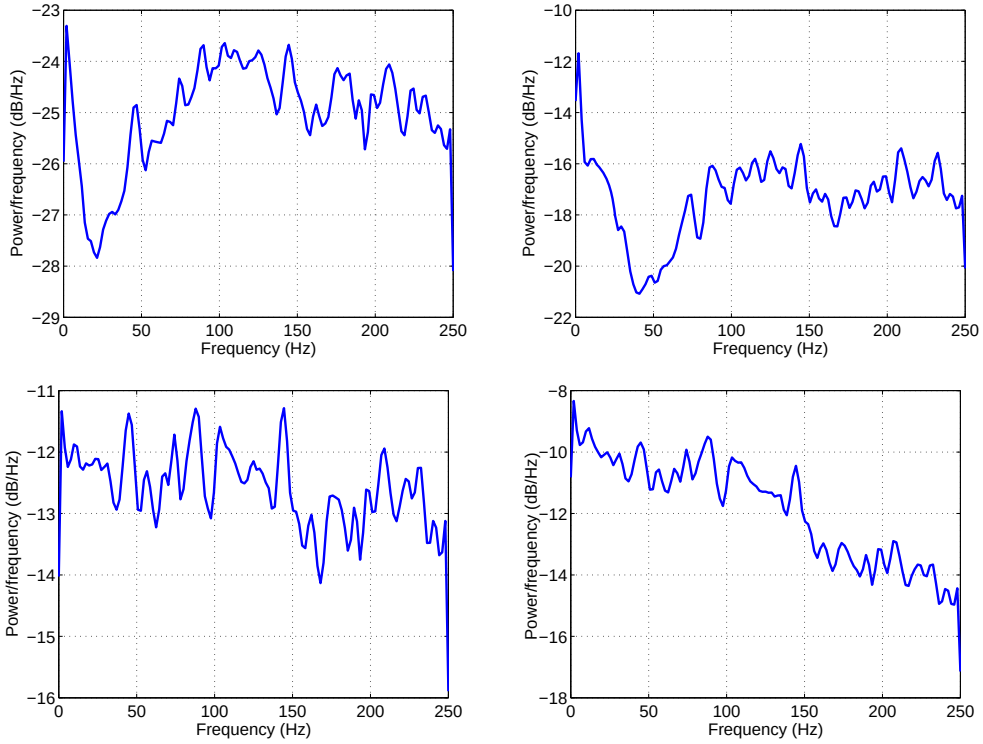

Figure 3.18: DSP plot of the force frequency response: (Top-right) yaw; (Top-left) pitch; (Bottom-right) roll; (Bottom left) translation.

3.6.2.2 Maximum capabilities

We devised a dedicated setup in order to evaluate technical performances of the assembled haptic device prototype. The performances obtained by experimentations are presented in Tables 3.7 and 3.8. In order to measure the device stiffness and maximum-torque capabilities, each axis was independently controlled in a fixed position using a proportional controller. By applying a maximum force that maintained the device in the controlled position, we measured the deviation of the position sensor and the level of the applied force. The ratio gave us the stiffness value for each axis separately.

For the rotational axis, the maximum maintained torques that can be generated by the device are superior to the required upper limits presented in subsection 3.2.2.2 according to [Rosen 1999] and [Rosen 2000]. The additional torques can be used for friction and eventually gravity compensation when needed. The maximum torque obtained for the translational axe is equivalent to an applied force of about $21N$, which is, to our best knowledge, an acceptable value for most tasks encountered in MIS.

The relatively high stiffness values are achieved by using high-precision bearing and aluminum material for manufacturing, which is light and strong in order to minimize the deflection due to the stiffness of the linkages.

Table 3.7: Performance evaluation of the haptic device.

	Dynamic Friction	Friction level	Stiffness	Maximum velocity	Maximum acceleration
Yaw axe	0.26N/m	7.8%	2750N/rd	5rd/s	95rd/s^2
Pitch axe	0.24N/m	7.2%	2400N/rd	5rd/s	95rd/s^2
Roll axe	0.025N/m	3.5%	3100N/rd	25rd/s	660rd/s^2
Translation	$-0.9, +1.6$N	4.3%, 7.6%	680N/cm	1.73m/s	6m/s^2

However, in our first prototype, the measured friction of the translational axis is superior to the allowed threshold (JND), although high precision bearings are used. This level is also asymmetric when moving the translational body in the two directions. This is certainly due to some imperfections in the assembling of the two parallel bars that guide the translational body; this problem can be easily solved by a more precise machining tool. In the case of the yaw and the pitch axes, the relatively high level of friction is due to the use of gear-reduction system, although the gear reduction ratio is small (1:4). An exception is the roll axis where the level of friction is less than the allowed one.

Finally, table 3.8 compares our prototype device to three commercial available ones that are designed also for MIS training. By comparing the workspaces boundaries, one can observe that our device is able to reach larger workspace in term of the pitch and yaw rotations and translation (insertion) with an equivalent sensing resolution. This additional workspace may be useful for future applications. However, our device is not able to give an unlimited self rotation (roll) with equivalent footprint. In term of workspace, force and torques capabilities, our device offers larger potentialities.

3.7 Position and force control

3.7.1 Position control

In order to assess the model and to evaluate the performances of the assembled device, basic position-control loops are implemented successfully using a PD controller. First, a trajectory (orientation and 3D position) is planned in the operational space, and then the desired joint positions are computed using the inverse kinematics model. After that, the desired positions of the active joints are derived from the kinematics constraints. The position control loops allow achieving the desired joint positions, (see Figure 3.20). The PD controller allows improving the time response of the system and eliminating the static error in the position control loop in a stable way. So that, and since the first instant, the resulting trajectory converges faster to the desired one (see Figure 3.19).

Table 3.8: Performances comparison of the designed haptic device with available devices.

	Laparoscopic Surgical Workstation	Xitact IHP^{TM}	EXOS	Designed device
Yaw (deg) (range/resolution)	100/0.01	100	140/0.1	140/0.009
Pitch(deg) (range/resolution)	100/0.01	100	140/0.1	140/0.009
Roll(deg) (range/resolution)	*Unlimited*/0.7	*Unlimited*	350/0.1	200/0.072
Insertion (mm) (range/resolution)	170/0.008	> 200	100/0.025	200/0.05
Pitch torque (Nm) (peak/ continuous)	0.85/0.47	1.4/1.0	0.4189/0.0852	5.6/3.3
Yaw torque(Nm) (peak/ continuous)	0.85/0.47	1.8/1.4	0.4189/0.0852	5.6/3.3
Roll torque (Nm) (peak/ continuous)	0.07/0.04	0.14/0.10	0.142/0.036	1.2/0.7
Insertion force(N) (peak/ continuous)	19/11	30/20	7/2	25/21
Footprint(cm)	30×34	$18 \times 16 \times 40$	$30 \times 33 \times 18$	35×35

3.7.2 Torque control

For torque control loop, the measured current of each link is converted into torque using the fitting equations established in subsection 3.4.3 and parameters presented in Table B. The parameters of the PID controllers (proportional gain (Kp), integral gain (Ki) and derivation gain (Kd)) are determined using classical control techniques and assessed experimentally (see Figure 3.20. We determined the parameters that: (i) keep the system stable (without exceeding in the transient phase), (ii) eliminate the static error, and (iii) reduce the response time, (see Figure 3.21), where a square input torque is desired). The PID gain factors are presented in Table 3.9.

3.8 Conclusion

We presented the mechatronics design, modeling and assembling of a new haptic device to be integrated in a MIS simulator. The proposed structure of this device is inspired from the real motions of the tool during practical use in real procedures. It is designed to provide adequate force feedback in 4 degrees of freedom as in most

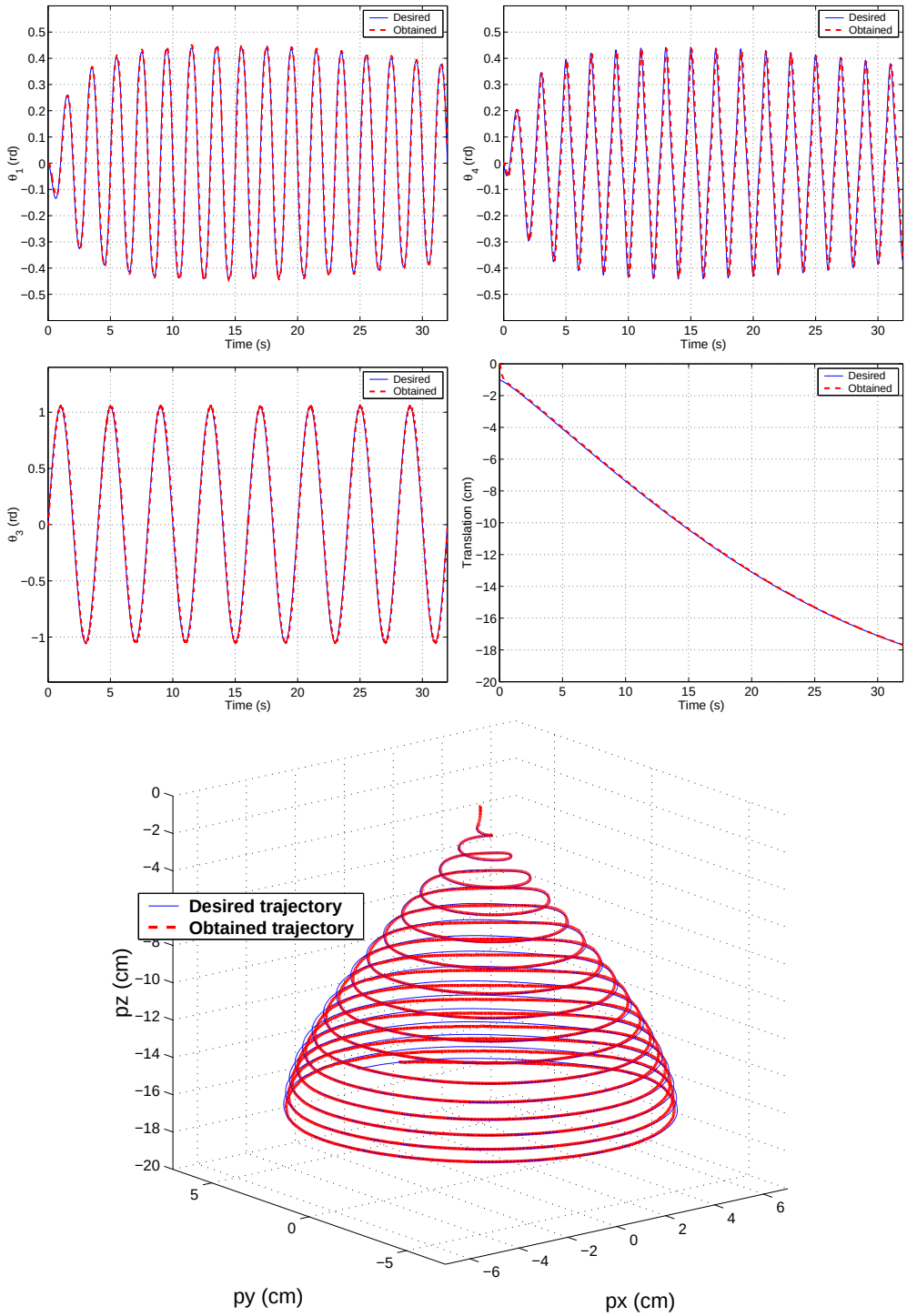

Figure 3.19: Position trajectory tracking example.

real MIS procedures. This device is designed to hold different surgical tools and to provide adequate force and torque capabilities. The motorized part, which pro-

Table 3.9: Torque controller gain factors.

	Kp	Ki	Kd
Axis 1	0.95	4	0.01
Axis 2	0.8	3.5	0.01
Axis 3	40	12	0.02
Axis 4	25	10	0.02

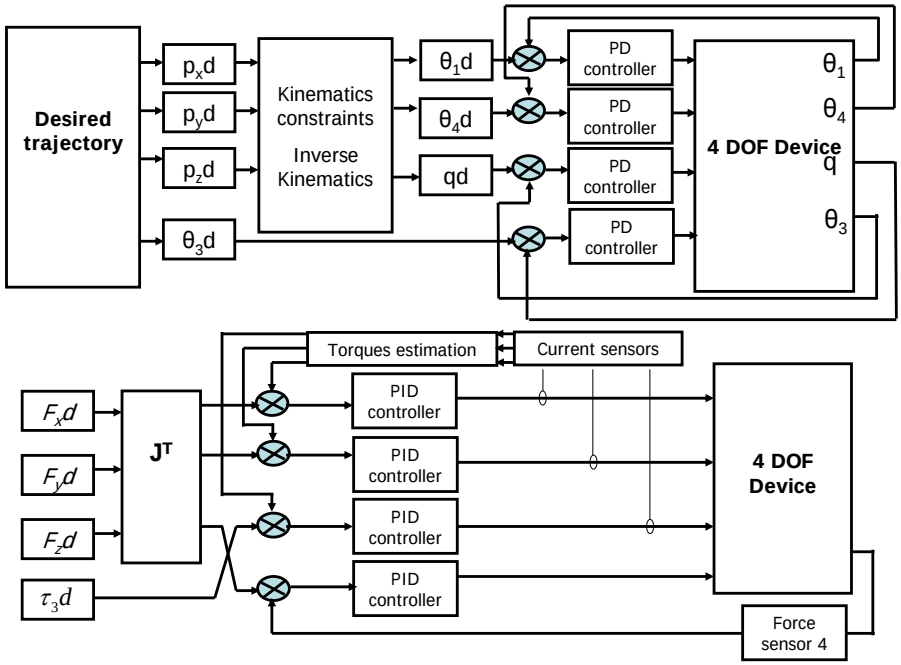

Figure 3.20: Position control (Top) and torque control schemes (Bottom).

vides force-feedback, consists of a hybrid configuration (parallel-serial) that allows combining a relatively high stiffness and a large workspace and that satisfies the general design considerations of haptic devices. Furthermore, the optimization and dimensioning procedure of actuators and workspace are performed using available measurements recorded during *in-vivo* MIS procedures in order to integrate successfully haptics with the environmental characteristics found in surgery. The forward and inverse kinematics models are expressed analytically using the DH convention. Basic dynamic equations are also formulated. The device is assembled and the electronics interfaces with sensor calibration are carried out. Then, the resulting prototype is characterized, evaluated and compared with some others available devices. Its main features such as bandwidth, stiffness, maximum forces/torques and velocity capabilities are determined experimentally. We also designed an electronics

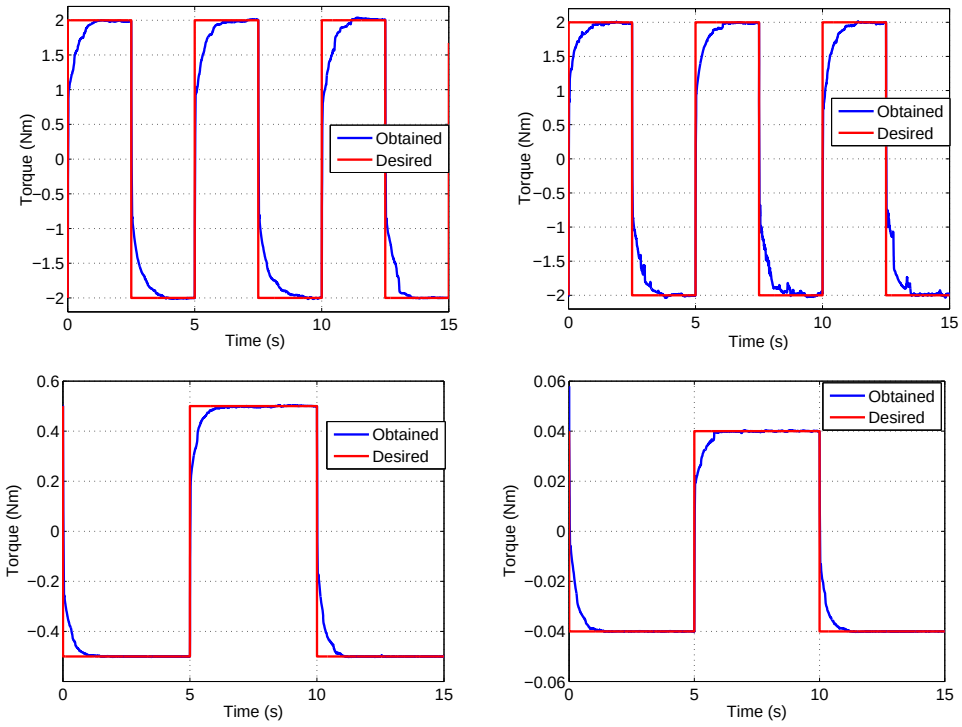

Figure 3.21: Torque control example.

interface that allows current and force sensing. Torques are estimated based on a fitting equation calculated from experimental calibration. This equation provides torque values that are closer to real torques than the conventional calculation using the torque constant of the DC motors. The resulting device is evaluated by implementing position and torque control loops based on basic PID controllers and the developed kinematics model. The obtained results show that desired position and orientation and torque are achieved successfully, which demonstrates the high ability of our device in position and torque tracking since these two measures are very important for force feedback generation in telepresence and VR applications. Using this device, the surgeon can train as in usual working conditions (except stress...) and embed the device with real surgical instruments that have to serve as haptic input devices since force-feedback is an important issue in VR-based surgery training. In the next chapter, we will address a new issue that was not considered in previous studies related to MIS. It concerns the adding thermal feedback. Justification and whole integration scheme is rather presented in the last chapter of this thesis. The next chapter addresses thermal modeling and rendering from a fundamental aspect regardless of the target application.

Chapter 4

Thermal Feedback for Telepresence and Virtual Reality Applications

Contents

4.1 Introduction

This study is conducted for a general purpose considering simply that we need to reproduce thermal feedback to the user (e.g. a surgeon or a medical stuff), from remote touch in real (telepresence) or virtual environments. The thermal sensation, permeating and accompanying our tactual impressions, influences considerably our capability to distinguish several objects in our surrounding world by the simple act of touching. When bare-touching an object, thermal exchange occurs through the area of contact between the human skin and this object, with the resulting warm/cool feeling as first sensation. This transient thermal contact feeling needs to be carefully investigated since it strongly affects one's first impressions [Monkman 1993][Jones 2003][Yamamoto 2004][Ho 2004][Ho 2006a][Ho 2006b]; it plays an important role and is inherent to our haptic sense.

Objects made of different materials that are all at the same temperature feel thermally different. For instance, wood generally feels warmer than metal, even though both materials are at room temperature. This effect is caused by differences in the thermal properties of these materials.

However, the idea of sensing temperature/thermal properties of an object to be manipulated is not new; but it tends to be ignored, even though thermal properties help in the identification of an unknown object and can serve as part of an object signature/model. Although this sensation is inherent to our haptic sense and the various possible applications in telepresence and virtual reality systems, thermal feedback has not been extensively investigated in comparison to force and other tactile feedback [Monkman 1993][Jones 2002][Drif 2005]. Thermo-electric module (TEM), in its proper configuration of heat-pump, is commonly used to produce a relative temperature on the finger of the operator [Benali-Khoudja 2003][Yamamoto 2004][Drif 2005][Yamamoto 2005].

4.1.1 State-of-the-art in thermal rendering

Recently, a state-of-the-art in thermal rendering has been thoroughly compiled in [Jones 2008]. From it, it appears that the human thermal perception process is still not well/totally understood. Few thermal displays exist that are really able to reproduce high-fidelity thermal sensations. On the other hand, no device or sensor developed so far is able to quantify our thermal perception in a reproducible way. Most of reported researches focus on the thermal threshold perception that allows distinguishing between warm and cold feeling [Cohen 1977][Katsuura 1998], while other researches deal with the human capability in materials discrimination using thermal cues [Jones 2002][Ho 2004]. In [Cho 2007], [Kim 2007] and [Kim 2008], thermal feedback systems have been investigated as a part of a multimodal device for prosthetic applications to provide thermal sensation for upper extremity amputees, especially those who have undergone targeted reinnervation surgery. Russel, in [Russell 1985][Russell 1988] conceived thermal sensors incorporated to slave manipulators for remote materials identification. Caldwell [Caldwell 1995], developed

an anthropomorphic teleoperation system integrating temperature sensors on a robot gripper and a temperature feedback on a master glove to stimulate the operator's index finger. In [Yamamoto 2004], the authors described a control technique for thermal tactile display. This technique is based on a decomposition of the thermal sense into two phases; they introduced the idea of relative effusivity. The technique is improved in [Yamamoto 2005], by the on-site thermal identification of the parameter of finger for each individual, just before thermal presentations. Some recent approaches use the physiological composition of the human finger (bone, blood and skin) and thermo-electricity laws to model and explain the heat exchange occurring in each part of the finger when touching an object. In [Benali-Khoudja 2003], a thermal model using electrical analogy is proposed for virtual reality. This model takes into consideration conduction and convection of air around the finger and around the touched material but it strongly depends on the human finger geometric dimensions and on its thermal properties. This model is based on electric analogy and takes into account various phenomena such as the applied pressure by the finger, the speed of the blood circulation, the surface state of the skin and the material. In [Deml 2006], the heat conduction between skin and objects is modeled by ordinary differential equations. Three different layers of tissue (epidermis, dermis and endodermis) are distinguished within the finger. The work of [Ho 2006b] proposes a prediction model for contact heat flux[1] and temperature based on an infrared camera during interactions phases. An infrared thermal measurement system is also designed in [Ho 2007b] so that it can be used to evaluate the performance of a thermal model implemented in a thermal display. This measurement system requires that the contact material be transparent in both the infrared and visible spectrum. It is therefore designed so that skin temperature can be measured more accurately during contact, but not as a system that would be integrated into a haptic interface. The objective of the studies presented in [Jones 2003][Ho 2004], is to measure material discrimination when thermal cues are the main source of information about the used material. These findings suggest that temperature cues can be used to discriminate between materials, but only when the thermal properties differences are large. This can facilitate object recognition when visual cues are limited. In [Jones 2002], the research provided the basis for further exploration of how thermal information is extracted from the environment and how effectively this can be presented in a haptic display.

Almost all thermal displays consist of a heat source, a Peltier pump or a power heater, embedded with a set of temperature sensors. The control technique used is simple and focuses on reproducing pre-measured and pre-computed temperature profiles on a thermal pad in contact with the human finger [Russell 1988][Caldwell 1995][Ottensmeyer 1997]. One way to provide the human operator with realistic impression of the thermal properties is to emulate the human sensing system with a thermal sensing device to get the relative temperature change that would be felt, and reproduce that temperature change to the user

[1] From now on, flux is meant to designate heat flux.

through the thermal display [Ho 2007a]. This is similar to that used by Russell and others [Russell 1988][Ho 2006b]. But, as stated by [Monkman 1993], the human tactile sense is not able to determine even relative temperatures by touching a selection of objects. Indeed, several results corroborate the fact that our fingertip sense thermal conductivity and diffusivity [Monkman 1993].

4.1.2 Problem statement

Most thermal feedback methods use a direct temperature control scheme and do not produce satisfactory thermal sensation since the human thermal perception relies on the heat transfer rate, and not solely on the temperature. An exception is the work presented in [Drif 2005] where the thermal feedback is based on a bilateral coupling scheme between the flux and the temperature using a four channel coupling scheme. The authors in [Drif 2005] presented a thermal teleoperator where rendering was achieved through bilateral coupling schemes between flux and temperature variables of the master and slave sides. Their idea was totally inspired by force reflecting teleoperators using bilateral coupling schemes through force (effort) and velocity (flux) variables. In the same way, the four-channel bilateral architecture established in [Lawrence 1993] was adopted as an architecture in their proposed thermal reflecting teleoperator, (Figure 4.1). Similarly to force reflecting bilateral coupling, four thermal bilateral coupling methods combining temperature and flux variables are possible. Those are: flux/flux, temperature/temperature, flux/temperature, and temperature/flux. A pair x/y means that the slave part is controlled according to desired measured/observed x variable coming from the master side, and the master side is controlled according to desired measured/observed y variable coming from the slave side. Here, the master device is simply an active thermal display and the slave an active thermal sensor; by active we mean that its output temperature/flux is controlled.

Experiments conducted in [Drif 2005] show that flux/flux scheme exhibits poor transparency (which is opposite to force reflecting systems where velocity/velocity tracking has good performance relative to force/force), and the stability depends strongly on the contact nature. An abrupt flux variation may lead to temperature divergence. Temperature/Flux or Flux/Temperature coupling have very superior (highest transparency) and stable performances. However, although very good performances are obtained, even in a temperature/temperature coupling scheme, these architectures do not reproduce realistic thermal interaction. Although the thermal active finger and the master display devices were exactly the same system, a confrontation of the heat exchange and evolution to similar direct contact conditions (i.e. direct touch of the material by the operator) highlights discrepancies in the behaviors: that is, the heat exchange signals (temperature and flux) obtained from the telepresence bilateral coupling set-up are different from those measured on a direct contact case (again, with similar conditions). The reason for this is simple: unless we have an artificial finger whose thermal properties are exactly the same as that of the human operator, the bilateral coupling scheme will certainly converge

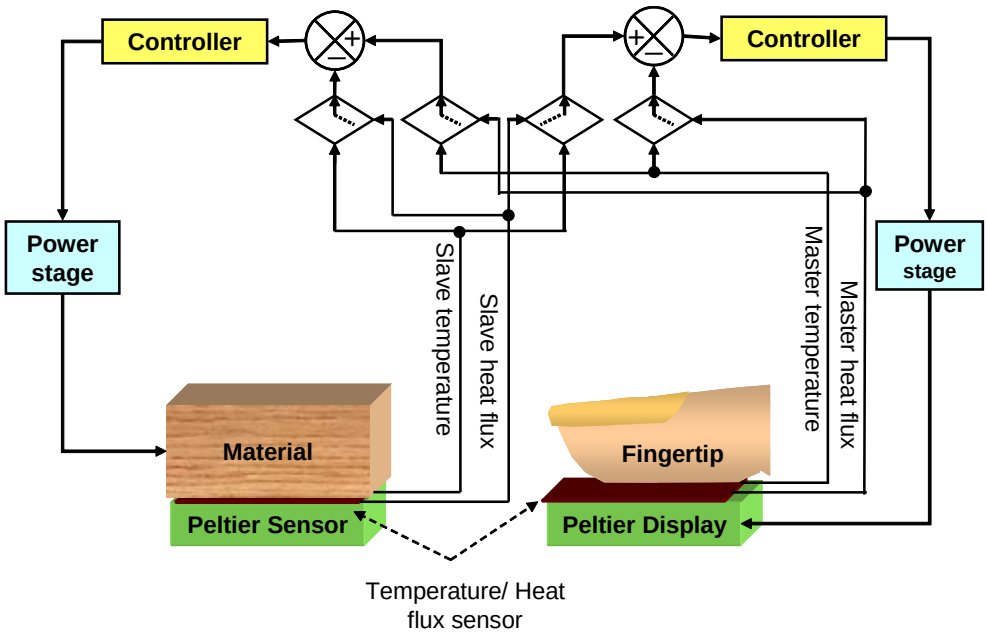

Figure 4.1: Overview of the thermal teleoperator and possible bilateral coupling.

toward equilibrium, but with a different behavior and a different state compared to the real case.

Thermal exchange is indeed driven by: (i) the intrinsic properties of the material, (ii) the nature of contacting area, and can hardly (not to say impossible) be compensated; unless one can change the intrinsic thermal properties of the material composing the sensor. The same applies for the display: it will have certainly different thermal properties from the object being explored (exception to objects made with the same material as that of the display surface). But, since humans are sensitive to flux behavior in identifying a given material, one can *cheat* by forcing the display to reproduce a given flux behavior through a closed-loop control.

4.1.3 Contributions

This chapter is organized as follows:

In section 4.2, we present the modeling and identification procedure of thermoelectric modules that we used as a thermal display (as many other researchers did), and also as an active sensor which may behave as the human fingertip for instance. We propose new models for both steady-state and unsteady-state dynamics based on Non-linear Autoregressive Moving Average Model (ARMA) models for temperature and flux. The proposed models can be used for simulation, control, electronic, and thermal engineering. They also help understanding the functionality of the heat pumps, and facilitating the solving of cooling/heating problems without the need for expertise in thermal engineering. The effectiveness of the models is assessed experimentally.

In section 4.3, these models are used in a novel rendering approach based on the estimation of the temperature in contact for both the finger and the touched object. The thermal feedback is provided by a bilateral control between the master (thermal display) and the slave (thermal robotic finger).

In section 4.4, we propose a new approach for thermal rendering in telepresence that improves thermal rendering transparency. We aim at reaching, as close as possible, what is experienced in similar real touch conditions. The proposed method is based on neural networks learning classifier that allows generating desired values for thermal controllers. Two databases are built from real measurements recorded during direct contact between the operator's finger and different materials. One database is used for training a classifier for an on-line identification of the material being explored in the remote side (probed site); the other one is used to generate desired flux trajectories for the two thermal control loops: the one acting for the artificial finger probe, and the other one acting for the thermal display. The learning bloc is based on Principal Component Analysis and Feed-Forward Neural Network.

In section 4.5, a theoretical and experimental study of a model describing the heat transfer that occurs when a finger touches an object is presented. This model accounts for the thermal dynamics of the finger, the sensor and the material by considering their thermal properties. Models of the heat exchange are developed and implemented on a thermal display incorporated to a haptic device for virtual reality applications. All the proposed techniques are validated experimentally; the obtained results are discussed in this chapter.

4.2 Modeling and control of thermoelectric modules

Thermoelectric modules, named also Peltier pumps, Peltier cooler, TEM cooler, or Peltier heat source... will be used as a display and possibly (depending on the application) as an active sensor that can replicate for instance a human fingertip. Thermal sensation is displayed to the human fingertip through a direct contact and hence two problems are to be solved:

1. a stable, robust and fast closed-loop control of the Peltier pump when used ad a display or as an active sensor (typically: temperature or flux closed-loop control); this call for classical control theory tools (modeling, identification, control synthesis, etc.);

2. having an intrinsic temperature sensor is difficult. Indeed, the sensor will be placed at the interface of the display/sensor and the contacted object and one need to isolate the resultant temperature to identify the quantity which is the contribution of the Peltier pump.

4.2.1 Thermoelectric modules

In this section, we give a brief review on the basic equations governing the thermal behavior of the TEM. Then, we define the proposed models for temperature dynam-

ics and flux as a function of current and temperature. These models would help us develop our temperature estimator for the Peltier modules used as a display and as an active sensor. After that, we present the experimental setup and the model identification procedure.

A thermoelectric module (TEM) consists of a multiple semiconductor junction connected in series electrically, in parallel thermally between two plates (Figure 4.2). The plates must, be both good conductors of heat and good electrical insulators. Ceramic materials fulfill this particular property: one plate is thermally connected to a radiator, and the other to the object whose temperature is to be controlled. Thanks to the Peltier physical effect, a current through the junctions creates a temperature difference between the plates whose polarity and magnitude depend on those of the current. Relatively to the ambient temperature, it then becomes possible to heat the object or cool it down (via one TEM plate). Today's technology allows single-module temperature differences as high as 84°C, and cascading arrangements can produce even higher differences.

TEMs are widely used today in many applications, from thermal stabilization to micro-refrigeration. TEMs can be used where cooling or temperature control of an object is required. Generally, TEMs are most often used:

1. in applications where an object needs to be cooled below the ambient temperature, or needs to be maintained at a constant temperature [Ciccarella 1989][Schütze 2001][Hodes 2007][Solbrekken 2008];

2. as a thermal-haptic display for virtual reality and telepresence systems [Benali-Khoudja 2003][Drif 2005][Citérin 2006]. Precisely in this case, we need to control the TEM in order to get fast and exact response both in temperature and in flux.

The main difficulty is to write accurate equations that relate the input current, driving the TEM, to the temperature of each side of the TEM. These equations are hard to determine and a precise analysis of the electro-thermal Peltier effect is difficult; this is because of the nonlinear behavior of the TEM that acts as a floating load for the voltage supply and the several phenomena that occur within it.

In [Lineykin 2007], a SPICE compatible equivalent circuit of TEM has been devised. Equivalent circuits are a convenient tool for electronic engineers. This helps representing the problem in 'electronic circuit language' and facilitates the solving of cooling/heating problems without the need for expertise in thermal engineering. In [Neto 2003], it has been shown that it is possible to describe the characteristics of a thermoelectric device with a second-order discrete-time ARMA model. The parameters of such a recursive second-order discrete-time model vary with the operating point, which is defined by the bias excitation current.

This section aims at providing a more general model of TEMs. We propose a non-linear dynamic representation based on a non-linear ARMA model for temperature control. We also propose a model for solving steady-state cooling/heating capacity

and establish a model to describe the temperature/heat flow relation. These models should help users synthesize control laws for achieving required performances.

4.2.2 Thermo-physical Models

When an electric current flows through a circuit composed of two different conductors $n-$type and $p-$type (see Figure 4.2) heat is liberated at one junction and absorbed by the other one, depending on the direction in which the current is flowing: this is called the Peltier effect. The quantity of heat P liberated per unit of time is proportional to the current [Carslaw 1959][Labudovic 2004]:

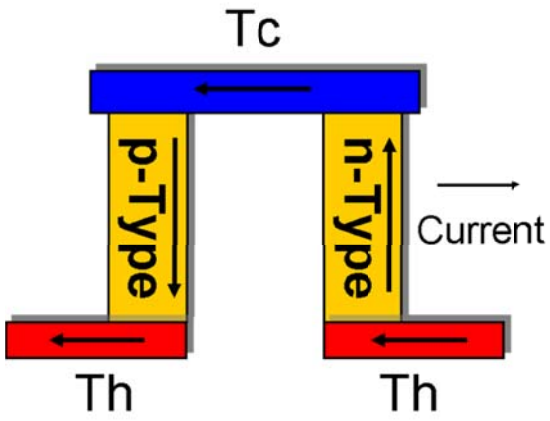

Figure 4.2: Construction of a Peltier semi-conductor element. In practice several elements are generally connected in series electrically, and in parallel thermally.

$$\frac{P}{t} = P_p = \pi\ I = \alpha\ T\ I \tag{4.1}$$

where π [V] is the Peltier coefficient, α [V·K^{-1}] the Seebeck coefficient, T [K] the absolute temperature and I [A] the electric current. If an electric current flows in a homogeneous conductor in the direction of a temperature gradient $\frac{dT}{dx}$, heat will be absorbed or given out, depending on the material: this is the Thomson effect,

$$P_T = \tau\ I\ \frac{dT}{dx} \tag{4.2}$$

where τ [V·K^{-1}] is the Thomson coefficient and x [m] the space variable. The direction in which the heat flows depends on: the sign of the Thomson coefficient, the direction in which the current flows, and the direction of the temperature gradient. At the other hand, heat is also generated due to Joule effect; this heating is assumed to be uniformly distributed on both sides.
If an electric current I flows in an isothermal conductor of resistance R, the Joule

effect is written as:

$$P_j = R\ I^2 \tag{4.3}$$

Because of heat conduction, heat also flows from the hot side (temperature T_h) to the cold side (temperature T_c), hence:

$$P_k = K\ (T_h - T_c) \tag{4.4}$$

where K is the thermal conductance. The heat capacity of the pump on the cold side (the steady-state cooling capacity) is:

$$P_c = n\left\{\alpha T_c I \pm \frac{\tau I\,(T_h - T_c)}{2e} - \frac{1}{2}RI^2 - K\,(T_h - T_c)\right\} \tag{4.5}$$

where e is the thickness of the Peltier component and n the number of components. The heat capacity of the pump on the hot side (the steady-state heating capacity) is:

$$P_h = n\left\{\alpha T_h I \pm \frac{\tau I\,(T_h - T_c)}{2e} + \frac{1}{2}RI^2 - K\,(T_h - T_c)\right\} \tag{4.6}$$

Equations (4.5) and (4.6) represent the steady-state behavior of the TEM, similar models can be found in [Martorana 1975][Hodes 2005][Martorana 2005][Harvey 2007][Beaudoin 2008]; the description of transient behavior is more complex. However transient behavior is required for real-time simulation and controller synthesis.

4.2.3 Proposed models

Based on the previous steady-state models, we assume that the dynamic behavior of the TEMs can be correctly described by the following discrete-time ARMA model [Neto 2003]:

$$T(t) = -\sum_{i=1}^{n} a_i\ T\,(t-i) + \sum_{j=0}^{m} b_j\ I\,(t-j) \tag{4.7}$$

where a_i and b_j are parameters depending on the current $I(t)$.

We propose recursive polynomial functions to describe the dependence of the parameters on current. That is:

$$a_i = \sum_{k=0}^{p} a_{ik} I\,(t-i)^k \tag{4.8}$$

$$b_j = \sum_{h=0}^{q} b_{jh} I\,(t-j)^h \tag{4.9}$$

The complete description leads to the non-linear ARMA model:

$$\begin{aligned} T(t) = &-\sum_{i=1}^{n}\sum_{k=0}^{p} a_{ik} I\,(t-i)^k T\,(t-i) \\ &+\sum_{j=1}^{m}\sum_{h=0}^{q} b_{jh} I\,(t-j)^h I\,(t-j) \end{aligned} \tag{4.10}$$

which is a linear model of the unknown parameters θ:

$$T(t) = \theta^T \varphi(t) \tag{4.11}$$

where

$$\begin{aligned} \theta = \quad & [a_{ik},\ \{i = 1 \cdots n,\ k = 0 \cdots p\}; \\ & b_{jh},\ \{j = 0 \cdots m,\ h = 0 \cdots q\}] \end{aligned}$$

is the vector of parameters of dimension $d = n(p+1) + m(q+1)$, and

$$\begin{aligned} \varphi(t) = \quad & \left[I(t-i)^k\ T(t-i),\ \{i = 1 \cdots n,\ k = 0 \cdots p\}; \right. \\ & \left. I(t-j)^{h+1},\ \{j = 0 \cdots m,\ h = 0 \cdots q\}\right], \end{aligned}$$

the regression vector of dimension d. For the relation between the temperature T and the flux Q, we also proposed an ARMA model:

$$Q(t) = -\sum_{i=1}^{n} c_i\, Q(t-i) + \sum_{j=0}^{m} d_j\, T(t-j) \tag{4.12}$$

where $c_i\ \{i = 1 \cdots n\}$ and $d_j\ \{j = 0 \cdots m\}$ are the model parameters to be identified.

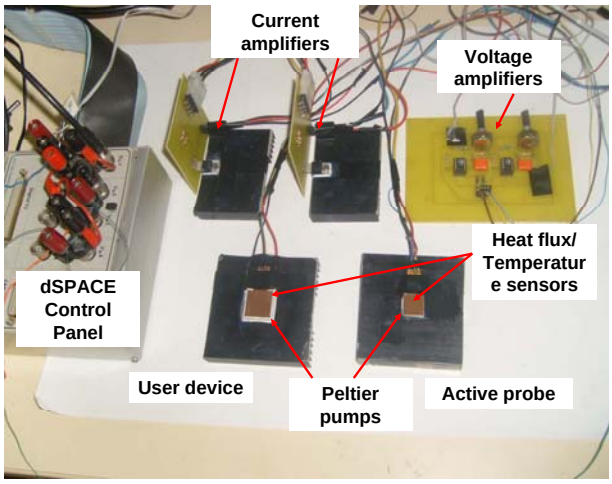

Figure 4.3: Master/slave thermal teleoperator site.

4.2.3.1 Experimental Setup

Figure 4.3 shows the experimental setup of the thermal teleoperator system. The master and the slave parts consist of a contact pad using one TEM from MELCOR Corp^{TM} of dimension 15mm×15mm×3.2mm. Each TEM is closed up to a dissipater with high thermal conductivity in one face, and to the flux sensor (with a sensitivity

of 1.24 $[\mu v/W/m^2]$) that incorporates a T-type thermocouple (with a sensitivity of 39 $\mu v/K$), on the other face.

From a performance standpoint, a thermocouple measurement is stable over time. Also, computing the temperature from thermocouple voltage is a straightforward one-step calculation.

With flux measurements, having good thermal contact between the flux sensor and the surrounding material is critical to achieving this goal. Without good thermal contact heat flow is disrupted. This causes some heat to flow around the sensor instead of through it, biasing the measurement. Therefore, the elimination of the air gaps around the sensor is the most common precaution that must be taken to maintain good thermal contact. For that reason, a silicone grease is used in order to decrease the contact resistance at the contact surface of the TEM.

Current amplifiers are used for driving the TEMs. Voltage amplifiers are used for the flux/temperature sensors signals; sensors measure the current provided to each device. In order to reduce the sensors sensibility to noises, the measured temperature and flux signals are filtered using a $2nd$-order low-pass digital filter. The system is controlled in real-time via a dSPACE 1104 Control Setup.

4.2.4 TEM Models Identification

4.2.4.1 Identification of the heating/cooling capacity models

Equations (4.5) and (4.6) can be also rewritten:

$$\begin{cases} P_c = \theta_{c1}T_cI + \theta_{c2}I^2 + \theta_{c3}T_c + \theta_{c4}I + \theta_{c5} = \theta_c^T\varphi_c \\ P_h = \theta_{h1}T_hI + \theta_{h2}I^2 + \theta_{h3}T_h + \theta_{h4}I + \theta_{h5} = \theta_h^T\varphi_h \end{cases} \tag{4.13}$$

with

$$\varphi_{h/c} = \left[T_{h/c}I, I^2, T_{h/c}, I, 1\right]^T$$

being the measure vectors and $\theta_{c/h}$ the unknown vectors.

Models given by equations (4.5) and (4.6) are linear functions of the parameters to be estimated. We propose a similar form for the model to be estimated:

$$\begin{cases} \hat{P}_{h/c} = \hat{\theta}_{h/c}^T\varphi_{h/c} \end{cases} \tag{4.14}$$

Experiment with $N = 14$ and different current values in the interval [−1.5A,+1.5A], has led to a set of measurements (current, temperature and flux) that illustrate the steady-state behavior of the device. The elements of the vectors $\theta_{h/c}$ can be determined by solving the following parametric optimization problem where:

$$\hat{\theta}_{h/c} = \arg\min_{\theta_{h/c}} \left\{ \sum_{t=1}^{N} \left[P_{h/c}(t) - \hat{P}_{h/c}(t) \right]^2 \right\} \tag{4.15}$$

where N denotes the length of the measurement vectors. Using the linear Least Square Method (LSM) we have:

$$\begin{cases} \hat{\theta}_{h/c} = \left(\Phi_{h/c}^T\Phi_{h/c}\right)^{-1}\Phi_{h/c}^T P_{h/c} \end{cases} \tag{4.16}$$

where:

$$\Phi_{h/c} = \left[\varphi_{h/c}(i), \;\; i = 1 \cdots N \right]$$

are measurement matrices. The estimated cooling/heating capacity by the identified model matches the real measurement (see Figure 4.4 and Figure 4.5). The estimated parameters are given in table A.1 of the appendix.

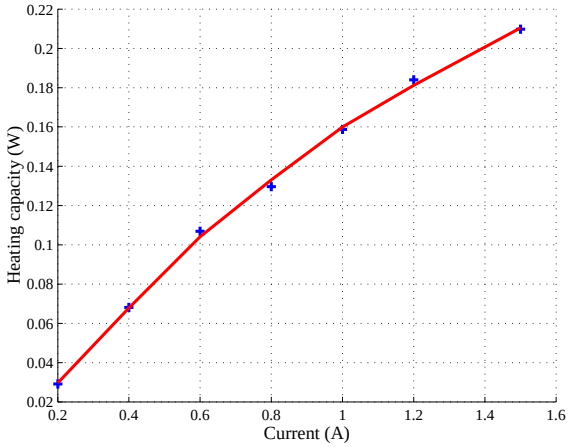

Figure 4.4: Estimated (line) and measured (cross) heat capacity.

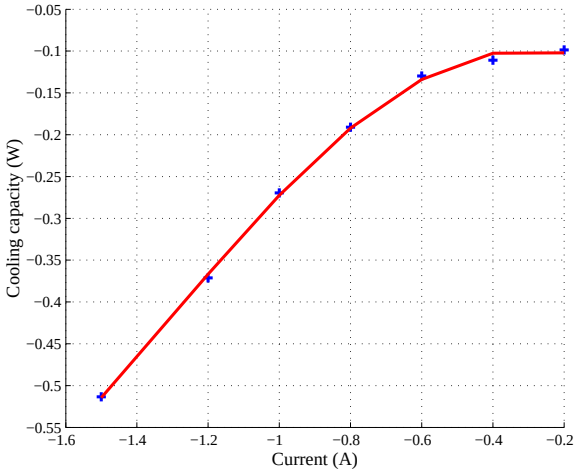

Figure 4.5: Estimated (line) and measured (cross) cooling capacity.

4.2.4.2 Identification of the Temperature Dynamic Model

An open-loop excitation is performed using a Pseudo Random Binary Sequence (PRBS) signal approximating a white noise signal with variable amplitude sampled

at 0.01sec. The same experiment is realized with the two TEMs. The parameters of the model equation (4.10) are determined by solving the following parametric optimization problem:

$$\hat{\theta}_{LS} = \arg\min_{\theta} \left\{ \sum_{t=n}^{M} \left[T(t) - \hat{T}(t) \right]^2 \right\} \tag{4.17}$$

where $\hat{\theta}_{LS}$ and $\hat{T}$ are the estimated parameters and the temperature respectively, $M = 10000$. The LSM algorithm is also used,

$$\hat{\theta}_{LS} = \left(\Phi^T \Phi\right)^{-1} \Phi^T Y$$

where $Y = \{T(t), t = n \cdots M\}$.

The above parametric optimization problem is improved by using the Recursive Least Square Method (RLSM):

$$\hat{\theta}(t) = \hat{\theta}(t-1) + K(t-1)\,\varphi(t)\,\varepsilon(t)$$

$\hat{\theta}(t)$ is the estimated vector at t, $K(t)$ the Kalman matrix gain, and $e(t)$ the estimation error defined as:

$$e(t) = \frac{y(t) - \theta(t-1)\,\varphi(t)}{1 + \varphi(t)^T K(t-1)\,\varphi(t)}$$

The Kalman gain update is computed as follows:

$$K(t) = \frac{1}{\lambda_1}\left[K(t-1) - \frac{K(t-1)\,\varphi(t)\,\varphi(t)^T K(t-1)}{\frac{\lambda_1}{\lambda_2} + \varphi(t)^T K(t-1)\,\varphi(t)} \right]$$

λ_1 and λ_2 are the forget factors, $K(0)$ the initial matrix gain (influences the convergence properties of the algorithm).

Figure 4.6 illustrates the measured TEM temperature compared to the estimated temperature, the identified model is for $n = p = m = q = 3$. In the worst case, the error between real and estimated temperatures reached 0.3°C. The estimated parameters are given in table A.3 of the appendix.

4.2.4.3 Identification of the temperature/flux dynamic model

The measurement sequences performed in the previous section are also used for the identification of the parameters of the temperature/flux model. The LSM algorithm is used to get the optimal solution. Figure 4.7 illustrates the measured TEM flux compared to the estimated one by the identified model with $n = m = 3$. The obtained results show good approximation of the real flux based on the previous measurement of the temperature. In the worst case, the error between the real and estimated flux reached 0.0025W. The estimated parameters are given in table A.2 of the appendix. The TEM can be used as a thermal display acting on the user fingertip or as an active sensor replicating user's finger behavior. The following will concentrate on designing higher level coupling controllers, i.e. those who generate appropriate reference signals to be tracked by the low level controllers.

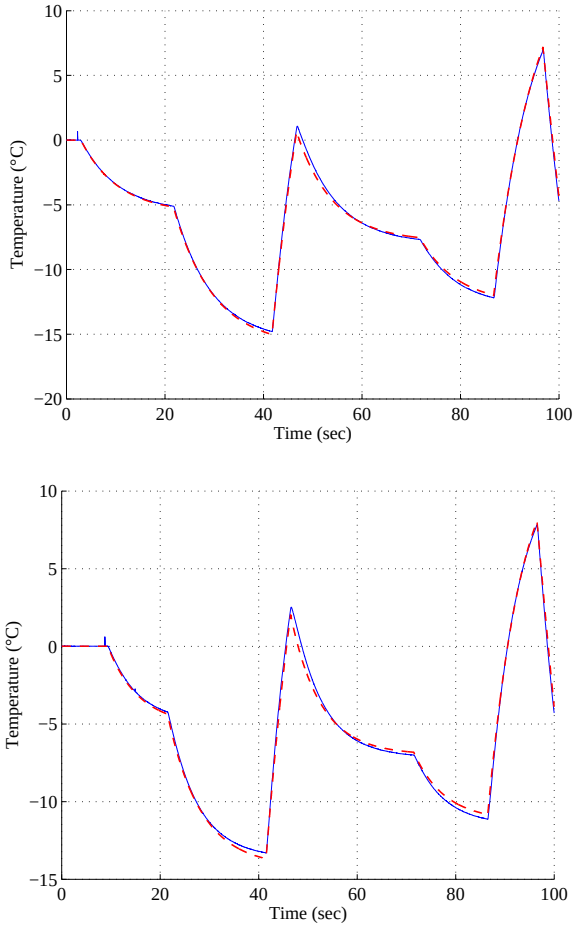

Figure 4.6: Estimated (dashed) and measured (solid) temperature of the TEM I (top) and II (bottom).

4.3 Thermal Feedback Based on Finger-Material Temperature Estimation for Telepresence Applications

4.3.1 Principle of the proposed approach

We propose a thermal feedback based on a new bilateral control scheme between the master side and the slave side of a teleoperator. The temperature evolution of each element of the coupled system is modeled and is identified for both the operator's finger and the remote object. In this control scheme, the slave device is asked to track the estimated temperature of the operator's finger, while the master device is asked to track the estimated temperature of the remote object. The material interface developed is used for thermal rendering and thermal identification of the remote touched object.

In this paragraph, we address the thermal transfer equations between two any

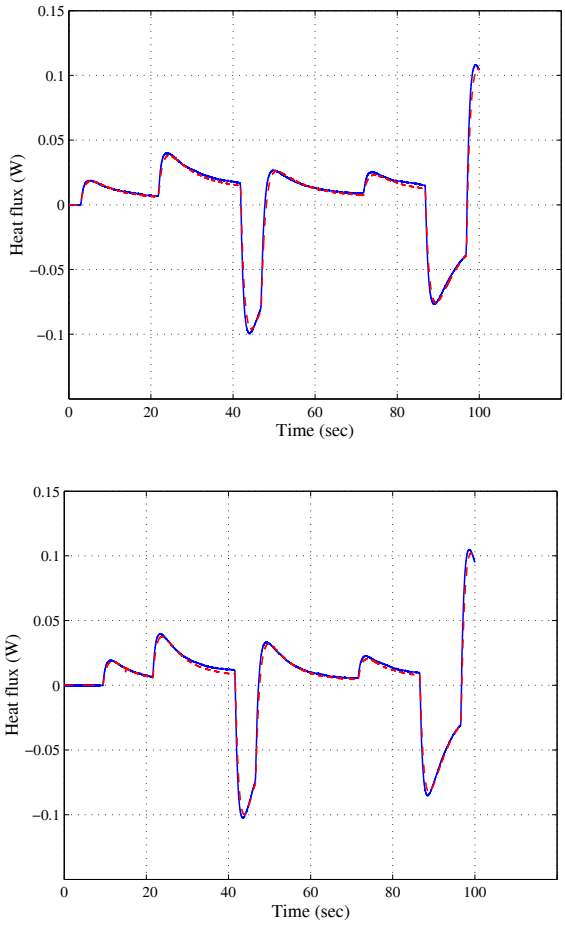

Figure 4.7: Estimated (dashed) and measured (solid) heat's flux of the TEM I (up) and II (bottom).

materials in contact with different thermal properties and initial temperatures. We also present the procedure for the material and finger temperature estimation based on the thermal transfer equations and the experimentally identified TEM models. Then, we address the thermal bilateral coupling scheme between the master and the slave with flux feed-forward control using temperature estimators. Then, we present the experimental results obtained from the implementation of the bilateral controller for different materials and discuss the thermal feedback performances.

In the master system, the TEM is used as a thermal display to stimulate the operator's finger which is controlled according to the estimated temperature and the flux of the touched object. In the slave part, the TEM is used to heat the touched object as a remote probe; it is driven according to the estimated temperature and the flux occurring at the operator's finger, see Figure 4.3. In this way, we ensure a bilateral control between the master and the slave sites that reproduces in a most transparent and stable way the thermal sensations experienced in both sides.

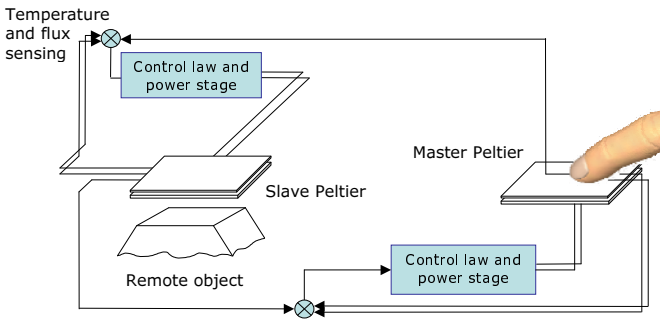

Figure 4.8: Overview of the thermal teleoperator.

4.3.2 Simplified thermal transfer equations

When two objects of different materials with different initial temperatures T_{1i} and T_{2i} respectively placed in contact, Figure 4.9, the temperature evolution during the transient contact phase, for 1D conduction heat transfer process, can be expressed using Fourier's law [Incropera 2006] as follows:

$$\frac{\partial T_k(x,t)}{\partial t} = \alpha_k \frac{\partial^2 T_k(x,t)}{\partial x^2} \tag{4.18}$$

where the index k states for the material 1 and 2, $\alpha_k = \lambda_k/\rho_k c_k$ is the thermal diffusivity, λ_k is the thermal conductivity, ρ_k is the mass density and c_k is the specific heat.

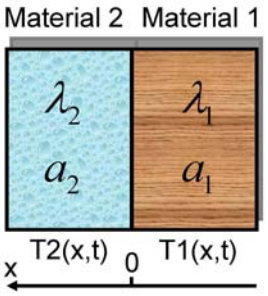

Figure 4.9: Thermal contact modeling.

The initial conditions are:

$$T_1(0,t) = T_{1i} \tag{4.19}$$

$$T_2(0,t) = T_{2i} \tag{4.20}$$

and the boundary conditions are:

$$\lambda_1 \frac{\partial T_1(0,t)}{\partial x} = \lambda_2 \frac{\partial T_2(0,t)}{\partial x} \tag{4.21}$$

$$T_1(0,t) = T_2(0,t) \tag{4.22}$$

A thin temperature and flux sensor is included between the two materials. The sensor is composed of two parallel cooper layers that encapsulates a T-type thermocouple. The sensor has a rectangular form with dimension of 15mm×15mm×420μm, so because of its small thickness, the thermal transfer within the sensor section may be assumed to be linear and homogeneous. The heat transferred will increase the

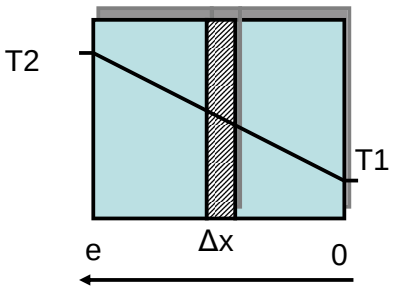

Figure 4.10: Temperature evolution inside the sensor.

temperature of the colder material and decrease that of the warmer material. The quantity of heat Q [W] stored and released by each material is defined by:

$$Q = \rho_k \, v_k c_k \frac{\partial T_k(x,t)}{\partial t} \tag{4.23}$$

where v_k is the volume of the material. The heat transfer at the limit of the contact area is equal along the x axis, $\varphi_x = \varphi_{x+dx}$, and the temperature equation becomes [Carslaw 1959]:

$$\alpha \frac{\partial^2 T(x,t)}{\partial x^2} = 0 \tag{4.24}$$

One general solution is $T(x) = c_1 x + c_2$, with the limit conditions $T_{x=0} = T_1$ and $T_{x=e} = T_2$ where e is the contact area thickness, we have:

$$T(x) = T_1 - \frac{x}{e}(T_1 - T_2) \tag{4.25}$$

The profile of the temperature evolution is linear and depends on the transfer direction x. Since the thermocouple is located at the center of the sensor, its temperature is calculated for $x = e/2$:

$$T_{e/2} = (T_1 + T_2)/2 \tag{4.26}$$

The flux evolution is:

$$Q = \frac{\lambda S(T_1 - T_2)}{e} = \frac{(T_1 - T_2)}{e/\lambda S} \tag{4.27}$$

Making analogy with Ohm's law in electricity, the difference $(T_1 - T_2)$ between two given points in each side, creates a temperature flux Q between these two points. This is equivalent to an electrical potential difference applied to the two ends of a resistance. We call thermal resistance R_{th} the quantity $\frac{e}{\lambda S}$. Under the influence of the temperature difference $(T_1 - T_2)$, the flux increases the temperature of the cold points in the contact area trying to reach equilibrium.

Taking into account the sensor outputs and the TEM identified models, the temperature evolution of the operator and the manipulated remote object, can be observed using the following expression:

$$T^{(h)} = 2\ T^{(m)} - T_p^{(m)} \tag{4.28}$$

$$T^{(r)} = 2\ T^{(s)} - T_p^{(s)} \tag{4.29}$$

where the variable $T_p^{(m,s)}$ state as the estimated temperature of the TEMs using the identified models in equation (4.10), $T^{(m,s)}$ the sensor temperature output and, $T^{(h,r)}$ denote the temperature evolutions observed for both human operator (h) and remote manipulated object (r).

4.3.3 Bilateral controller implementation

4.3.3.1 Temperature control

A typical TEM temperature controller uses a PID function. Although the PID controller is useful, it suffers from a dependence on the ambient temperature condition. The differential term attempts to measure the heating/cooling rate of the TEM to overcome this problem; but being a derivative, it is inherently unstable for fast temperature variations as it is the case of an abrupt contact. The flux sensor used offers an elegant alternative to the differential term because it measures directly the heating/cooling rate in the TEM and does not depend on the thermal ambient conditions and perturbations.

The PID controller function using the flux sensor essentially replaces the derivative term with the sensor output, as follows:

$$u(t) = k_p\ e(t) + k_i \int e(t)\ dt + k_Q\ Q \tag{4.30}$$

where k_p and k_i are respectively the proportional and integral gains, $e(t)$ is the temperature error, and k_Q the flux factor. The use of the flux term effectively predicts where the temperature is going and allows a feed-forward control of the Peltier device [Lartz 1994]. We have also designed and implemented a sliding mode controller based on the proposed TEM's ARMA model (see Appendix C). However, the obtained result shows the presence of the chattering phenomenon. This undesirable behavior induces enormous variations in flux generation that is inherent for

sensation. Therefore, we use only PID controller to control the TEM temperature in our experiments.

4.3.3.2 Bilateral temperature control

We use a temperature/temperature bilateral coupling between the master and the slave with flux feed-forward control as described above. Figure 4.11 shows a general view of the bilateral controller: The control laws for both the master (m) and the

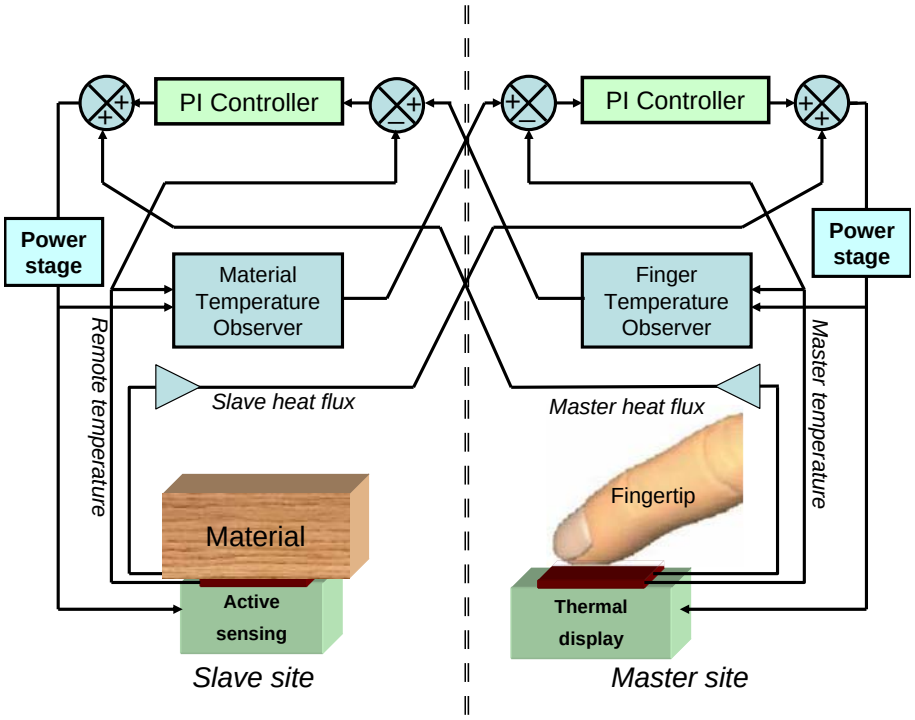

Figure 4.11: Overall bilateral controller of the thermal teleoperator.

slave (s) are defined, in the Laplace domain, as follows:

$$u^{(m)} = \left\{ k_p^{(m)} + \frac{k_i^{(m)}}{s} \right\} (T^{(r)} - T_p^{(m)}) + k_Q^{(m)} \, Q^{(s)} \tag{4.31}$$

$$u^{(s)} = \left\{ k_p^{(s)} + \frac{k_i^{(s)}}{s} \right\} (T^{(h)} - T_p^{(s)}) + k_Q^{(s)} \, Q^{(m)} \tag{4.32}$$

where $u^{(m,s)}$ denote the control output, $T_p^{(m,s)}$ the estimated TEM temperature, $T^{(h,r)}$ denote the estimated temperature for the human operator (h) and the remote object (r) in (4.29) , $Q^{(m,s)}$ is the measured flux, $k_p^{(m,s)}$, $k_i^{(m,s)}$ and $k_Q^{(m,s)}$ are the proportional, the integral and the feed-forward gain factors, respectively.

4.3.3.3 Experimental results and discussion

In this experiment, objects made of aluminum, steel, wood are used as remote objects in contact with the slave part. The surface of the objects is smoothened to reduce roughness and ensure a minimal thermal contact resistance with a constant pressure force. The experimental curves in the case of contact with wood and aluminum blocks are shown on the Figure 4.12. The proposed method gives a good tracking of temperature between the master and the slave parts. The operator is more sensitive to temperature drop and flux changes in the slave part when the contact is established. Note that the same experimental object temperature is reproduced under the operator's finger, which leads to good thermal sensations.

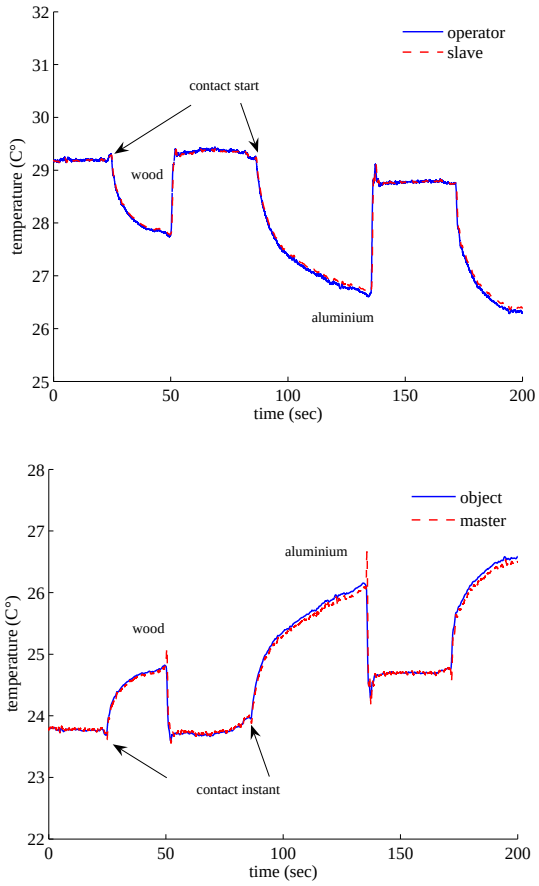

Figure 4.12: Slave Peltier temperature controlled with the estimated finger temperature during consecutive contact (top). Master Peltier temperature controlled with the estimated temperature of touched objects (bottom).

Materials with large thermal conductivity are found to be easier to discriminate compared to object having smaller thermal conductivity, especially in the case of consecutive contact (small or no thermal adaptation of the finger). This demonstrates a satisfactory accordance as in the case of consecutive contact with real

objects. Materials with relatively similar heat conductivity, such as wood and PVC are difficult to distinguish. This is due, from our first trials, to an imperfect contact.

The fact that the master device reproduces the touched material behavior and the slave device reproduces the finger thermal behavior improves the thermal interaction realism so that it improves transparency too.

However, the temperature estimation procedure is influenced by the existence of a thermal resistance between the finger and the thermal display in one side, and between the remote object and the remote probe in the other side due to the imperfect contact conditions. In addition, the thermal dynamic parameters of the finger are to be included in the estimation.

4.4 Thermal Display for Telepresence based on Neural Identification and Heat Flux Generation

To overcome the lack of information concerning the finger properties and the contact conditions evoked in the previous section, we propose a new approach based on a learning technique for thermal rendering in telepresence which improves transparency; it aims at reaching, as closely as possible, what is experienced in similar direct touch conditions. This technique reproduces, in a more realistic way, the thermal interaction that occurs when a finger of an operator touches a remote or virtual object.

First, a set of experiments is performed using different materials characterized by their dissimilar thermal properties. This set of experiments consists of a Peltier pump as a heat sink. Then, by creating a temperature gradient between the heat sink and the materials, we record the flux that occurs during contact. Each experiment is repeated several times. Based on this set of experiment, we built a database whose purpose is used to train and validate a material identifier module. The material recognition is performed using principal component analysis (PCA) combined to a feed-forward neural network (FNN); its role is to identify which material is actually in contact with the heat sink. Another set of experiments is performed to record the heat exchange behavior resulting from a human bare finger touching the materials used in the first set of experiments. Several persons were asked to participate in this set of experiments. The flux evolution during contact is recorded for each person and each material. Collected data (the database) is used to train a set of FNN. This set of FNN would act as a model predictor bloc that produces the resulting flux created in such realistic situations.

The last set of experiments consists of evaluating the overall thermal telepresence system. The remotely probed material is identified thanks to the trained material identifier module. Then, based on the predictive model carried out, the desired flux is generated and conveyed concurrently to (i) the thermal display controller, in order to replicate realistic thermal sensation based on flux control and to (ii) the local thermal remote probe (i.e., active sensor) controller, in order to replicate the human finger thermal influence on the probed object's surface..

4.4.1 Proposed thermal telepresence controller

Thermal telepresence using bilateral coupling is an efficient method that has proved to be simple to implement. Our idea can be stated simply as follows: since it is difficult to design an active thermal probe having intrinsic thermal properties similar to those of any user experiencing the system, we will make use of any active thermal probe to simply identify the material. Then, the bilateral thermal coupling is performed on the predictive behavior of the thermal exchange using signals from the master side as input to the model-based computation of the identified material. In this method, the thermal sensor will have a secondary role but can be kept active to refine the identification of the model or assert the behavior exchange continuously. The output of our method is temperature or flux estimates that are used as desired trajectories for the thermal display controller. To implement this method, we proceed to experimental observation of the heat exchange that occurs when a fingertip touches several objects characterized by different thermal parameters. These objects are used as reference samples. These observations are exploited in order to build a new database by recording the flux and temperature evolution for each material. Another database results from the observation of contact between the material samples and the thermal sensing device. As for humans, thermal perception needs a learning phase to build the knowledge on various materials found in real environments. From this point of view, the observation database is used to train a classifier whose purpose is the identification of the material in the remote side. This process takes place as soon as the material is touched by the remote thermal probe. When the material is identified, model-based signals are produced for both the remote thermal probe and for the thermal display. In addition, the control model uses the initial temperature gap between the operator fingertip and the remote probed material, and information provided by the classifier. Additional sensors are used in order to detect contact and to measure the user's applied forces.

4.4.2 Modeling

As previously stated, when two objects having different materials and/or different initial conditions are put in contact, the temperature's drop –across the contact area (or the interface)– could be significant. This temperature behavior is complex to model precisely; it is however attributed to what is known as the thermal contact resistance. The thermal interaction between the finger and a given touched material is mostly driven by heat conduction phenomenon. According to [Ho 2006b], heat Q is exchanged across the interface by conduction and flows through a thermal contact resistance as follows:

$$Q(t) = \frac{T_{2,i} - T_{1,i}}{R_c} \exp(\alpha_1 \psi^2 t) \mathrm{erfc}\left[\psi\sqrt{\alpha_1 t}\right] \tag{4.33}$$

where ψ is given by:

$$\psi = \frac{1}{\lambda_1}\left[1 + \sqrt{\frac{\beta_1}{\beta_2}}\right]$$

where index ($k = 1$) states for the fingertip and ($k = 2$) states for the material surface, $T_{k,i}$ is the initial temperature, R_c is the thermal contact resistance and $\beta_k = \sqrt{\lambda_k \rho_k c_k}$ is the thermal effusivity.

This equation shows that the flux exchanged, during contact, depends on the thermal properties of both the fingertip and the material. This flux is also proportional to the initial temperature gap between the finger and the material. In our method, thermal data are later normalized by dividing the fluxes by this initial temperature gap.

The existence of a contact resistance is mainly due to surface roughness effects [Incropera 2006]. Therefore, heat transfer is due to conduction across the actual contact area and to conduction and/or convection through other possible interfaces (air). The contact resistance may be lowered by increasing pressure at the contacting area or by selecting an interfacial fluid of large thermal conductivity. Silicone-based thermal greases are attractive because of their ability to fill out completely the interstices with material whose thermal conductivity is as much as 50 times that of the air [Khatri 2001]. Although theories have been developed for predicting R_c [Yovanovich 1982][Yovanovich 1997][Savija 2003][Xu 2005][Ho 2006b], the most reliable results are those obtained experimentally [Defer 1998]. The thermal contact resistance is a function of materials' mechanical, thermophysical, and surface properties. More details are provided is section 4.5.1.

4.4.3 Material Identification and Heat Flux Generation

Two databases are constructed from direct touch experiments: the first one is used to instruct and to validate the material identification module. The second one allows the generation of the desired thermal variables to be tracked by the closed-loop controllers of both devices. Seven different materials are selected. These materials are characterized by different thermal properties and equal volume.

To build the first database, (see Figure4.13), which is used for training the material identification bloc, we made ten tests with each material. At first, the room temperature is measured using infrared thermometer to obtain the initial temperature of the material. Then, the TEM is heated until the temperature reaches 10°C above than that of the samples (this corresponds to the average difference between the temperatures of the fingertip and that of the samples). For each experiment, the flux signal is recorded for one second, starting from the first instance of contact between the pad and the material. Then, the recorded data are filtered. To make this section self-contained, let us recall PCA and FNN basics.

4.4.3.1 PCA Algorithm

Principal Component Analysis (PCA) is a commonly used technique for reducing data dimension and extracting useful information. Let x_i be the recorded data for a sample i, N the size (cardinality) of the learning set, and $M+1$ the length of the

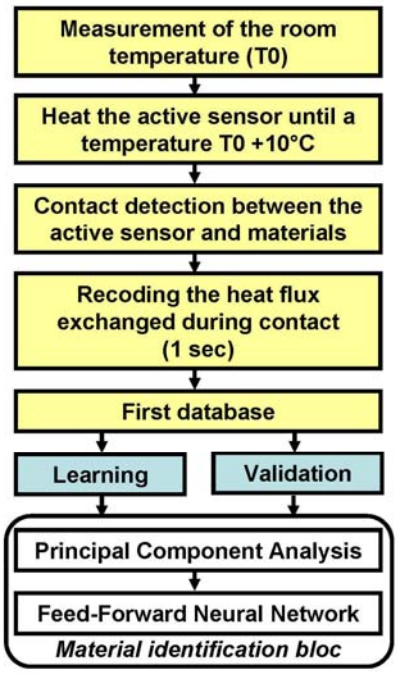

Figure 4.13: First database building for training the material identification bloc.

sampled data. First, the average signal is computed as [Bishop 1995]:

$$x_m(t) = \frac{1}{N}\sum_{i=1}^{N} x_i(t) \quad t = 0, \cdots, M \tag{4.34}$$

then, the average is subtracted from the original data, that is $y_i(t) = x_i(t) - x_m(t)$. The obtained data is prearranged in the following matrix form:

$$Y_{(M+1)\times N}(t) = [y_1(t), \cdots, y_i(t), \cdots, y_N(t)] \quad t = 0 \cdots M \tag{4.35}$$

Let $A = \frac{1}{\sqrt{N}}Y$, we get the new orthogonal base as follows:

$$\phi_i = \frac{1}{\sqrt{\lambda_i}} A \nu_i^T \tag{4.36}$$

where λ_i are the eigenvalues and ν_i are the corresponding eigenvector of the covariance matrix $C = A^T A$. For each measurement, the projection of Y on the base $\Phi = [\phi_1, \cdots, \phi_i, \cdots, \phi_N]$, gives

$$u_i = y_i^T \Phi \tag{4.37}$$

u_i is then the new representation of the sample i.

4.4.3.2 FNN Algorithm

FNN with one hidden layer is used (see Figure 4.14). The number of neurons in the input layer is chosen to be the dimension of the input vector, and the number

of neurons of the output layer is equal to the number of classes (seven). Sigmoid activation functions are used [Hertz 1991][Bishop 1995].

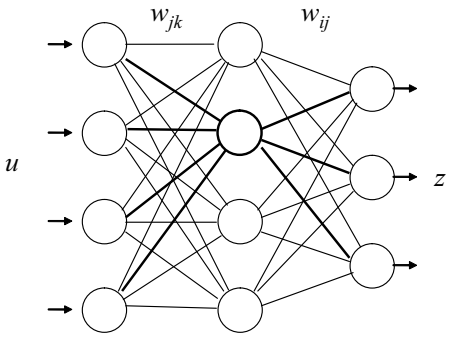

Figure 4.14: Feedforward Neural Network.

The mean squared error criterion determines the size of the error to be back propagated:

$$E = \frac{1}{2N} \sum_{k=1}^{N} \sum_{p=1}^{N_o} \left[d_k^p - z_k^p \right]^2 \tag{4.38}$$

where d_k^p is the desired output for unit k when pattern p is clamped, z_k^p is the actual output and N_o is the number of outputs. The objective during training is to minimise this error by choosing the appropriate weights. In this work, we use the well-known Levenberg-Marquardt rule. The new weight is determined by the learning algorithm as follows:

$$w^{t+1} = w^t - \left(\mathbf{H} + \lambda \mathrm{diag} \left[\mathbf{H} \right] \right)^{-1} \mathbf{J} \varepsilon \left(w^t \right) \tag{4.39}$$

where λ is a positive gain, $\mathbf{J} = \nabla z(t)$ is the Jacobian matrix that contains first derivatives of the network errors with respect to the weights w, $\varepsilon \left(w^t \right) = \left[d(t) - z(t) \right]$ is the error on the previous weights and $\mathbf{H}$ is the Hessian matrix. Using this matrix causes the learning algorithm to converge faster. It is, however, computationally expensive and sometimes even impossible to compute for large neural networks. Therefore, we use the outer products approximation of the Hessian given by $\mathbf{H} = \mathbf{J}\mathbf{J}^T$.

For building the second database, (see Figure 4.15), experiments were performed with five persons. Before each experiment, the temperatures of the index fingertip of the subject and that of the material were measured. Subjects were instructed and trained to keep their index fingertip on the support and to apply a force of 10N approximately at the first instance of contact in order to get a similar contact surface in all cases. The exchanged flux is recorded during 60sec. A sample profile is presented in Figures 4.16 and 4.17. The difference between the flux profiles and the temperature profiles of each material appears clearly. The difference between the flux profiles and the temperature profiles is apparent. Note that the temperature

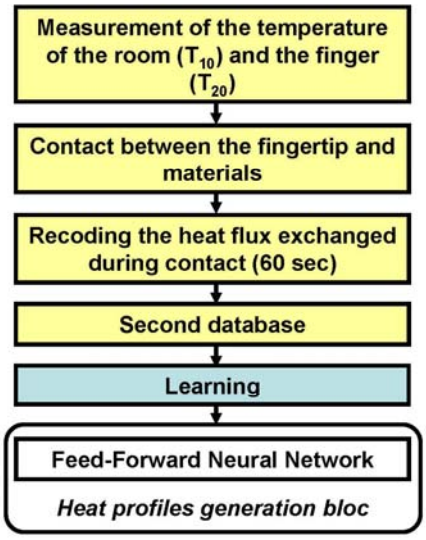

Figure 4.15: Second database building for heat profiles generation bloc.

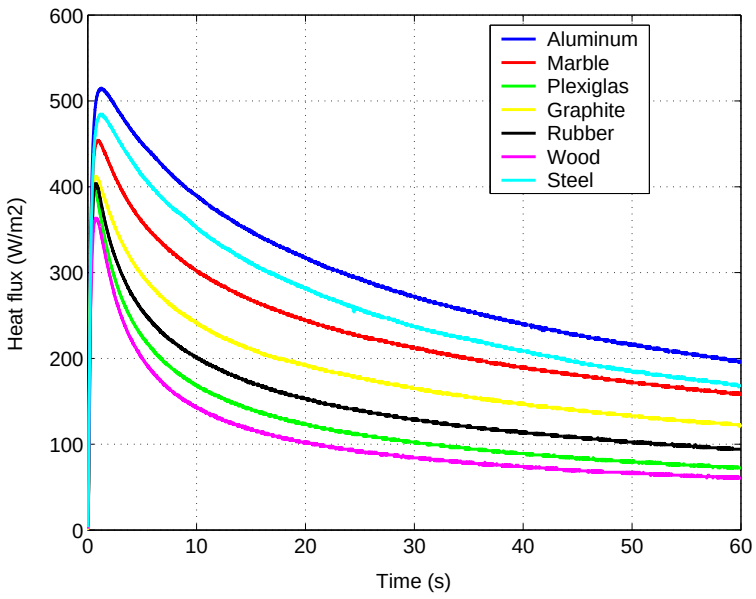

Figure 4.16: Thermal heat flux exchanged during real contact between finger and materials.

variation is conversely proportional to the thermal effusivity of the materials at the opposite of the exchanged flux.

The performance of the classification bloc depends on the time-length allowed for

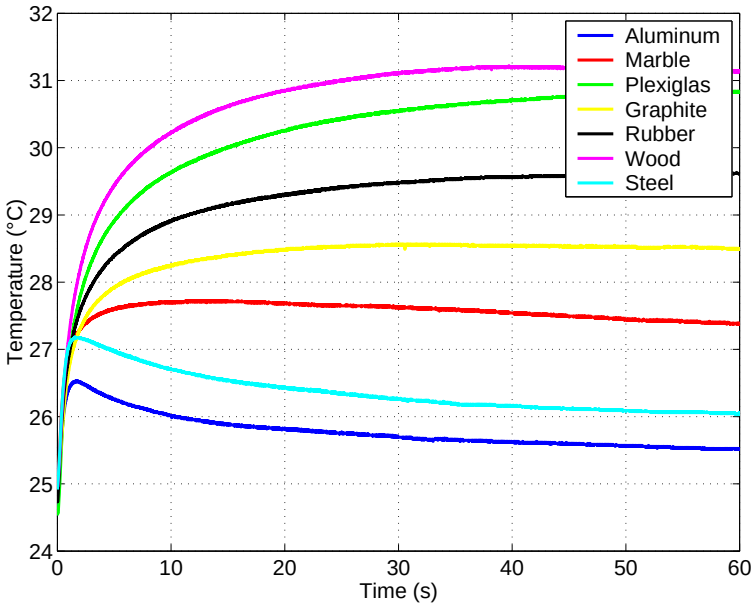

Figure 4.17: Temperature evolution during real contact between finger and materials.

identification processing. For a 1sec sequence, and seven classes, confusion occurs between the aluminum and steel and between graphite and rubber (see table 4.1). This is probably due to their close thermal properties. By gathering the confused materials in two classes, the result is improved though for sequences of 0.75sec 100% of good identification is obtained. However, if the time-length is decreased, the performances deteriorate, (see tables 4.2 and 4.3).

Table 4.1: Validation result with seven classes (1 sec sequence).

	Aluminum	Marble	Plexiglas	Graphite	Rubber	Wood	Steel
Aluminum	xxx						xx
Marble		xxxxx					
Plexiglas			xxxxx				
Graphite				xxx	xx		
Rubber				xx	xxx		
Wood						xxxxx	
Steel							xxxxx

Concerning the second database, for each material, the average data was computed and used to train the FNN module responsible of the flux generation to be used primarily as a reference variable for the thermal display. This choice is made because [Drif 2005] show that rendering flux at the master side has superior transparency and stability performances. We used one FNN with linear output for each material.

Table 4.2: Validation result with five classes (0.25 sec sequence).

	Aluminum-Steel	Marble	Plexiglas	Graphite-Rubber	Wood
Aluminum	xxxxx				
Marble	x	xxx			
Plexiglas			xxx	x	x
Graphite				xxxx	x
Rubber		x		xxxx	
Wood					xxxxx
Steel	xxxxx				

Table 4.3: Validation result with five classes (0.5 sec sequence).

	Aluminum-Steel	Marble	Plexiglas	Graphite-Rubber	Wood
Aluminum	xxxx	x			
Marble	xx	xxx			
Plexiglas			xxxxx		
Graphite				xxxxx	
Rubber				xxxxx	
Wood					xxxxx
Steel	xxxxx				

4.4.4 Result analysis and discussion

The experimental setup is similar to that presented in paragraph 4.2.3.1. A PID controller is used to regulate the flux control loops (Figure 4.18). The parameters of each PID controller are adjusted using the models developed in section 4.2.

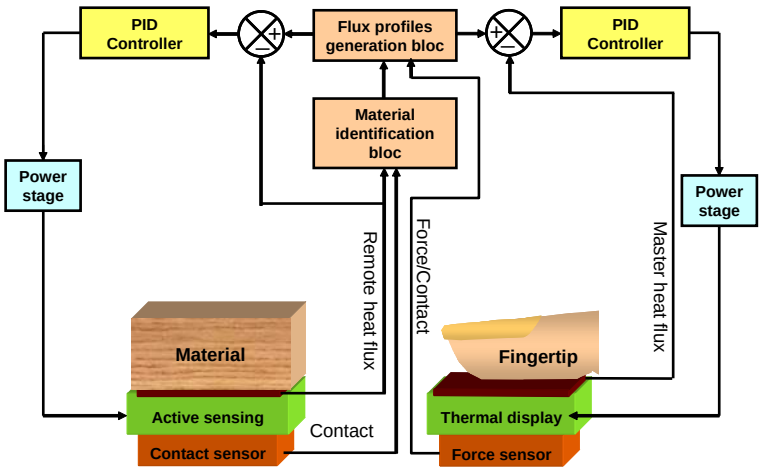

Figure 4.18: Thermal control scheme.

Three experimental scenarios are performed. In all experiments, we use sequences of 1 second for identification, and the seven classes of material used pre-

viously. The three scenarios differ in the manner and the instant the contact is established in the remote and in the user sides.

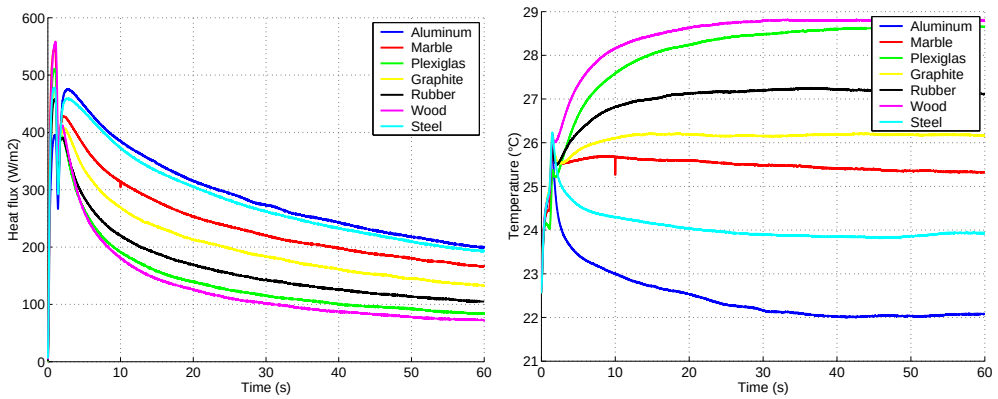

Figure 4.19: Thermal heat flux (left) and temperature (right) exchanged in the user side in the case of scenario 1.

4.4.4.1 Scenario 1

In this scenario the bilateral coupling is triggered once the contact is established at the same time at the user and the telepresence sides. Once the material identification is made, the desired flux is computed and weighted by the initial temperature gap between the finger and the material (this is because the output signal is normalized). The resulting output is sent as a desired state for the inner low-level control loops of both the display and the remote thermal probe Because of the delay needed for material identification, the first impression of contact displayed to the user is induced by thermal intrinsic properties of the display's material, as shown in Figure 4.19, left panel. Although an independent flux control is performed at both sides, the obtained temperature exchange profiles are very similar to those recorded for direct fingertip/material contact, as shown in Figure 4.19, right panel. This scenario is typical in telepresence systems involving encounter-type haptic displays [Kheddar 2004] and using an artificial robotic finger with active thermal behavior as a remote probe.

4.4.4.2 Scenario 2

In order to get rid of the undesirable transient behavior experienced in scenario 1, we implemented a predictive-like scheme. The contact is realized, at first, in the remote side. Following this, the contact is made afterward between the user's fingertip and the thermal display. The thermal desired flux signal is generated from the model-based module. As in scenario 1, the resulting signal is sent to the thermal display and to the thermal probe low-level control loops. In this case, we obtain good reproduction of the flux profiles (see Figure 4.20), from the very first instant of (the user's finger/ display) contact. Indeed, the latency experienced in scenario 1 is compensated for by the prior predictive contact established in the remote side. This

procedure is typical to virtual reality telepresence applications since virtual objects' thermal properties are known prior to establishing the virtual contact [Citérin 2006]. Indeed, by using any proximity-distance algorithm, we can set a distance threshold from which the object is identified as nearly being touched. This method can also be used in teleoperation setups where an intermediary representation is allowed [Kheddar 2001]. A problem however arises for its applicability in direct bilateral coupling teleoperation. First, it is not easy to decide the amount and the direction of the position shift between the master device and the slave probe. Assuming this problem is solved, if force feedback is also provided concurrently with thermal feedback, it is not stable to achieve force feedback with a predictive shift on the motion, unless compliance is embedded in the remote site.

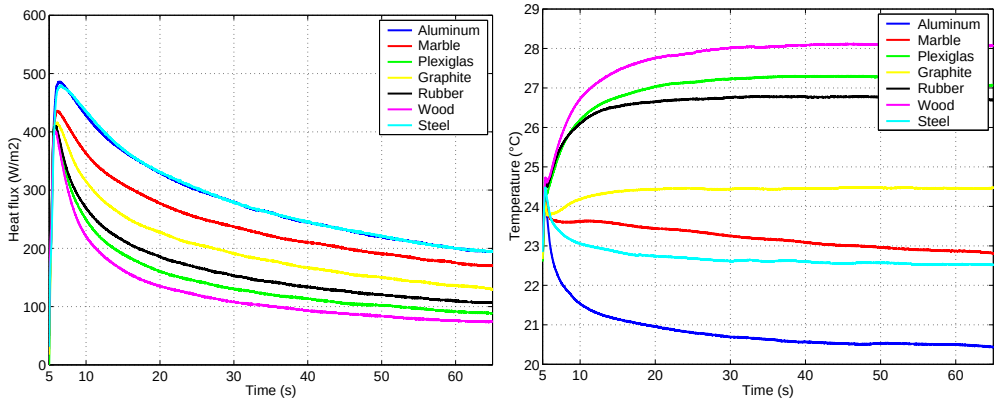

Figure 4.20: Thermal heat flux (left) and temperature (right) exchanged in the master side in the case of scenario 2.

4.4.4.3 Scenario 3

In this case study, the user fingertip is maintained the entire time in contact with the thermal display. When the contact is detected between the material and the sensing probe, a thermal feedback signal is generated in that is similar to the two previous scenarios. (see Figure 4.21). This situation is typical in wearable master devices where the fingers of the operator are always in contact with the device (e.g., a glove or a force feedback handle).

In all cases, the flux is reproduced accurately. Notice that the obtained temperature profiles are very similar to those recorded during direct contact. This result shows that we have an interaction that is close to what has been observed and recorded during direct contact.

4.4.5 Transient response comparison

Table 4.4 illustrates a signal-comparison between transient temperatures and fluxes occurring at the user side (i.e., recorded at the display/finger interaction) during the first instants of contact (the first 5 s of contact) in the cases of the direct contact

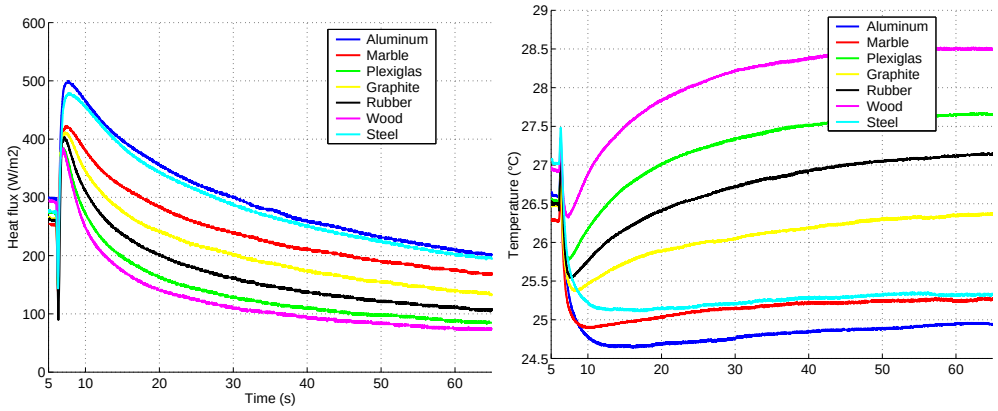

Figure 4.21: Thermal heat flux (left) and temperature (right) exchanged in the master side in the case of scenario 3.

and the three scenarios. By comparing profiles, it is apparent that the order of magnitude of signals is always kept in direct contact and in all the three scenarios. Moreover, this holds for both temperature and flux. The difference between profiles is, however, observed in (i) the transition from initial situation to contact situation, and in (ii) the magnitude of signals. This is due to the difference in initial conditions, including the inescapable individual variation of each experiment, which cannot be kept exactly the same by the very nature of the investigation.

In summary, to reproduce realistic thermal sensations, we have proposed a new approach based on a neural-network learning technique. It uses record-and-replay signals obtained from real measurements of thermal flux exchanged during contact between operator's finger and several materials with dissimilar thermal properties. This technique avoids having to determine the thermal contact resistance, which is known to be extremely difficult to measure or compute.

The identification of the material on the remote side allows the generation of model-based flux references. The rate of good classification depends on the length of the temporal sequence used for learning and/or for validation. The performance of the rendering depends on the instant and on the type of contact. Also, the constructed databases may be used for studying the evolution of the contact flux and for determinating the thermal parameters of the touched object.

To validate this approach, an experimental setup was realized and a set of experiments was performed. The obtained results demonstrate a clear improvement of the thermal rendering when manipulating virtual or remote object via haptic interfaces.

One challenging issue to be investigated is rapid identification of objects' material intrinsic thermal properties together with the thermal resistance from an instant abrupt contact and without prior training or classification. This identification will then be used in either a classical thermal bilateral coupling scheme or as a more generic preview model that can interpolate intrinsic properties from a few learned models and a brief instant thermal exchange behavior. In robotics, these methods

Table 4.4: Temperature and flux evolution during the five first second of contact.

Temperature	Flux
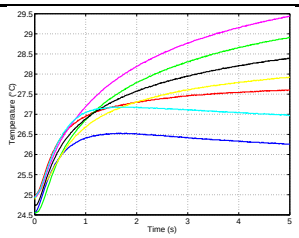	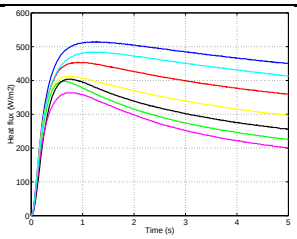
Recorded	
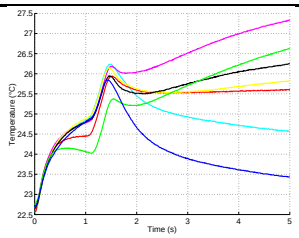	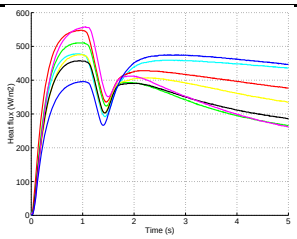
Scenario 1	
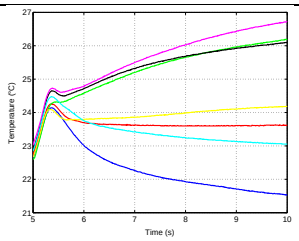	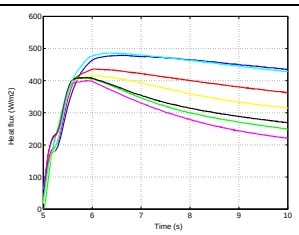
Scenario 2	
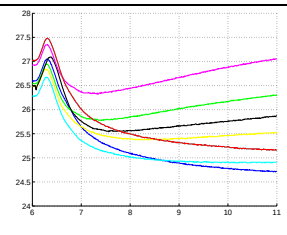	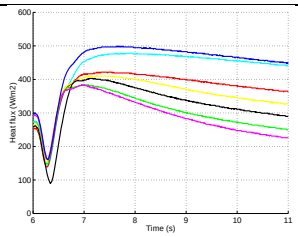
Scenario 3	

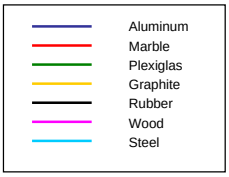

could apply perfectly in various ways; for example, thermal identification could be combined with vision for fast object recognition and material identification from active touch or during grasping. Such an approach would be useful and perfectly applicable for any medical purposes that call for thermal sensing either through a

direct touch or via a tool. Real MIS using a robotic system is an example as it will be addressed in chapter 5

4.5 Heat Transfer Model for Thermal Feedback in Virtual Environments

The results obtained in the last section show the existence of a latency in flux and temperature profiles, which is due to the time needed for the material recognition process in the slave side.

In this section, we perform a theoretical and experimental study of a more general model describing the heat transfer that occurs when a finger touches an object. Models of the heat exchange are developed and implemented on a thermal display incorporated to a haptic device. This model accounts for the thermal dynamics of the finger, the sensor and the material by considering their thermal properties. Experimental results validating the proposed thermal model are evaluated when touching virtual objects in virtual environments. The developed interface is used for thermal rendering and thermal identification of virtual touched object.

We use a sensorized TEM as a thermal display to stimulate the operator's finger. In addition, a force sensor is introduced in order to measure the force applied by the operator's finger.

4.5.1 Thermal Interaction Modeling

The quantitative characterization of heat transfer, in general, and that of the conduction heat transfer, in particular, relies on the evaluation of the heat-transfer rate.

When three objects made of different materials with different initial temperatures $T_{1,i}$ and $T_{2,i} = T_{3,i}$, respectively, are made in contact, Figure 4.22, the temperature evolution during the transient contact phase can be expressed using (4.18). Here, subscribes 1, 2 and 3 denote, respectively, the operator's finger, the sensor and the material.

Mathematically, the macroscopic diffusion equation of heat transfer is a partial differential equation, in space and time. Consequently, the heat transfer problem is a well-posed problem in the Hadamard sense, that is, there exists a solution, which is unique and depends continuously on the boundary conditions if consistent initial conditions (ICs) and boundary conditions (BCs) for the temperature are prescribed and if the heat-source definitions are specified [Marghitu 2001] under the hypothesis of semi-infinite body for both the finger and the material:

$$\lambda_1 \frac{\partial T_1(0,t)}{\partial x} = \lambda_2 \frac{\partial T_2(0,t)}{\partial x} \tag{4.40}$$

$$\lambda_1 \frac{\partial T_1(0,t)}{\partial x} = h\ \left(T_1(0,t) - T_2(0,t)\right) \tag{4.41}$$

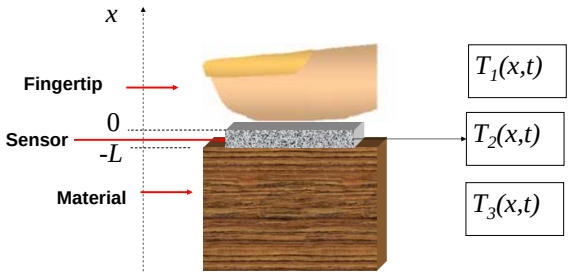

Figure 4.22: Three-layer modeling.

$$\lambda_2 \frac{\partial T_2(-L,t)}{\partial x} = \lambda_3 \frac{\partial T_3(-L,t)}{\partial x} \tag{4.42}$$

$$T_2(-L,t) = T_3(-L,t) \tag{4.43}$$

L represents the thickness of the sensor and $h = 1/R_c$ represents the inverse of the thermal contact resistance.
An important concept introduced through (4.41), is the contact thermal resistance. This type of thermal resistance is common to all technical applications and it is due to the real, imperfect, mechanical contact between the two parts of a composite structure. The heat transfer is then accompanied by a supplementary temperature drop at these interface levels, by combined convection and/or radiation transfer.

By replacing $\tilde{T}_k = T_k - T_{k,i}$, introducing the Laplace transform in (4.18) gives:

$$\frac{\partial^2 \theta_k(x,s)}{\partial x^2} = \frac{s}{\alpha_k} \theta_k(x,s) \tag{4.44}$$

where $\theta_k(x,s)$ represents the Laplace transform of $\tilde{T}_k(x,s)$ for $k = 1, 2$ and 3, s is the common Laplace variable. A trivial general solution is to take:

$$\theta_1(x,s) = A_1 \exp(-p_1 x) + B_1 \exp(p_1 x) \quad , \quad x \geq 0 \tag{4.45}$$

$$\theta_2(x,s) = A_2 \exp(-p_2 x) + B_2 \exp(p_2 x) \quad , \quad -L \leq x \leq 0 \tag{4.46}$$

$$\theta_3(x,s) = A_3 \exp(-p_3 x) + B_3 \exp(p_3 x) \quad , \quad x \leq -L \tag{4.47}$$

Where: $p_1 = \sqrt{\frac{s}{\alpha_1}}$, $p_2 = \sqrt{\frac{s}{\alpha_2}}$, $p_3 = \sqrt{\frac{s}{\alpha_3}}$, A_1, B_1, A_2, B_2, A_3, B_3 are to be computed. The temperature T_1 gets a finite value when x tends toward $+\infty$ and the temperature T_3 gets a finite value when x tends toward $-\infty$. So that: $B_1 = 0$ and $A_3 = 0$.

The Laplace transform of (4.40), (4.41), (4.42) and (4.43) gives:

$$\begin{cases} \lambda_1 p_1 A_1 - \lambda_2 p_2 A_2 + \lambda_2 p_2 B_2 = 0 \\ (h\ + \lambda_1 p_1) A_1 - \quad hA_2 - hB_2 = h\frac{T_{i2}-T_{i1}}{s} \\ \lambda_2 p_2 \exp(Lp_2) A_2 - \lambda_2 p_2 \exp(-Lp_2) B_2 + \lambda_3 p_3 \exp(-Lp_3) B_3 = 0 \\ \exp(Lp_2) A_2 + \exp(-Lp_2) B_2 - \exp(-Lp_3) B_3 = 0 \end{cases} \tag{4.48}$$

The resolution of that system leads to:

$$A_1 = \frac{\left(A_{10} + A_{11} \exp\left(-2L\sqrt{\frac{s}{\alpha_2}}\right)\right)}{s\left(C_1 + C_2 \exp\left(-2L\sqrt{\frac{s}{\alpha_2}}\right)\right)} \tag{4.49}$$

$$A_2 = \frac{A_{20} \exp\left(-2L\sqrt{\frac{s}{\alpha_2}}\right)}{s\left(C_1 + C_2 \exp\left(-2L\sqrt{\frac{s}{\alpha_2}}\right)\right)} \tag{4.50}$$

$$B_2 = \frac{B_{20}}{s\left(C_1 + C_2 \exp\left(-2L\sqrt{\frac{s}{\alpha_2}}\right)\right)} \tag{4.51}$$

$$B_3 = \frac{\left(B_{30} \exp\left(-3L\sqrt{\frac{s}{\alpha_2}}\right) + B_{31} \exp\left(L\sqrt{\frac{s}{\alpha_2}}\right)\right)}{s\left(C_1 + C_2 \exp\left(-2L\sqrt{\frac{s}{\alpha_2}}\right)\right)} \tag{4.52}$$

$$\theta_1(x,s) = \frac{A_{10} \exp\left(-x\sqrt{\frac{s}{\alpha_2}}\right) + A_{11} \exp\left(-\left(\frac{2L}{\sqrt{\alpha_2}} + \frac{x}{\sqrt{\alpha_1}}\right)\sqrt{s}\right)}{s\left(C_1 + C_2 e^{-2L\sqrt{\frac{s}{\alpha_2}}}\right)} \tag{4.53}$$

$$\theta_2(x,s) = \frac{A_{20} \exp\left(-(2L+x)\sqrt{\frac{s}{\alpha_2}}\right) + B_{20} \exp\left(x\sqrt{\frac{s}{\alpha_2}}\right)}{s\left(C_1 + C_2 \exp\left(-2L\sqrt{\frac{s}{\alpha_2}}\right)\right)} \tag{4.54}$$

$$\theta_3(x,s) = \frac{B_{30} \exp\left(\left(\frac{x}{\sqrt{\alpha_3}} - \frac{3L}{\sqrt{\alpha_2}}\right)\sqrt{s}\right) + B_{31} \exp\left(\left(\frac{x}{\sqrt{\alpha_3}} + \frac{L}{\sqrt{\alpha_2}}\right)\sqrt{s}\right)}{s\left(C_1 + C_2 \exp\left(-2L\sqrt{\frac{s}{\alpha_2}}\right)\right)} \tag{4.55}$$

where:

$$A_{10} = h\beta_2 (T_{2,i} - T_{1,i})(\beta_3 + \beta_2)$$

$$A_{11} = h\beta_2 (T_{2,i} - T_{1,i})(\beta_3 - \beta_2)$$

$$A_{20} = \beta_1 h (T_{2,i} - T_{2,i})(\beta_3 - \beta_2)$$

Table 4.5: Thermal properties of candidate materials.

	Thermal conductivity	Mass density	Specific heat	Diffusivity	Effusivity
	$(W/m.K)$	(Kg/m^3)	$(J/Kg.K)$	(m^2/s)	$(W/\sqrt{s}.m^2.K)$
Aluminum	238	2700	917	9.61e-005	24274
Plexiglas	0.19	1190	1465	1.09e-007	575
Rubber	0.28	2010	1100	1.27e-007	787
Wood	0.23	675	3156	1.08e-007	700
Steel	52	7870	447	1.48e-005	13525

$$B_{20} = h\beta_1 \left(\beta_3 + \beta_2\right) \left(T_{1,i} - T_{2,i}\right)$$

$$B_{30} = \frac{h\beta_1\beta_2}{\beta_3} \left(\beta_3 - \beta_2\right) \left(T_{1,i} - T_{2,i}\right)$$

$$B_{31} = \frac{h\beta_1\beta_2}{\beta_3} \left(\beta_3 + \beta_2\right) \left(T_{1,i} - T_{2,i}\right)$$

$$C_1 = \left(h\left(\beta_1 + \beta_2\right) + \beta_1\beta_2\sqrt{s}\right)\left(\beta_3 + \beta_2\right)$$

$$C_2 = \left(h\left(\beta_2 - \beta_1\right) + \beta_1\beta_2\sqrt{s}\right)\left(\beta_3 - \beta_2\right)$$

Sight the complexity of the resulting function, the inverse Laplace transform of the function is calculated numerically using the simple precision Stehfest method $(N = 10)$ [Stehfest 1970].

$$T_k\left(x,t\right) = \frac{\ln\left(2\right)}{t} \sum_{j=1}^{N} V_j \theta_k \left(x, \frac{j\ln\left(2\right)}{t}\right) + T_{k,i} \tag{4.56}$$

where:
$V = [0.083333, \ -32.083333, \ 1279.000076, \ -15623.666890, \ 84244.169460, \ -236957.512900,$
$375911.692300, \ -340071.692300, \ 164062.512800, \ -32812.502560];$

4.5.2 Determination of the thermal contact resistance and the thermal properties of the sensor

In this experiment, we selected five materials from the those presented in section4.3: Aluminum, Plexiglas, Rubber, Wood and Steel. These materials have known thermal properties, (see table 4.5).

In this experiment, we use the recorded data presented in Figure4.17 for $T_{1,i} = 36^oC$ and $T_{2,i} = 24.5^oC$. The thermal properties of the sensor and the thermal contact resistance are computed using a Least Square Criterion and the Newton

Table 4.6: Thermal contact resistance of candidate materials

Material	*Aluminum*	*Plexiglas*	*Rubber*	*Wood*	*Steel*
Thermal contact resistance $(K.m^2/W)$	0.0013	0.0028	0.0042	0.0011	0.0009

optimization algorithm while the thermal properties of the finger (skin) are: $\lambda = 0.34$, $c = 3340$ and $\rho = 1200$. The computed thermal properties of the sensor are found to be: $\beta_2 = 992(W/\sqrt{s}.m^2.K)$, $\alpha_2 = 1,036\text{e}^{-7}(m^2/s)$. The obtained thermal contact resistances are given in table (4.6).

4.5.3 Including the thermal display to a haptic interface

In order to able including the thermal display to a haptic interface, we use a PHANTOM Omni haptic device coupled to a planar table. The thermal display is incorporated to the mobile part of the planar table, (see Figure 4.23). The PHANTOM device permeating kinesthetic feedback is also used as input device that provides the position of the finger in the 3D space. The mobile part is controlled to track the position XY of the PHANTOM device. A virtual world including virtual material is simulated in order to provide visual rendering. The thermal behavior of each

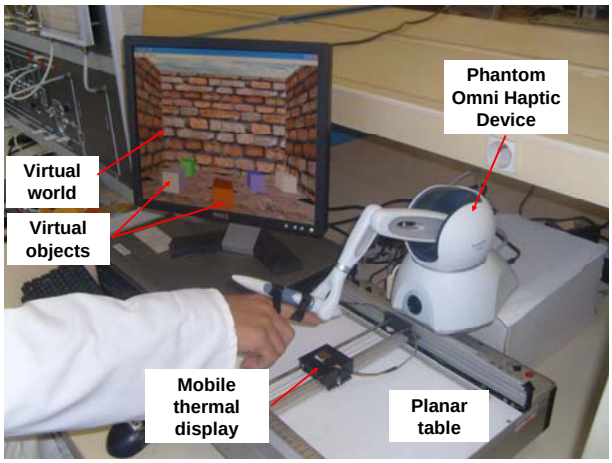

Figure 4.23: Haptic interface including the thermal display.

material is simulated using the model developed in (4.54) and the parameters identified in table 4.6 including the thermal properties of the sensor. The temperature is controlled according to the paragraph (4.3.3.1)) for $x = -L/2$. The simulation algorithm is quite simple: the fingertip's position is given by the PHANTOM (since the finger is attached to its handle) and is sent to the virtual environment. A collision detection algorithm checks for the proximity distance between the virtual finger model and the virtual objects that are used in the experiment. Once a contact is

determined, the touched material is identified and the predicted temperature of the sensor is computed by our model (that is $T_2(t, x)$). This temperature is then sent as a command for the display at the operator's side.

Figure (4.24, right) shows that the temperature profiles are reproduced with accuracy in comparison to Figure (4.17) under the same initial conditions. Note that the same experimental object's temperature is reproduced under the operator's finger.

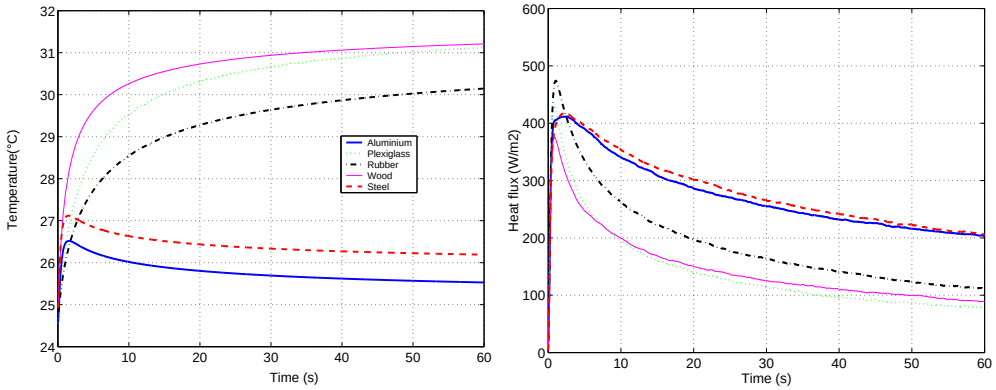

Figure 4.24: Thermal heat flux (left) and temperature (right) exchanged during contact with virtual materials.

However, Figure (4.24, left) shows that the flux profiles are slightly different in amplitude in comparison to Figure (4.16). The reasons have two origins: (i) we did not impose a 10N force to be maintained (which may influences the contact area in the real experiment) and, (ii) the feed-forward controller at the master site is made in a nearly unilateral way and based on temperature servoying. This results are thus in accordance with remarks made in [Drif 2005].

In perceptual term, experiments show that the operator is more sensitive to temperature drop and flux changes when the contact is established. Materials with large thermal conductivity/effusivity (metals) are found to be easier to discriminate compared to object having smaller one, especially in the case of consecutive contact (small or no thermal adaptation of the finger). This demonstrates a satisfactory accordance as in the case of consecutive contact with real object. Materials with relatively similar heat conductivity/effusivity are difficult to be distinguished. The fact that the thermal display reproduces the touched material behavior in contact with the finger, improves the thermal interaction realism.

Results of this section perfectly apply to virtual MIS that make usage of thermal feedback: bare-finger or tool interactions are both possible to simulate with our proposed method.

4.6 Conclusion

In this chapter, we addressed new fundamental approaches for thermal rendering in order to improve the realism while interacting with virtual or remote environments. The thermal display (master side) and the remote probe (slave side) are carried out based on TEMs. So, first we began by a study of the static and dynamic behavior of these devices. We proposed new mathematical models those describe these behaviors. The proposed models have been identified using the LSM and RLSM algorithms and assessed experimentally. They proved to be efficient for analyzing the TEM flux and temperature behavior using linear and non-linear recursive ARMA. Using the identified models of the TEMs, we proposed a new approach for thermal feedback based on the material and finger temperature estimation with flux feed-forward control. The candidates' materials have been selected so that they have dissimilar thermal properties. The rendering scheme used a bilateral coupling law to reproduce, perfectly, the operator and the remote material thermal interaction in order to ensure realistic thermal sensation. The experimental validation of this control scheme has shown that it contributes to the improvement of the thermal sensation in the aimed application. However, the temperature estimation procedure was influenced by the thermal dynamic parameters of the finger and mechanical properties of the contact surface such as the thermal contact resistance. So these parameters had to be included in the estimation.

In order to reduce the difficulties in the determination of the thermal contact resistance and to avoid the use of complex mathematical models, we proposed a learning approach for the thermal bilateral coupling. This new approach is based on a neural network learning technique that uses record-and-replay signals obtained from real measurements of thermal flux exchanged during contact between operator's finger and several materials. To validate this approach, a set of experiments has been performed. The results have shown the ability to discriminate between materials at the user side that improves the thermal sensation. However, we have observed the existence of a latency, which is due to delay needed to identify the material in the remote site. One challenging issue we addressed is fast identification of objects' material intrinsic thermal properties together with the thermal resistance from an instant abrupt contact. This identification would then be used in either a classical thermal bilateral coupling scheme or as a more generic preview model that could interpolate intrinsic properties from few learned models and a brief instant thermal exchange behavior.

We also presented an analytical method representing the temperature evolution when contact occurs between a finger and a material taking into account the influence of the sensor thermal properties and thermal contact resistance. Experiments have shown that the drop of the temperature of the finger depended on the thermal properties of the materials and the initial conditions. The temperature profiles were reproduced perfectly when touching a virtual material so that realistic thermal sensation (from a signal viewpoint) is guaranteed by our developed model and a feed-forward control scheme.

The obtained results encourage the use of the thermal rendering in future works in order to get more realistic sensations when manipulating virtual or remote object via haptic interfaces. We expect that the proposed techniques for thermal feedback would increase the operator's feeling immersion and would assist the operator in material identification. Alternatively, thermal feedback could be used as a sensory substitute or adjunct for visual and/or tactile feedback for surgery applications.

Chapter 5

Multimodal integration experiments

Contents

5.1 Introduction

Previous chapter presented motivation, the design and the control of haptic device dedicated to MIS which role is to track the induced motion subsequent to the interaction between a surgical instrument and the user's hand and then to provide realistic force feedback computed from simulation of MIS procedures. MIS instruments with real handles can be inserted and removed freely, as it is common to use different type of such tools during a real operation. Another important issue of our work deals with the fundamentals of thermal feedback in telepresence and in virtual environment simulations.

The aim of this chapter is to integrate our hardware and methods (including force with thermal feedback) within interactive simulation software. We choose the framework SOFA to achieve this integration. SOFA is an open software platform to

benchmark wide research development in the domain of MIS interactive simulation and which is being developed and maintained by a consortium of well know and established researchers, it is also open for academia. Our contribution to SOFA is in integrating the thermal feedback in the simulation hardware and software using our established models in chapter 4.

In order to investigate the role that can play thermal sensation in surgery, we pooled a simple questionnaire to a group of surgeons, namely: "would the adjunction of a temperature sensor in the tip of the laparoscopic instrument and displaying this temperature on their fingertip could help them take adequate decisions?" More than 50% of them have welcomed the idea and have encouraged the development of such an innovative instrumentation, some others were curious about the initiative. Especially that the lack of haptics in robotic assisted surgery might benefit from this idea. However, the use of thermal cues for organs discrimination is not possible since most tissues and organs have the same temperature and very similar thermo-physical properties. We suggest that the adjunction of a thermal display to the handle may contribute to the creation of a full interaction, with real or simulated organs, when tactile sensation is absent. The force/thermal sensation should help the surgeon in taking appropriate decisions during real or simulated MIS operations. The content of this chapter is rather technical and several issues are yet to be improved prior to investigations on end-users' performance evaluation from usability and teaching quality assessments point-of-views.

5.2 Visual feedback

5.2.1 Visual feedback as a part of surgical simulator

Visual rendering and physically based simulation play an important role in any interactive simulator [Castet 2008] and especially in surgery simulators. This is particularly important in MIS, since by essence minimally invasive means a relatively restrictive opening and access. Endoscopic cameras are generally used to overcome the lack of direct vision of the operation location. Hence, an entire visual feedback of the body using various rendering techniques such as blending and transparency provides the user with a 3D virtual representation of the human organs and anatomy; it is used as a teaching step so that a general view of the context and of what's happening is presented. A restricted virtual rendering similar to that of an endoscopic camera is used to simulate read operation conditions. Physically based simulation, including collision detection and contact force rendering replicates the behavior of the tissues composing the organs of interest in a given MIS simulation. Both representations must be as close as possible to the real situation in order to enhance the simulation realism, yet this is still subject to discussion since reduced representations could also be as efficient as fully 'realistic' ones. Organs behavior is often modeled based on their biomechanical equations, deformation of which is usually simulated using mass-spring models or finite element methods. For the past few years, software toolkits have been designed for medical simula-

tion with the aim of providing an open-source answer to the various challenges of medical simulation research and developments. These toolkits include, for example, the KISMET [Kuhn 1996], VRASS [Baraff 1998], SPRING [Montgomery 2002], CHAI 3D [Conti 2003], GiPSi [Goktekin 2004], SSTML [Bacon 2006], HYSTIM [Tuchschmid 2006], and recently SOFA [Allard 2007][Faure 2007].

5.2.2 The SOFA framework

Our force/thermal integrated haptic device prototype is interfaced with the SOFA framework, which is an open-source C++ library designed for physical simulation, primarily targeted to medical simulation and industry research. Our choice for this platform has been dictated by its source code openness, the availability of the support and the possibility of collaboration with its research and development team.

The main features of SOFA, compared with other toolkits, are its flexibility and modularity. It allows the use of multiple interacting (and at different resolution) models for the same object, typically, a mechanical model with mass and constitutive laws, a collision model with simple geometry, and a visual model with detailed geometry and rendering parameters, see Figure 5.1. Each model can be designed independently from the others in terms of data structure and processing; it is connected to other through data structure interfaces.

In addition, this open-source framework allows independently-developed algorithms to interact within a common simulation. This flexibility allows one to focus on his own domain of competence, while re-using the other's contributions on other topics that reduce the development time required for integration. More details concerning the SOFA framework can be found in (`www.sofa-framework.org`).

5.2.3 Laparoscopic simulation

A laparoscopic graphics simulation system has been developed under SOFA, in which the liver and intestines are modeled as deformable models that can be manipulated using a laparoscopic instrument and that can collide with the ribs, as illustrated in Figure 5.2. The modularity of the SOFA architecture allows us to experiment easily different constitutive models for the organs. For example, the liver is modeled as a finite-element model (FEM) and the intestines as a spring-based grid [Allard 2007][Faure 2007]. The separation between Visual, Collision, and Behavior models allows us to generate visually appealing simulations at interactive rates. Tissue deformations and force feedback are computed at real-time rates and are rendered both visually and haptically to the user. However, some usual phenomenon, such as blood circulation, tissues cutting, welding or suturing, are still under development by the SOFA team.

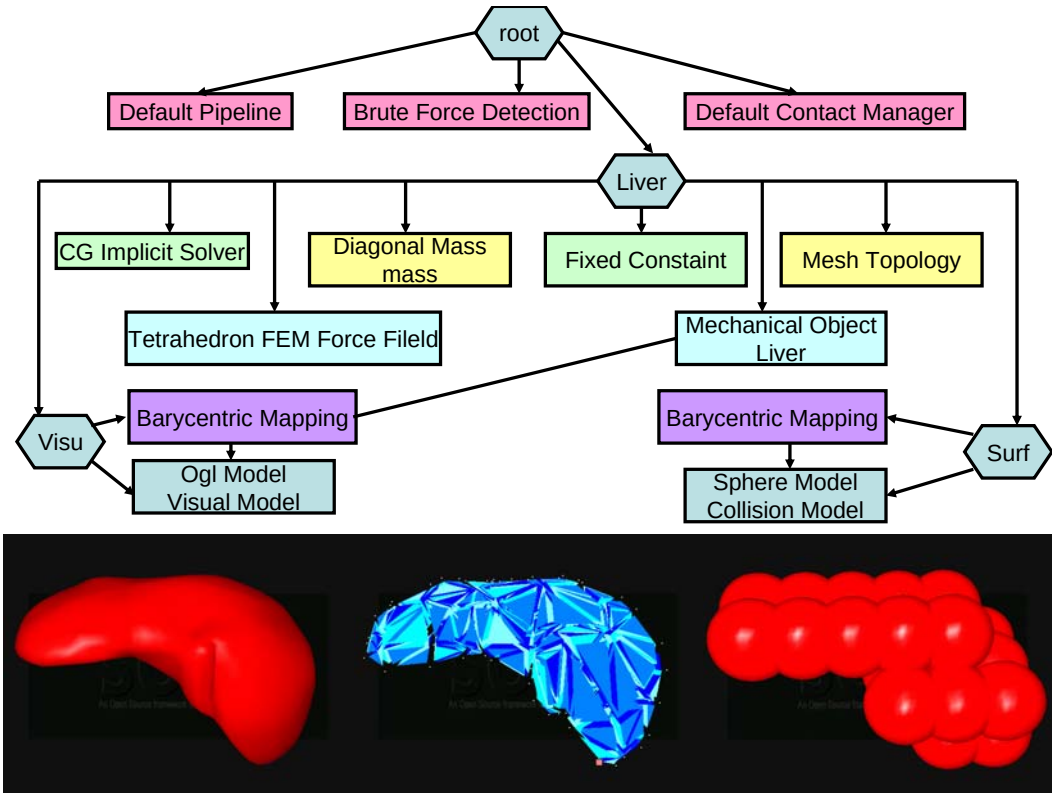

Figure 5.1: SOFA example.

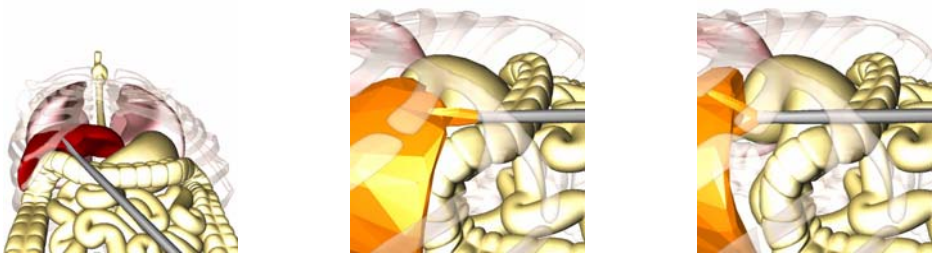

Figure 5.2: Laparoscopic simulation under SOFA framework.

5.3 Force feedback integration

5.3.1 Force propagation model

The force propagation model describes the relationship between the applied torques at the active joints of the haptic device as a function of the calculated force generated through the graphical simulation as shown in Figure 5.3. In general, this relationship can be written as follows:

$$\vec{M} = \vec{P}_C \times \vec{F} \tag{5.1}$$

where $\vec{P}_C = \begin{pmatrix} p_{cx} & p_{cy} & p_{cz} \end{pmatrix}^T$ represents the location of the contact between the surgical tool and the virtual organ and $\vec{F} = \begin{pmatrix} F_x & F_y & F_z \end{pmatrix}^T$ is the generated force due to the pushing or pulling actions, for example. Or, in a general case, through the Jacobian matrix.

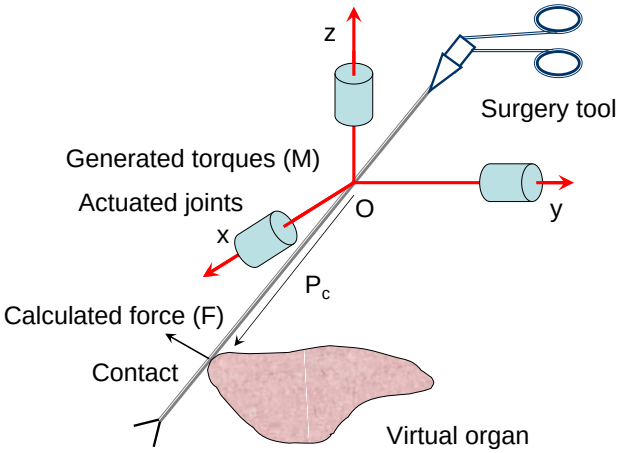

Figure 5.3: Force propagation in the MIS tool.

5.3.2 Haptic control loop

Figure 5.4 is a model of a 1DOF haptic loop system as proposed in [Colgate 1994] and [Colgate 1997]. In this scheme, m represents the mass of the moving part including the actuator rotor and the handle, which behave as a rigid body with viscous friction b, while u is the controller torque. The feedback signal is sampled at the rate T_s, and the control signal is passed through a zero-order hold. The virtual environment is represented by a stable linear, shift-invariant transfer function $H(z)$. According to [Colgate 1997]: "*the necessary and sufficient condition for passivity-based stability of the sampled data system in Fig. 5.4 (without the unilateral constraint) is:*"

$$b > \frac{T_s}{2}\frac{1}{1-\cos\omega T_s}\mathrm{Re}\left\{\left(1-e^{-j\omega T_s}\right)H\left(e^{j\omega T_s}\right)\right\} \quad 0 \leq \omega \leq \omega_N \tag{5.2}$$

where $\omega_N = \pi/T_s$ is the Nyquist frequency.

However, useful virtual environments cannot be composed strictly of linear operators, especially in the case of soft human organs. At the least, it is necessary to include the nonlinear element pictured in Figure 5.4. This nonlinear element, i.e. the unilateral constraint, is omnipresent in the physical world and it need to be accounted for collisions and complex contact models. Design of haptic systems that guarantee stable interaction with nonlinear environments is well discussed

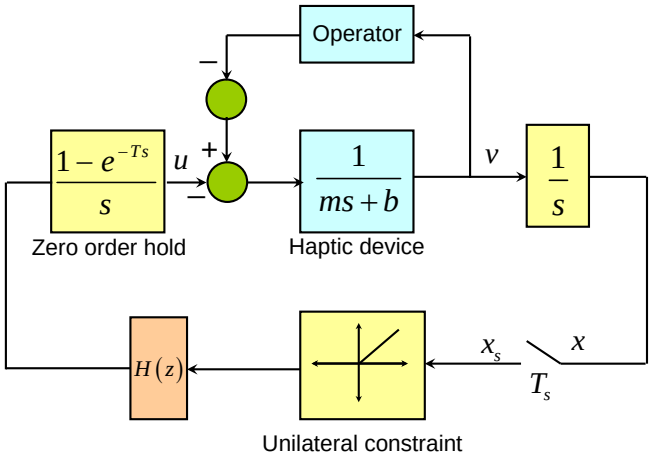

Figure 5.4: 1 DOF Haptic control loop according to [Colgate 1994].

in [Miller 2000].

The haptic device can simulate mechanical impedance, where position/velocity is sent to the VE where eventual contact forces resulting on the manipulated tool are computed and sent back as feedback to constraint the user's motion. It can also simulate mechanical admittance where we acting forces on the haptic device's handle are monitored and sent to the VE where resultant motion of the manipulated tool is computed and sent back as position/velocity feedback to accompany the user's applied forces [Salisbury 2004]. In our application, we used the impedance control scheme in which, position and quaternion rotation of the tool are sent to the simulation where contact forces and moments are computed and forwarded to the haptic device [Henry 2006]. The surgical tool is treated as a volumetric rigid object exchanging forces/torques and positions/rotations with the user.

Several modules compose a typical haptic rendering algorithm, as illustrated in Figure 5.5:

- low-level controller read the haptic device embedded sensors to replicate in real-time desired feedback trajectories (position, velocity, force or any causal combination of them) taking into account stability and transparency at best.

- simple monitoring processes collect user's intention in terms of tool's actions to be transmitted to the virtual reality physically-based engine; these intentions can be derived from the haptic device internal state (actual position, velocity...) or external state (like external applied forces).

- collision or proximity detection algorithms are used detect eventual close contacts or interferences between the virtual representations of the tool and the objects of interest. Depending on the scheme that is used to compute the

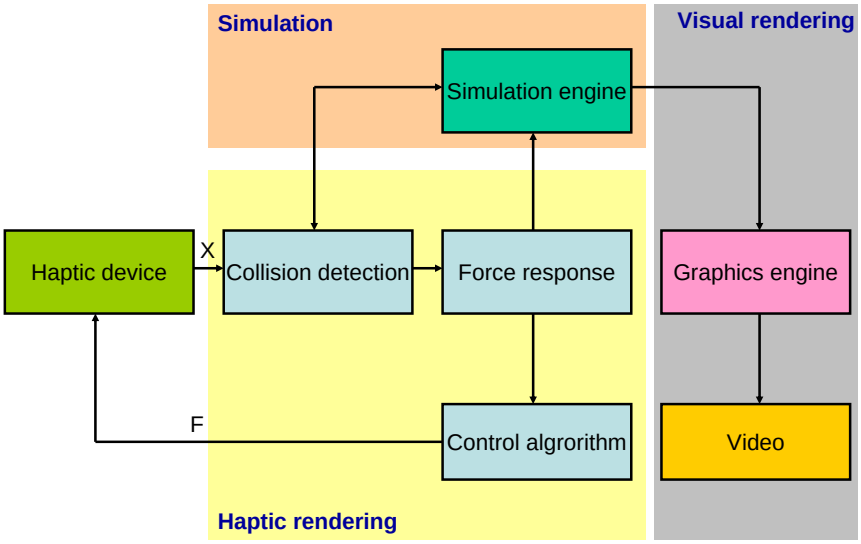

Figure 5.5: Haptic rendering architecture.

contact forces, collision/proximity detection yields information about where, when, and ideally to what extent collisions have occurred.

- computer haptics algorithms compute interaction forces between the tool and virtual objects involved when a collision/proximity is detected. Ideally, computed force approximates as closely as possible the contact forces that would normally arise during real contact. Force-response algorithms operate on the tool position, the position of all objects in the virtual environment, and the collision state between the tool and virtual objects. In our experiments, we used a penalty-based scheme for force feedback computation (see Figures 5.6and 5.7). However, constraint-based method using linear or non-linear complementarity problem (NLCP, LCP) [Duriez 2006] can be also used by simply replacing one component with another, without changing the mass distribution, the collision geometry, the time integration scheme, etc. This is possible thanks to the modularity of SOFA. The returned values are force and torque vectors that are either directly applied to the haptic device or update the virtual tool spatial parameters state from which feedback is derived to the control algorithms. The result is in any case a desired feedback trajectory applied implicitly to the operator through the haptic device inner control loops while maintaining a stable overall behavior.

- the simulation engine computes the effect of the interaction forces on objects in the virtual environment and updates the state of the scene.

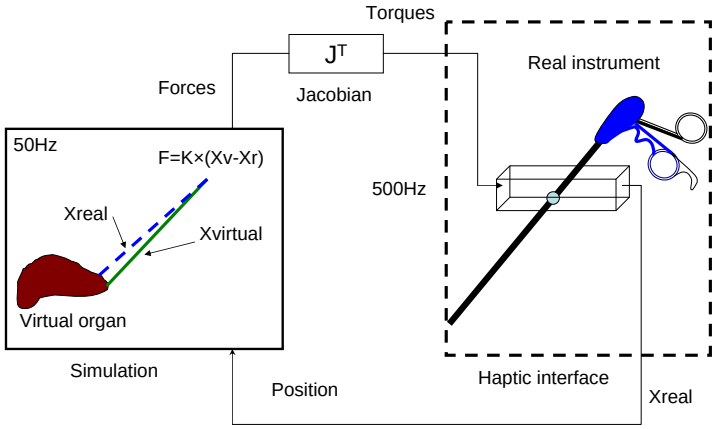

Figure 5.6: Implemented open-loop control scheme.

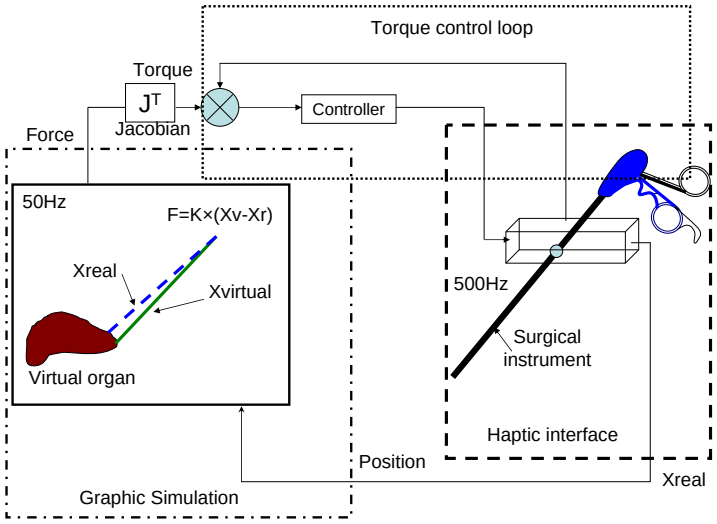

Figure 5.7: Implemented closed-loop control scheme.

Hardware limitations prevent haptic devices from applying the exact force computed by the force-response algorithms to the user when operating in open loop, (see Figure 5.6). However, closed-loop control algorithm command the haptic device according to desired force and torque vectors computed by force response algorithms in such a way that the error between ideal and applicable forces is minimized, (see Figure 5.7). PID controllers are used to command the device torques. The stability of the PID-based control for haptic interface is well discussed in [Zhang 2007].

In our experiments, we only use basic haptic-rendering and force-response algo-

rithms (i.e. those already available with SOFA). The haptic loop is updated every 0.002s (500Hz) while the graphics simulation is updated every 0.02s (50Hz). The synchronization is guaranteed thanks to the use of multi-thread programming. These rates seem to be a subjectively acceptable compromise permitting presentation of complex objects, including multiple-point interaction to grasp and manipulate virtual organs. Therefore, the instrument handle is equipped with an angular sensor (potentiometer) that translates the grasping angle (see Fig. 5.8). Figure 5.9 shows

Figure 5.8: Handle sensorization for grasping angle sensing.

a sample representing the good and high force tracking capability of the assembled prototype.

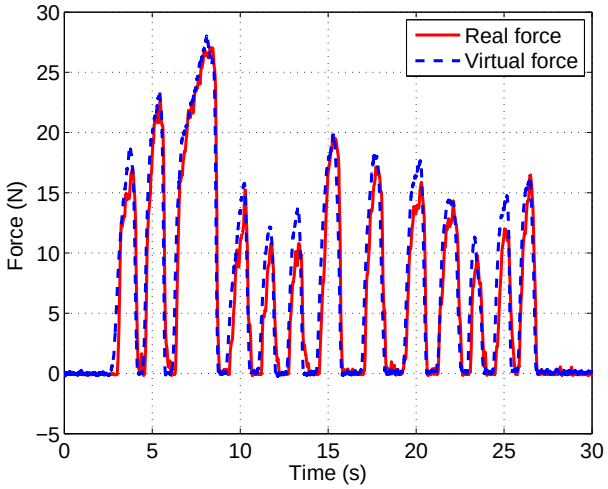

Figure 5.9: Force control example.

5.4 Thermal feedback

5.4.1 Temperature monitoring for therapeutic applications

Knowledge on heat transfer in living tissues has been widely used in medical applications. The applications of the heat transfer model include simulations of hyperthermia [Liu 2000] and cryosurgery, thermal diagnostics [Ng 2004], thermal comfort analysis, thermal parameter estimation [Zhang 2000], burn injury evaluation [Liu 2008] and thermal ablation of tumors.

The ablation is a corrective procedure that involves removal of faulty tissues, can involve abrasion, surgery, or heating energy. Applications include cardiac, endometrial, tumor, bone marrow and brain tissue ablation, as well as roto-ablation to clean blood vessels. Recent developments in interventional imaging have opened a wide range of promising medical applications. For example, several techniques for minimally-invasive percutaneous tumor ablation have been developed; some relying on heating (focused ultrasound, laser or radiofrequency) and some on freezing (cryotherapy) the tissue to kill the cells. Exposure of both normal and cancer cells to heat above 50°C causes the death of cells. With thermal ablation, cells are exposed to temperatures up to 110°C for periods of up to 14 minutes, resulting in cellular destruction [Liu 2008]. Therefore, heat energy must be controlled precisely to prevent undesired healthy tissue damage when using heat to correct the damaged tissue during ablation procedures. In addition, when using laser for tissue welding, controlling the temperature of the target organ can be critical. Laser energy activates tissue bonds between the surgical surfaces, fusing them together. If there is too much heat, the tissue is damaged and poor healing results; but, on the other hand, if there is not enough heat, the bonds do not form.

5.4.2 Temperature sensing for diagnosis

Another possible use of thermal cues in surgery is in the area of diagnosis. The real-time diagnosis of the tissue's pathology would allow the surgeon to choose a suitable therapy. Therefore, minimally invasive diagnosis of the tissue of interest can be obtained by incorporating temperature, biochemical and tactile sensors into surgical tools since it is well known that differences in energy consumption exist for normal and cancerous tissue. So that, researchers are looking into ways to make catheters more intelligent, while retaining their miniscule sizes [Carrozza 2003][Zhao 2008].

Any abnormality in the tissue, such as the presence of a tumor, alters the normal temperature on the tissue surface due to increased metabolic activity of the tumor [Paruch 2007]. Therefore, abnormal tissue temperature profiles are an indication of diseases such as mastitis, benign tumors, fibrocystic breast disease, and cancer [Liu 2000][Ng 2004][Salhab 2005][Mital 2008]. Thermography and infrared imaging has been used in the detection of different types of cancer since the local temperatures of the tissue over a tumor is generally significantly higher (about $2-3$°C) than normal tissue temperatures. According to [Mital 2008], this temperature difference is due to convection effects associated with increased blood perfusion,

and increased metabolism around the tumor. Clinical studies with steerable thermography catheters also showed that the difference of the temperature between normal tissue and a neoplastic area could be a useful criterion in the diagnosis of the malignancy of urinary bladder tumors [Stefanadis 2001] gastric lesions and lung lesions [Stefanadis 2003]. This also shows that embedding thermal sensing within catheters is already possible. For example, a study performed in [Stefanadis 2003] investigated the existence of thermal heterogeneity in bronchial lesions, in vivo, and tested the hypothesis whether there is any thermal distinction between benign and malignant lung lesions. Their analysis showed that, in benign (chronic inflammation) lesions, the mean temperature differences was $0.71 \pm 0.6°\mathrm{C}$, while the temperatures differences in malignant tumors was found to be $1.23 \pm 0.4°\mathrm{C}$. Very similar results have been found in [Zhao 2008] where the authors used a thermocouple needle which has been inserted into the tumor. These investigations show that temperature difference can be a significant marker for the discrimination of the type of malignant or benign tumor.

5.4.3 Modeling heat exchange for surgery simulation

Due to its simplicity and validity, most of the work published so far has been based on the Pennes' Bio Heat Transfer Equation (BHTE). This equation considers the different body tissues as a continuum model and takes into account heat transport by blood perfusion and metabolic heat generation [Arkin 1994][Zhong-Shan 2002][Xu 2008] that makes the behavior of living tissue complex and thermally active. Therefore, the calculations made in the present study are mainly based on the Pennes equation as follows:

$$\rho_{\mathrm{org}} c_{\mathrm{org}} \frac{\partial T_{\mathrm{org}}}{\partial t} = \lambda_{\mathrm{org}} \frac{\partial^2 T_{\mathrm{org}}}{\partial x^2} + \dot{m}_b c_b \left(T_{\mathrm{ar}} - T_{\mathrm{org}}\right) + Q_{\mathrm{org}} \tag{5.3}$$

where ρ_{org}, c_{org}, and λ_{org} are, respectively, the density, the specific heat, and the thermal conductivity of the organ tissue; m_b and c_b denote the blood perfusion rate and the specific heat of blood; in the organ; Q_{org} is the metabolic heat generation; T_{ar} is the arterial blood temperature, x is the positive space variable, t is time and T_{org} is the organ temperature.

5.4.3.1 Model for thermal therapy

The thermal therapy is modeled as a heat source with constant heat flux Φ imposed to the surface of the organ. The following boundary conditions express the principle of heat flux conservation on the surface of the semi-infinite heated organ:

$$\begin{cases} -\lambda_{\mathrm{org}} \frac{\partial T_{\mathrm{org}}(0,t)}{\partial x} = \Phi \\ T_{\mathrm{org}}(x,0) = T_i \\ T_{\mathrm{org}}(\infty,t) = T_i \end{cases} \tag{5.4}$$

Equation (5.3) is rewritten as follows:

$$\frac{\partial T_{\mathrm{org}}}{\partial t} = \alpha_{\mathrm{org}} \frac{\partial^2 T_{\mathrm{org}}}{\partial x^2} - a T_{\mathrm{org}} + a T_{\mathrm{ar}} + b Q_{\mathrm{org}} \tag{5.5}$$

where $a = \frac{\dot{m}c_b}{\rho_{\text{org}}c_{\text{org}}}$ and $b = \frac{1}{\rho_{\text{org}}c_{\text{org}}}$

By replacing $\tilde{T}_{\text{org}} = T_{\text{org}} - T_i$, then (5.5) becomes :

$$\frac{\partial \tilde{T}_{\text{org}}}{\partial t} = \alpha_{\text{org}} \frac{\partial^2 \tilde{T}_{\text{org}}}{\partial x^2} - a\tilde{T}_{\text{org}} + a\left(T_{\text{ar}} - T_i\right) + bQ_{\text{org}} \tag{5.6}$$

By introducing the Laplace transform, (5.6) can be written as follows:

$$s\theta_{\text{org}}(x,s) = \alpha_{\text{org}} \frac{\partial^2 \theta_{\text{org}}(x,s)}{\partial x^2} - a\theta_{\text{org}}(x,s) + \frac{a\left(T_{\text{ar}} - T_i\right) + bQ_{\text{org}}}{s} \tag{5.7}$$

where s represents the Laplace variable. This equation is rewritten as follows:

$$\frac{\partial^2 \theta_{\text{org}}(x,s)}{\partial x^2} - q_{\text{org}}^2 \theta_{\text{org}}(x,s) = -d \tag{5.8}$$

This expression represents a second-order differential equation with second member, where: $c = a\left(\tilde{T}_{\text{ar}} - T_i\right) + bQ_{\text{org}}$, $d = \frac{c}{\alpha_{\text{org}} s}$ and $q_{\text{org}}^2 = \frac{s+a}{\alpha_{\text{org}}}$, α_{org} represents the thermal diffusivity in the organ. The general solution of this equation is a combination of the solution of homogonous equation and a particular solution.
The solution of the homogonous equation is expressed as follows:

$$\theta_{\text{org}}^h(x,s) = A_{\text{org}} \exp\left(-q_{\text{org}}x\right) + B_{\text{org}} \exp\left(q_{\text{org}}x\right) \tag{5.9}$$

where A_{org} and B_{org} are to be calculated. Since the temperature is finite when $x \to +\infty$, then $B_{\text{org}} = 0$.

A trivial particular solution is to take:

$$\theta_{\text{org}}^p(x,s) = \frac{d}{q_{\text{org}}^2} = B \tag{5.10}$$

The general solution is then:

$$\theta_{\text{org}}^g(x,s) = \theta_{\text{org}}^h(x,s) + \theta_{\text{org}}^p(x,s) \tag{5.11}$$

By replacing in (5.4), we get :

$$A_{\text{org}} = \frac{\Phi}{\lambda_{\text{org}} q_{\text{org}} s} \tag{5.12}$$

Therefore, the general solution in the Laplace domain is:

$$\theta_{\text{org}}(x,s) = \frac{c\beta_{\text{org}} + \Phi\sqrt{s+a}\, a\, exp\left(-\sqrt{\frac{s+a}{\alpha_{\text{org}}}}x\right)}{\beta_{\text{org}} s\left(s+a\right)} \tag{5.13}$$

The temporal solution is calculated numerically using the simple-precision Stehfest method ($N = 10$) presented in chapter 4, equation 4.56.

5.4.3.2 Model for temperature-based diagnosis

In this section, we consider a scenario where the surgeon's fingertip with an initial temperature T_{if} palpates an organ that has an initial temperature T_{io}. The temeprature of the organ is governed by (5.3) and the temperature of fingertip is then governed as follows :

$$\rho_{\text{finger}} c_{\text{finger}} \frac{\partial T_{\text{finger}}}{\partial t} = \lambda_{\text{finger}} \frac{\partial^2 T_{\text{finger}}}{\partial x^2} \tag{5.14}$$

where ρ_{finger}, c_{finger}, and λ_{finger} are, respectively, the density, the specific heat, and the thermal conductivity of the fingertip; T_{finger} is the fingertip temperature.

At the surface, the temperature is continuous and the effect of the heat source is represented by the interface contact condition assuming the existence of a thermal contact conductance h. The boundary conditions are expressed in the following equations:

$$\begin{cases} \lambda_{\text{org}} \frac{\partial T_{\text{org}}(0,t)}{\partial x} = \lambda_{\text{finger}} \frac{\partial T_{\text{finger}}(0,t)}{\partial x} \\ \lambda_{\text{org}} \frac{\partial T_{\text{org}}(0,t)}{\partial x} = h \left(T_{\text{org}}(0,t) - T_{\text{finger}}(0,t) \right) \end{cases} \tag{5.15}$$

The general solution of (finger) can be expressed as follows:

$$\theta^h_{\text{finger}}(x,s) = A_{\text{finger}} \exp\left(q_{\text{finger}} x\right) + B_{\text{finger}} \exp\left(-q_{\text{org}} x\right) \tag{5.16}$$

where $q^2_{\text{finger}} = \frac{s}{\alpha_{\text{finger}}}$ and α_{finger} represents the thermal diffusivity of the finger. Since the temperature of the finger is finite when $x \to -\infty$, $B_{\text{finger}} = 0$.

By introducing the Laplace transform in (5.15), we get the following system of equations:

$$\begin{cases} -\lambda_{\text{org}} A_{\text{org}} q_{\text{org}} = \lambda_{\text{finger}} A_{\text{finger}} q_{\text{finger}} \\ -\lambda_{\text{org}} A_{\text{org}} q_{\text{org}} = h \left(A_{\text{org}} + B - A_{\text{finger}} + \frac{1}{s} \left(T_{if} - T_{io} \right) \right) \end{cases} \tag{5.17}$$

The solution of this system of equations gives:

$$\begin{cases} A_{\text{org}} = \frac{h \lambda_{\text{org}} q_{\text{org}} \left(T_{if} - T_{io} + Bs \right)}{s \left\{ \lambda_{\text{org}} \lambda_{\text{finger}} q_{\text{org}} q_{\text{finger}} + h \left(\lambda_{\text{org}} q_{\text{org}} + \lambda_{\text{finger}} q_{\text{finger}} \right) \right\}} \\ A_{\text{finger}} = \frac{-h \lambda_{\text{org}} q_{\text{org}} \left(T_{if} - T_{io} + Bs \right)}{s \left\{ \lambda_{\text{org}} \lambda_{\text{finger}} q_{\text{org}} q_{\text{finger}} + h \left(\lambda_{\text{org}} q_{\text{org}} + \lambda_{\text{finger}} q_{\text{finger}} \right) \right\}} \end{cases} \tag{5.18}$$

Finally A_{org} and A_{finger} are formulated as follows:

$$\begin{cases} A_{\text{org}} = \frac{h \beta_{\text{finger}} \left(\left(T_{if} - T_{io} \right)(s+a) + C \right)}{(s+a) \left\{ \beta_{\text{org}} \beta_{\text{finger}} s \sqrt{s+a} + h \left(\beta_{\text{org}} \sqrt{s(s+a)} + \beta_{\text{finger}} s \right) \right\}} \\ A_{\text{finger}} = \frac{-h \beta_{\text{org}} \sqrt{s+a} \left(\left(T_{if} - T_{io} \right)(s+a) + C \right)}{s(s+a) \left\{ \beta_{\text{org}} \beta_{\text{finger}} \sqrt{s(s+a)} + h \left(\beta_{\text{org}} \sqrt{s+a} + \beta_{\text{finger}} \sqrt{s} \right) \right\}} \end{cases} \tag{5.19}$$

where β_{org} and β_{finger} represent the thermal effusivity of the organ and the finger, respectively.

The general solution is then expressed as follows:

$$\begin{cases} \theta_{\text{org}}(x,s) = B + A_{\text{org}} \exp(-q_{\text{org}} x) & x \geq 0 \\ \theta_{\text{finger}}(x,s) = A_{\text{finger}} \exp(q_{\text{finger}} x) & x \leq 0 \end{cases} \tag{5.20}$$

The temporal solution is also calculated numerically using Stehfest-method.

5.4.4 Thermal display integration

In order to integrate the thermal display to our setup, two main solutions are possible. The first solution consists of placing the thermal display outside the laparoscopic instrument. However, this solution maus be rejected since the surgery tasks are usually bimanual; the second solution is to include the thermal display on the handle of the surgery instrument. In order to decide of the best placement of the thermal display, four possibilities are to be studied (see Figure 5.10. The most ergonomic placement appears to be the one presented in 'D' where the thermal display could be in contact with the index finger. We did not perform a thorough usability or performance studies to assess this choice, this came from ad-hoc trials, but we definitely need to investigate this issue more thoroughly.

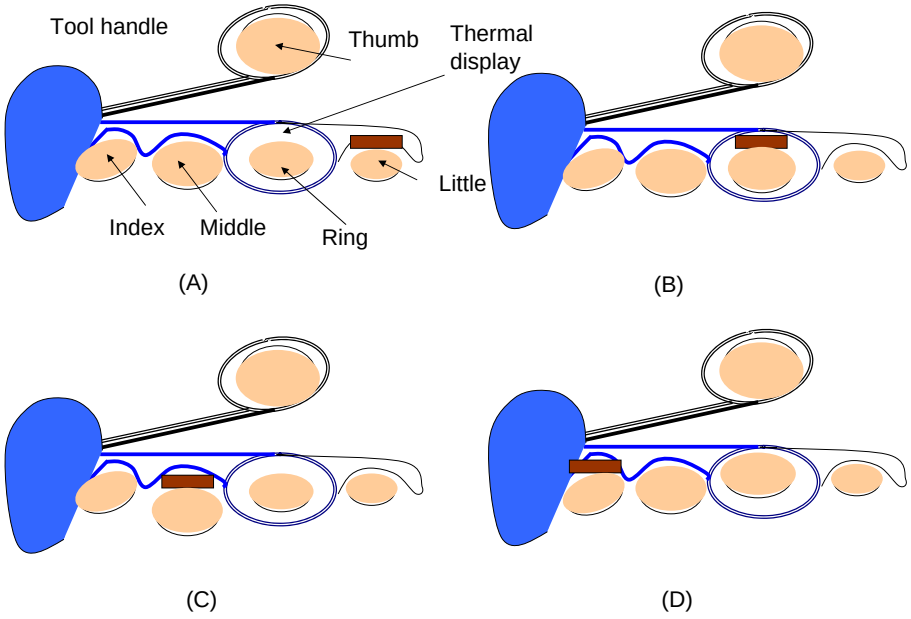

Figure 5.10: Thermal display integration possibilities.

Temperature models developed in (5.13) and (5.20) are implemented in the SOFA framework. When contact between the virtual tool and organs is detected, thermal desired trajectories are generated to the inner thermal (temperature or flux) control loop, (see Figure 5.11). The temperature control law is based on a PI controller with heat flux feed-forward. Organ's model with different initial temperatures and/or

Table 5.1: Thermo-physical properties of living human organs

	Thermal conductivity (W/m.K)	Mass density (Kg/m^3)	Specific heat (J/Kg.K)	Metabolism rate (W/m^3)
Liver	0.57	1050	3600	6150
Kidney	0.54	1050	3900	1290
Heart	0.59	1060	3700	6320
Fat	0.19-0.20	1010-1050	3600-3800	/

different metabolic rates simulating the presence on anomalies are also implemented.

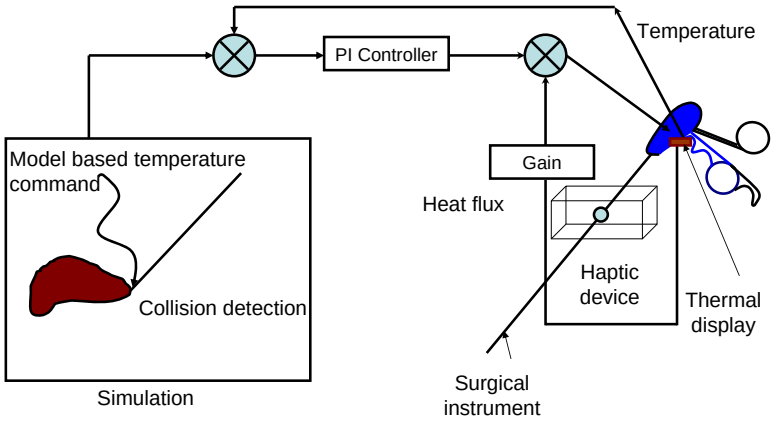

Figure 5.11: Thermal display control scheme.

A picture of the integration in SOFA of the assembled haptic interface with thermal display is shown in figure 5.12.

5.4.5 Experimental results and discussion

5.4.5.1 Experiments for diagnosis

The first set of experiments simulates the thermal behavior of a living organ (the liver) using the thermo-physical properties presented in Table 5.1 and the model presented in (5.20). The presence of anomalies is simulated by considering higher initial temperatures of the organ [Stefanadis 2001] [Stefanadis 2003][Zhao 2008], and/or

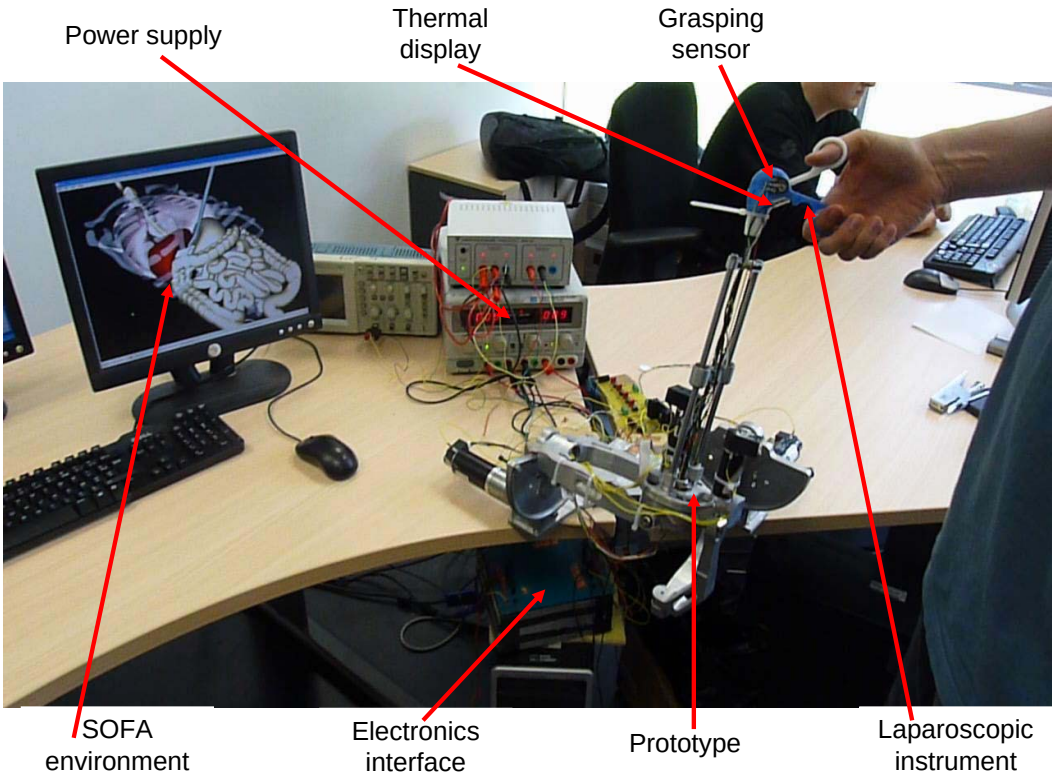

Figure 5.12: An overview of the designed interface integrating visual, haptic and themal feedbacks.

higher metabolism rates [Paruch 2007][Mital 2008]. Figure 5.13 presents the evolu-

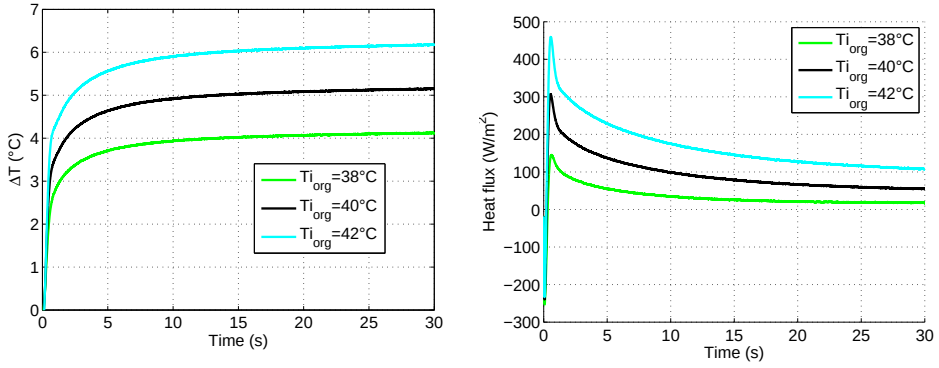

Figure 5.13: Temperature variation of the fingertip (left) and heat flux (right) exchanged for different initial conditions.

tion of temperature rendered to the user fingertip during simulated palpation of the liver with different initial temperatures (38, 40 and 42°C). On one hand, the results

show the existence of a large difference in the rendered temperatures proportional to the initial temperatures, and that, both during transient and steady-state phases. However, the perceived temperature difference is approximately 50% from the initial difference (an initial temperature difference of 2°C is presented as 1°C). This is affected by the thermal display dynamics (Peltier pump + temperature/flux sensor) and the neglected thermal phenomenon such as convection and radiation. From perception point-of-view, the ability to perceive variations in temperature depends not only on their amplitudes but also on their rates of change. Since the differential threshold for warming is 0.20°C at a rate of 2.1°C/s according to [Jones 2008], and considering the transfer factor of 50%, 0.4°C is the minimum initial temperature difference that can be perceived by the user.

On the other hand, the heat flux exchange gives a comprehensible image of the heat perceived by the user. The picks presented in the beginning of the simulation show that the largest quantities of heat is exchanged during the transient phase that stimulates significantly the user thermal sense. This phase is very short since it does not exceed 1 second.

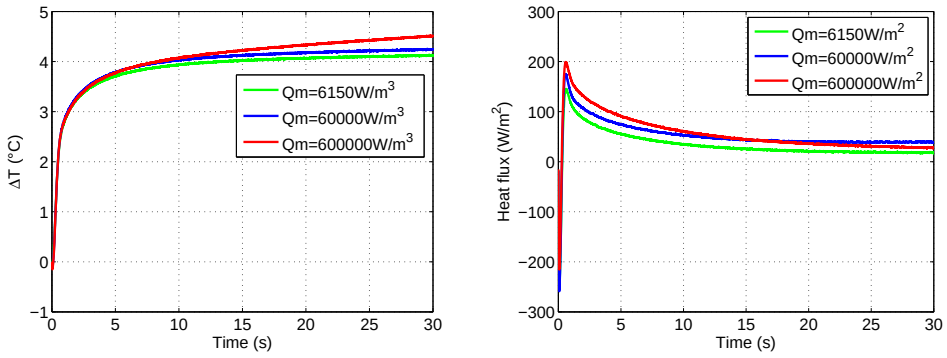

Figure 5.14: Temperature variation of the fingertip (left) and heat flux (right) exchanged for different metabolism rates.

Figure 5.13 presents the evolution of temperature rendered to the user fingertip and the heat flux exchange during simulated palpation of the liver with different metabolism rate that mimics the presence of superficial tumors with 10 times and 100 times the normal metabolism of healthy tissue, (see [Zhao 2008]). The results show the existence of small differences between the temperature profiles in the steady state phase. This difference is proportional to the metabolism rate and it is about 0.1°C and 0.4°C, respectively. However, in the transient phase, which characterizes the thermal sensation, the three profiles are approximately close in spite of the existence of a difference about 25W/m^2 and 30W/m^2, respectively, in term of flux profiles. Therefore, more psychophysical studies are required to conclude about the perception of heat flux. In order to increase temperature differences perception, we propose to use a scaling factor that emphasizes this difference. The calculation of this factor has to be performed based on the differential thresholds presented in [Jones 2008] depending on the aim of the simulation.

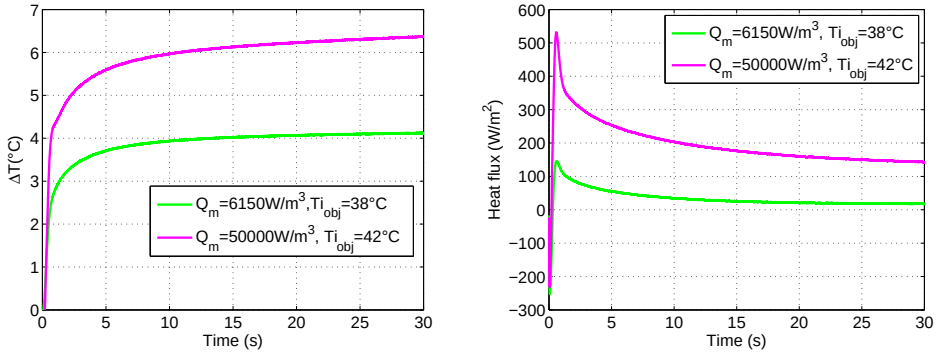

Figure 5.15: Temperature variation of the fingertip (left) and heat flux (right) exchanged flux, for different initial conditions and different metabolism rates.

Figure 5.13 simulates a more realistic case in which we consider the presence of an abnormal initial temperature and abnormal metabolism rate. The result shows a transfer factor of about 56%, which reflects a combination of the two cases presented previously.

5.4.5.2 Experiments for therapy simulation

The second set of experiments simulates the influence of the application of an external heat source on the surface of a living organ (the liver) according to (5.13). The aim of these experiments is to allow a real-time monitoring of the temperature and heat exchange during such procedures. The temperature evolution can be visualized on a monitor or rendered to the user fingertip thanks to the thermal display. However, the use of a scaling factor is to be considered since this temperature can exceed 100°C during a few minutes while the application of a temperature of about 46 to 48°C will cause damage to the user fingertip.

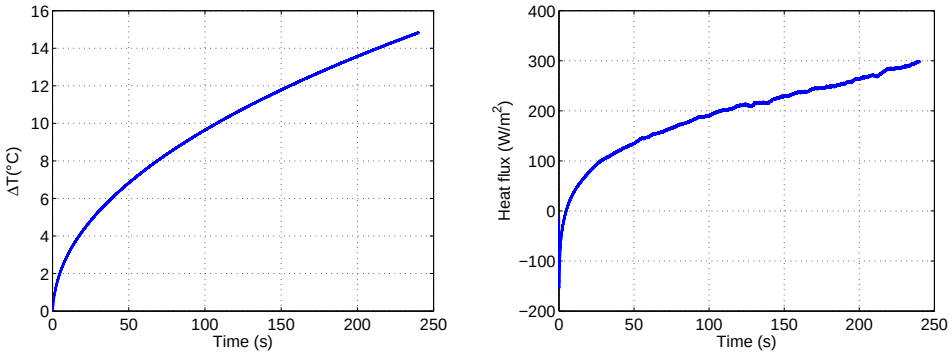

Figure 5.16: Temperature variation (left) and heat flux (right) evolution during the application of a heat source of 1000W/m^2.

Figures 5.16, 5.17 and 5.18 present the heat flux exchange and the temperature

variation when rendering the temperature of the heated organ to the user fingertip for three different source's power levels. In each experiment, the fingertip is maintained in contact with the thermal display until an approximate temperature $46 - 48°C$. The time required to achieve this temperature depends on the quantity of heat provided by the thermal source (inversely proportional).

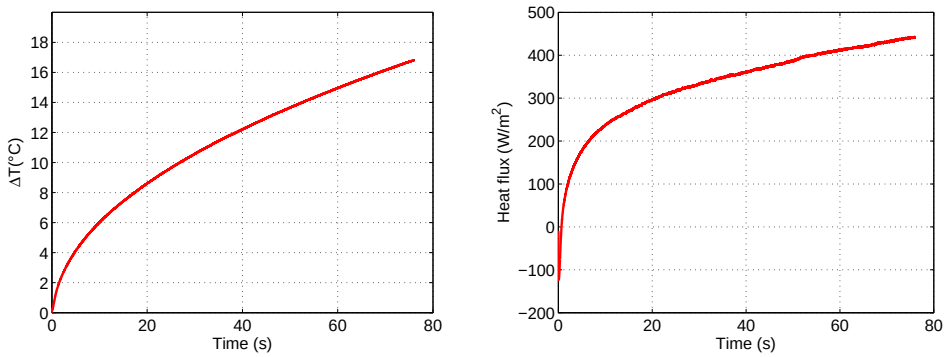

Figure 5.17: Temperature variation (left) and heat flux (right) evolution during the application of a heat source of 2000W/m^2.

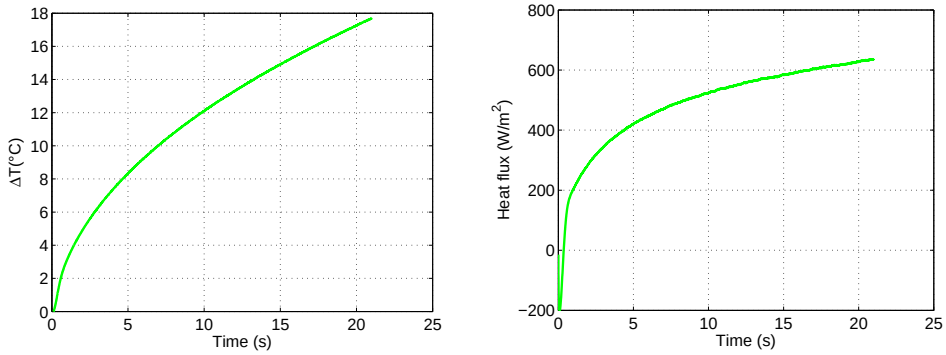

Figure 5.18: Temperature variation (left) and heat flux (right) evolution during the application of a heat source of 4000W/m^2.

5.5 Conclusion

The assembled prototype of the 4-DOF device designed for MIS training has been integrated successfully. The graphics component of the simulator is created based on the SOFA framework, which offers a modular and flexible solution for haptic algorithm implementation and hardware integration. Although simple haptic control schemes have been implemented, the integration of the force-feedback enhanced the interactivity of simulation in performing virtual MIS procedures. In addition to haptics and graphics, we integrated the thermal sensation, which so far has not

been considered in virtual MIS prior to this work, though it has a real significance for medical application since the detection of abnormal temperatures informs about the eventual existence of tumors in the living human organs. In order to achieve a physically plausible replication of this sensation with the haptic and the graphic interfaces, we have modeled the heat exchange inside the body, added a thermal display on the surgical instrument's handle and then implemented the developed models in conjunction with the haptic and graphic's rendering. Another model has been developed and implemented in order to simulate the temperature evolution of an organ under the application of external heat source usually used for tumor ablation, therapy or welding. The performed experiments show that it is possible to include thermal sensation in the conventional simulator without recalling into question their functioning design. In fact, the adjunction of this sensation do not disturb the interaction in practical use.

Nevertheless, these preliminary results must be rather seen as potential investigations; we spent a lot of time dealing with technical aspects of integration of the device with the software which are still to be improved. Only then, more thorough studies on usability and performance of the overall set-up can be conducted.

Chapter 6

Conclusion

In this research, we devised a new haptic feedback device for MIS interactive simulation which is able to combine force and thermal senses and rendering. This device is coupled with the SOFA engine for visual rendering and physically-based simulation of the interaction and the deformation of the organs.

Our particular novelty is in using of thermal stimulation from both a fundamental and an MIS applied perspectives. Interesting sensations have been recorded which have a direct bearing on the ability to distinguish between objects in the surrounding environment and particularly in the medical field where temperature sensing correlates with anomalies in some know diseases. The incorporation of the thermal sensory and its integration with the visual and haptics cues can likely open doors for next generation of surgical simulators. But the first step of this research was to develop our dedicated haptic device in order to gain experience and knowledge and to have an open system for the control law implementation, computer haptics research in MIS domain, and improvement of the system toward low cost accessible devices for advanced teaching and training.

For the design of the device, we analysed surgical tasks in terms of required dexterity, workspace, force and torque. The mechanical design constraints have been considered with respect to the general requirements for haptic interface design from what has been well established in the haptics literature. These requirements include the minimization of friction, backlash, and apparent inertia while maximizing force and position bandwidths, stiffness, motions and force/torque capability.

The proposed mechanism for the haptic device consists in a 4 DOF hybrid parallel-serial structure to combine good stiffness properties with a relatively large workspace while satisfying general design considerations of haptic devices. Its design is made so that it can hold different surgical tools (as a handle) which can be added and removed easily. Hence, the handle of our haptic device is a real surgical instrument that however is slightly adapted to be embedded with sensors serving in user intentions/actions tracking and/or in inner close-loop feedbacks for rendering. The dimensioning of the actuators and the assessment for the workspace and the mechanical structure are performed using CAD software. The mechanical pieces composing the device are assembled and the electronics interface including the power stage and the current and force sensor's conditioning circuits has been also realized. Experiments for sensor calibration are also performed in order to determine the relationship between measures and the sensor's output. The confirmed linearity characteristic of the used sensor offers an adequate low-cost solution for

force monitoring.

The forward and inverse kinematics models are expressed analytically using the DH convention and basic dynamic equations are also formulated for a good compensation of gravitational effects. A set of experiments is completed in order to evaluate the device characteristics. This evaluation included workspace, stiffness, friction, maximum velocity and acceleration, force/torque, and bandwidths. The main features of our device compared to the existed commercial ones lie in its larger workspace and force capability. However we have noticed non-negligible friction (i.e. superior to the acceptable thresholds) in some axes which is due to the assembling process; therefore, exact friction estimation and compensation appears to be necessary. Simple PID based control loops appear to be sufficient to well control the device's position and torques. For each axis, the desired position and torque are achieved with very good precision and in a stable manner.

Before incorporating thermal cues into the force feedback interface, we investigated fundamentals of thermal rendering in a general context, i.e. in telepresence and in virtual reality schemes. Thermal display is carried out based on Peltier pump (TEM) that convert electric current into heat. The dynamic of this device is modeled based on the fundamental thermo-physical equations describing the relationship between the input current, temperature and heat flux. We also proposed new representative models which describe this dynamic using linear and non-linear recursive ARMA equations. The proposed models have been identified and assessed experimentally and proved to be efficient for analyzing the TEM heat flux and temperature behavior. A symmetric thermal telepresence system is carried out using similar TEMs and incorporating heat flux sensors with integrated temperature sensor (thermocouple).Then, using the proposed model, we implemented a new approach for thermal feedback based on the material and finger temperature estimation when they are in contact with the active sensor and the thermal display respectively. The coupling scheme is based on temperature command with heat flux feed-forward control. In order to evaluate the proposed control scheme, we selected some materials which compose object's surfaces encountered in daily activities. Direct contact test showed the possibility to distinguish between these materials by thermal sensing especially when the thermal properties are very scatter. The experimental implementation of the bilateral coupling law reproduces the thermal exchange experienced in a remote interaction of the operator with a given material. However, this experiment also revealed that thermal rendering was influenced by the thermal dynamic (due to intrinsic thermal properties) of the finger and the material composing the Peltier sensor/display. Therefore we proposed another bilateral coupling scheme based on a learning approach. The learning algorithm uses a Neural Network technique combined with the PCA method. In this case, the remote thermal sensor role could be reduced to that of a probe (even a passive one) which role is to identify which material composes the surface of the object that is being contacted in the remote site. The training data are the real measurements of thermal heat flux exchanged during direct contact situation. The results have shown a higher ability to discriminate between materials in the user side that improves the

thermal sensation. However, there exists latency due to that of the sensor time response which sum-up with another latency due to the unavoidable delay needed to identify the material in the remote site. This latency time would be reduced by using faster sensors.

In order to take into account together the sensor's dynamic, the finger thermal properties, and the contact conditions, we developed an analytical model representing the evolution of the temperature when contact occurs between a fingertip and a material. This model is implemented in virtual reality application where different materials are modeled using their intrinsic thermo-physical properties. Based on temperature command from the virtual environment, the thermal display reliably produces temperature profiles when touching a virtual material that guarantees realistic thermal sensation (from a signal viewpoint).

These results promote the application of thermal cue rendering in interactive interfaces in order to enhance the quality (or realism) of the operator's immersion feeling and assist the operator in material identification when manipulating virtual or remote object. Otherwise, thermal cues could also be used as a sensory substitution or as an adjunct to visual and/or haptic feedback. Thermal rendering being investigated for general telepresence and virtual reality applications; we also explored its role in medical applications and precisely in surgery. In view of these technical developments, consideration is made as to whether thermal modality can actually help surgeon to take adequate decision. In practice discrimination between healthy and pathological tissues can potentially be perceived from thermal sensing in conjunction with simultaneous information available from visual and tactile senses. In addition the monitoring of the tissues temperature is particularly important when they are heated during therapeutic procedures.

The device has been interfaced with an existing open source VR simulator (SOFA). We added in SOFA the necessary software dealing with thermal modeling and physically based simulation using built-in data structure and methods. The integration was successful and a realistic simulation scenario with both visual and thermal feedback was achieved. Representative data were obtained from biological tissues simulation demonstrating that the developed interface has potential applications in virtual systems or robotic tele-medical care. However, in using systems capable of providing multisensory information, it is important to find out how these multiple sensations can be perceived efficiently. In this way redundancy or overload of information can be avoided. The psycho-physiological analysis should give a response to this fundamental question. Incorporating thermal sensation in surgery simulator is expected to find practical clinical application as well as an aid for improving teaching of the surgical skills and a test-bed for evaluation of future instrumentation.

Finally, there are still much efforts needed to implement this complex system with a more effective realistic simulation of tissue properties and a combined thermal/force feedback. At short-term developments, there are some additional issues to be improved. Our suggestions for future work are:

1. concerning the haptic interface and force rendering:
    - optimizing the mechanical design for low-cost devices based on lessons learned from the realization (from scratched) of our prototype;
    - model based identification and compensation of device friction and inertia in order to enhance the transparency of the interface;
    - improvement of the computer haptics algorithms in order to improve the realism of the perceived feedback forces
2. concerning the thermal rendering:
    - we will develop closed-loop theories based on thermal impedance scheme: thermal rendering can benefit from such an approach;
    - investigating other possibilities for thermal rendering in medical applications and other fields in conjunction with force, tactile and visual feedbacks;
    - psychophysical studies in order to perform an efficient integration of the thermal sensory information without distribution of the surgeon attention.

More generally, we hope to conduct assessment studies on user performance and usability of this technology in MIS surgical operation and spread its usage.

Appendix A

Thermal-model identified parameters

A.1 Heating/Cooling identified model parameters

Table A.1: Heating/Cooling identified model parameters

Heating capacity model	Cooling capacity model
$\theta_{h1} = 0.0020$	$\theta_{c1} = -0.0040$
$\theta_{h2} = -0.0622$	$\theta_{c2} = -0.5872$
$\theta_{h3} = 0.0047$	$\theta_{c3} = -0.0021$
$\theta_{h4} = -0.0186$	$\theta_{c4} = -0.1311$
$\theta_{h5} = 0.4186$	$\theta_{c5} = -0.3356$

A.2 Identified TEM Heat flux model parameters

Table A.2: Identified TEM Heat flux model parameters

	TEM pump 1	TEM pump 2
c_1	1.0138	1.0902
c_2	0.2722	0.2734
c_3	−0.2920	−0.3689
d_0	−0.0078	−0.0065
d_1	−0.0037	−0.0035
d_2	0.0116	0.0100

A.3 Identified TEM temperature model parameters

Table A.3: Identified TEM temperature model parameters

	TEM pump 1	TEM pump 2
a_{10}	0.6951	0.7341
a_{20}	0.3019	0.2921
a_{30}	0.0018	−0.0276
a_{11}	−0.0024	0.0009
a_{21}	0.0256	0.0364
a_{31}	−0.0009	0.0004
a_{12}	0.0033	−0.0126
a_{22}	0.0038	−0.0007
a_{32}	−0.0277	−0.0215
b_{10}	−0.1196	−0.1438
b_{20}	−0.0204	0.0386
b_{30}	0.1835	0.1472
b_{11}	0.1581	0.2166
b_{21}	0.3164	0.4830
b_{31}	0.0168	−0.0598
b_{12}	0.0446	−0.1497
b_{22}	−0.1613	−0.1497
b_{32}	−0.3549	−0.1375

Appendix B

CAD model and inertial parameters of the designed mechanical parts

B.1 CAD model of the designed mechanical parts

B.2 Masse and inertial parameters of the different parts

Part Number	1	2	3	4	5	6
I_{xx} (g.mm^2)	1639440	240709	3650540	2959303	1360616	164536
I_{yy} (g.mm^2)	2652541	58381	3516277	2059748	1041127	198608
I_{zz} (g.mm^2)	1932954	285510	448371	1613624	790073	47717
I_{xy} (g.mm^2)	-196192	85496	42475	173959	15628	1752
I_{xy} (g.mm^2)	1078410	0	-18203	275883	-38188	-222
I_{yz} (g.mm^2)	201304	0	19590	-51383	-445955	-16924
Masse (g)	500	149	557	600	559	66

Table B.1: Masse and inertial parameters of the different parts

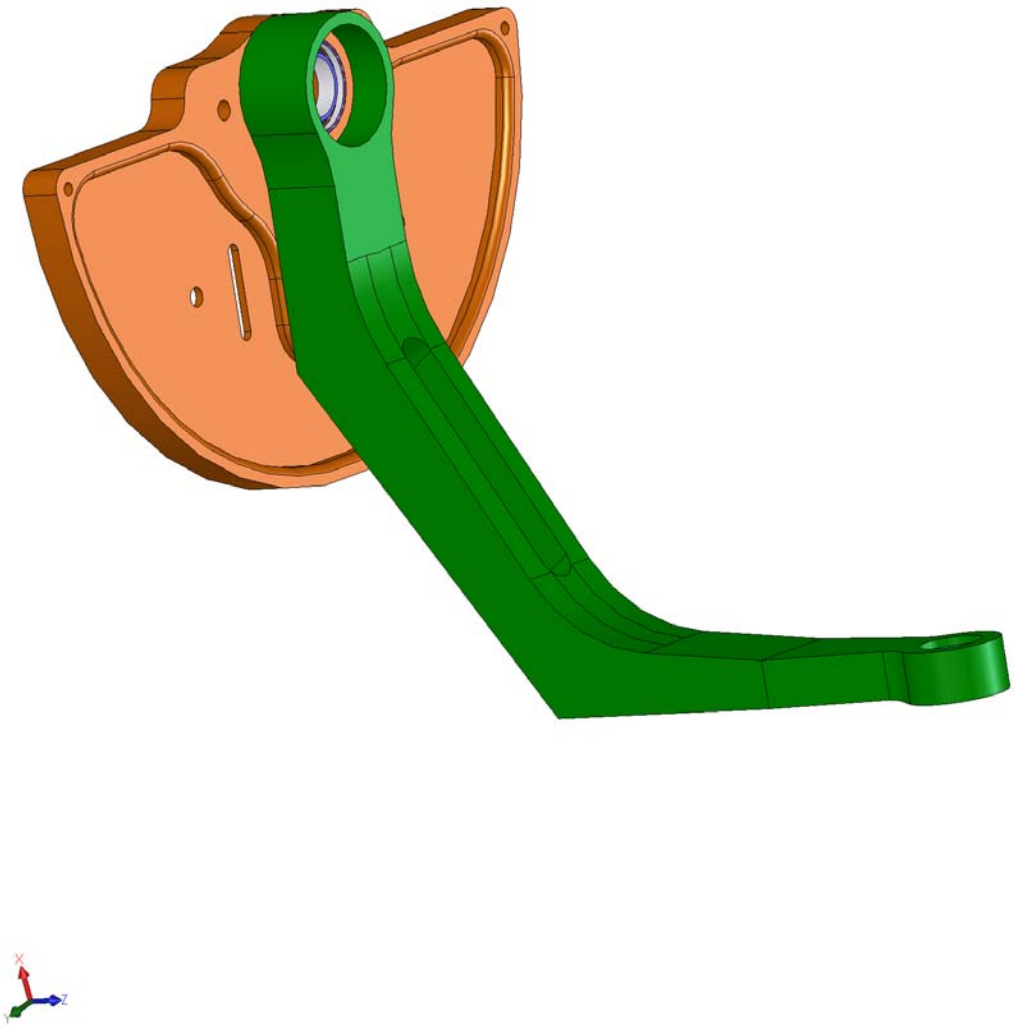

Figure B.1: CAD Model of Part 1 *(Capstan 2 + Body 4)*.

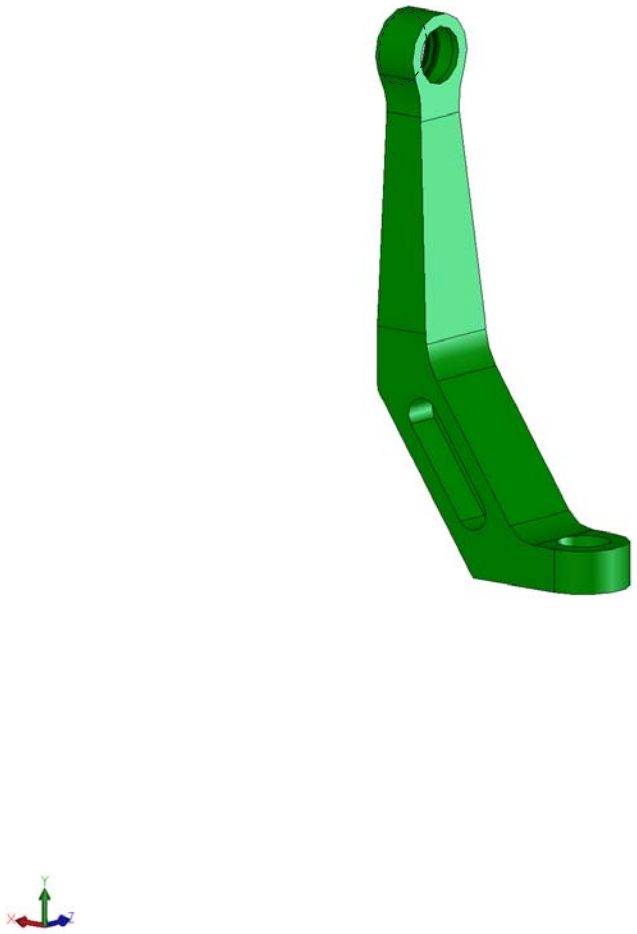

Figure B.2: CAD Model of Part 2 *(Body 5)*.

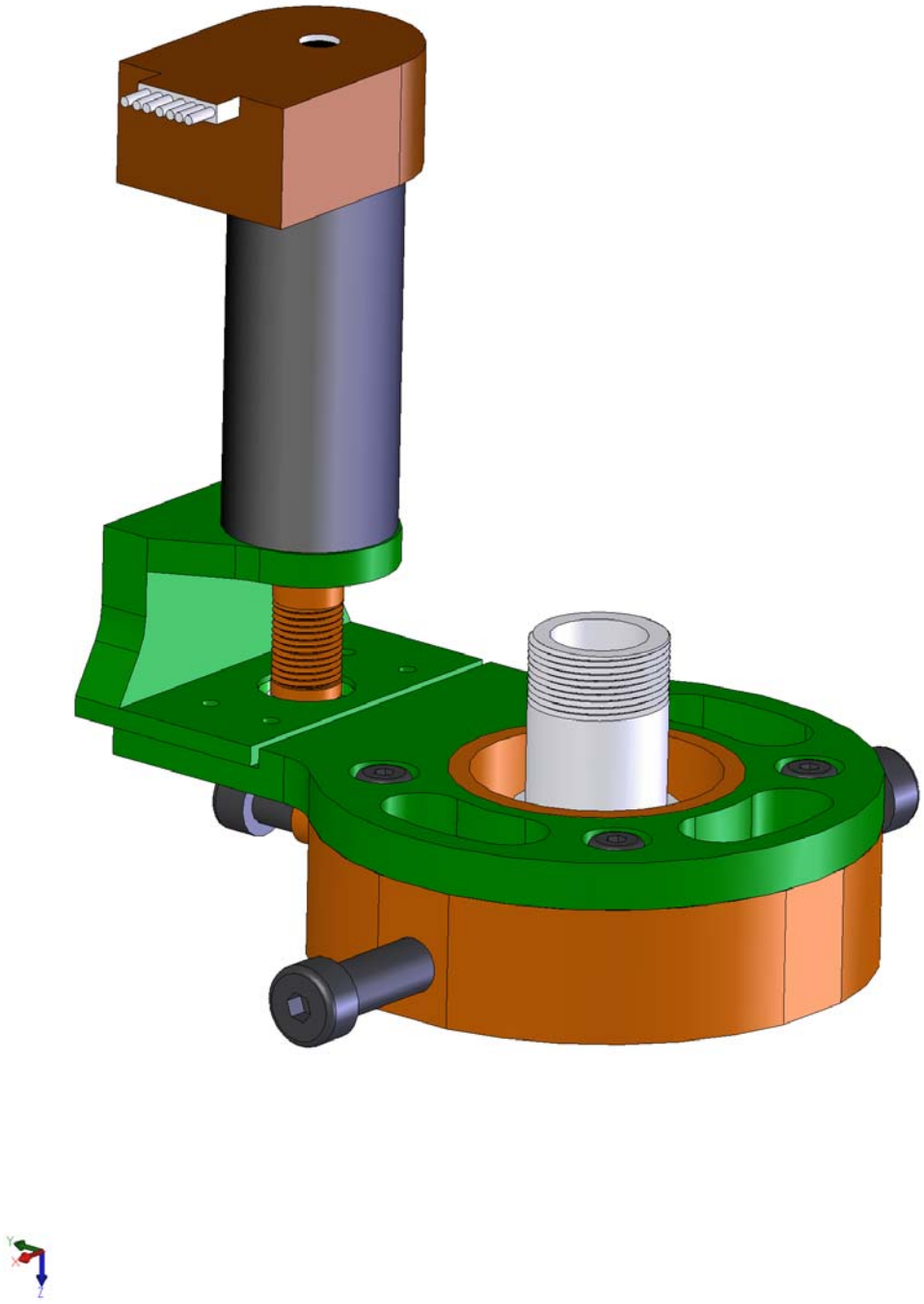

Figure B.3: CAD Model of Part 3 *(Body 2 + Motor 3)*.

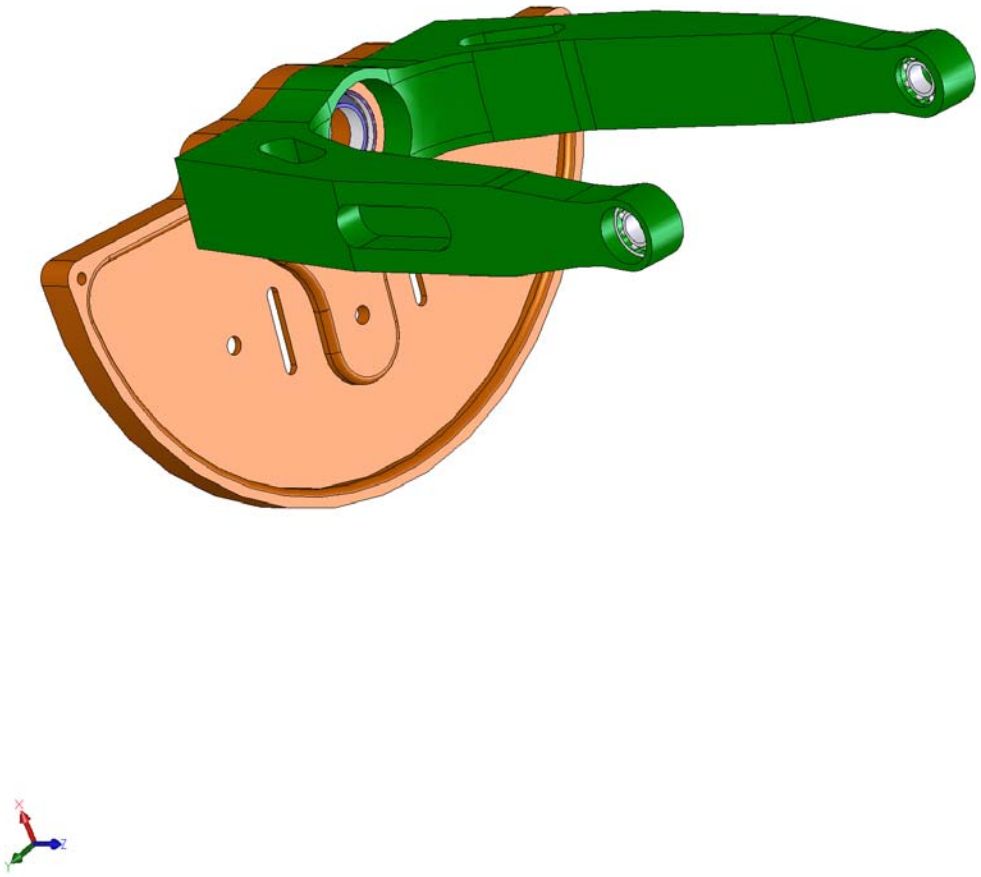

Figure B.4: CAD Model of Part 4 *(Capstan 1 + Body 1)*.

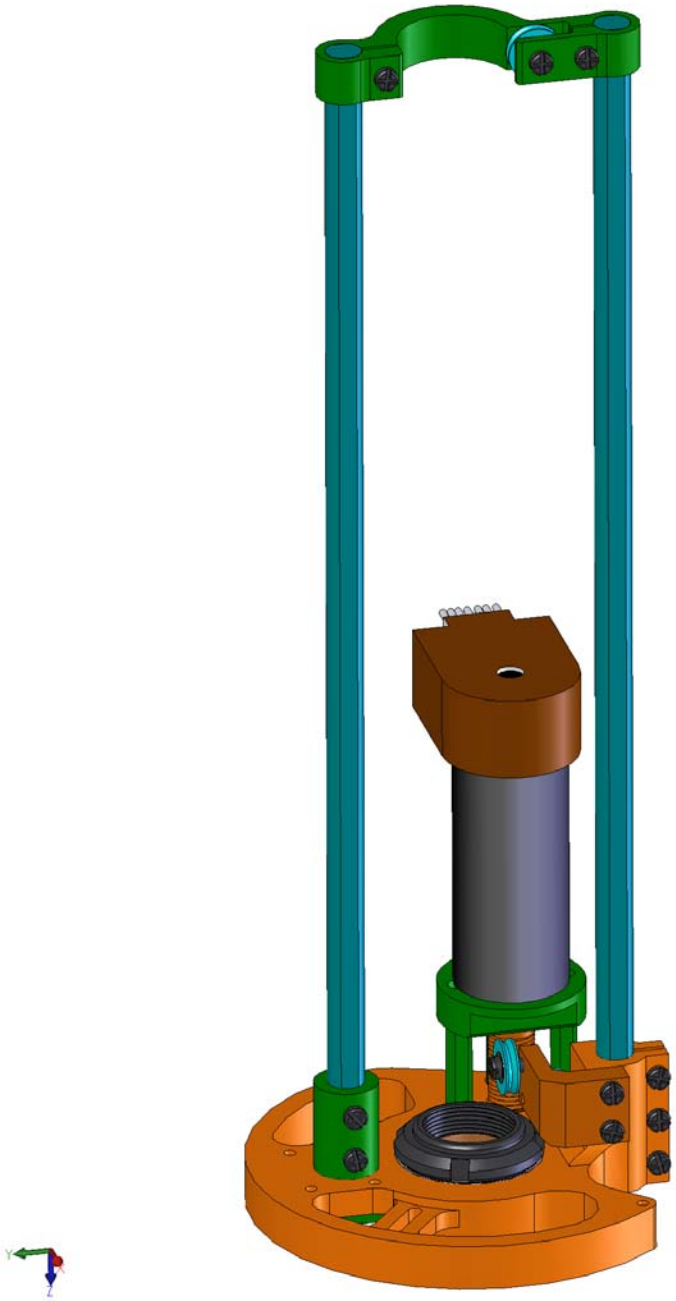

Figure B.5: CAD Model of Part 5 *(Capstan 3 + Body 3 + Motor 4)*.

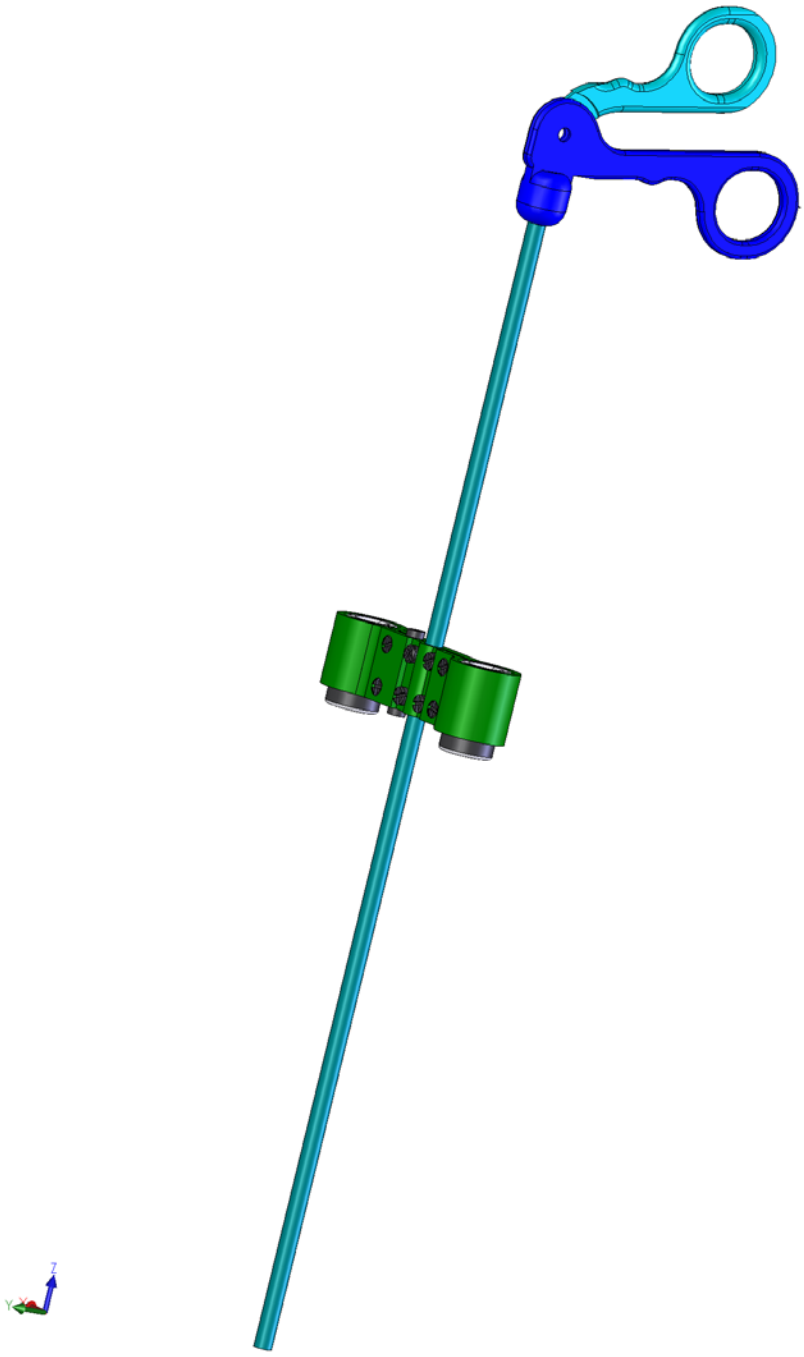

Figure B.6: CAD Model of Part 6 *(Body 6 + Tool)*.

Appendix C

Sliding Mode Temperature Control

We present in this appendix the synthesis of a robust controller based on the identified non-linear recursive ARMA equations governing the TEMs thermal dynamics.

C.1 Robust controller design

This paragraph presents the design of a sliding mode controller for the identified TEC temperature model. Starting with temperature ARMA model, the equation (4.10) can be rewritten as follow:

$$T(t) = -\sum_{i=1}^{n} a_{i0}\ T\,(t-i) + \sum_{j=0}^{m} b_{j0}\ I\,(t-j) + \xi(I,T,t) \tag{C.1}$$

where $\xi(I,T,t)$ is the non-linear dynamic of the model. The simplified linear ARMA model is then derived as:

$$T(t) = -\sum_{i=1}^{n} a_{i0}\ T\,(t-i) + \sum_{j=0}^{m} b_{j0}\ I\,(t-j) \tag{C.2}$$

From (C.2) we get a discrete-continuous transformation using the zero-order holder method:

$$\begin{aligned} \frac{d^3T(t)}{dt^3} + l_1\frac{d^2T(t)}{dt^2} + l_2\frac{dT(t)}{dt} + l_3\ T(t) = \\ m_1\frac{d^2I(t)}{dt^2} + m_2\frac{dI(t)}{dt} + m_3\ I(t) \end{aligned} \tag{C.3}$$

From (C.3), the state space model writes:

$$\left\{ \begin{array}{rcrcl} \dot{x}(t) & = & A\ x(t) & + & B\ u(t) \\ y(t) & = & C\ x(t) & = & T(t) \end{array} \right. \tag{C.4}$$

where $x(t)$ is the state vector, $u(t)$ is the control input and $y(t)$ is the output. The matrices A, B and C are defined as follows:

$$A = \begin{bmatrix} 0 & 1 & 0 \\ 0 & 0 & 1 \\ -l_3 & -l_2 & -l_1 \end{bmatrix}$$

$$B = \begin{bmatrix} 1 & 0 & 0 \\ l_2 & 1 & 0 \\ l_3 & l_2 & 1 \end{bmatrix}^{-1} \begin{bmatrix} m_1 \\ m_2 \\ m_3 \end{bmatrix} = \begin{bmatrix} \alpha_1 \\ \alpha_2 \\ \alpha_3 \end{bmatrix}$$

and[1]

$$C = [1 \;\; 0 \;\; 0]$$

We define the sliding surface according to [Slotine 1991]:

$$s(t) = \dot{e}(t) + \lambda \; e(t) \tag{C.5}$$

where λ is a strict positive constant, and $e(t) = y_d(t) - y(t)$ the output error and $y_d(t)$ the desired state. Substituting the state space expression in the sliding surface equation we have:

$$s(t) = [\dot{y}_d(t) + \lambda y_d(t)] - [\lambda x_1(t) + x_2(t) + \alpha_1 u(t)] \tag{C.6}$$

differentiating the sliding variable yields:

$$\dot{s}(t) = [\ddot{y}_d(t) + \lambda \dot{y}_d(t)] - [\lambda \dot{x}_1(t) + \dot{x}_2(t) + \alpha_1 \dot{u}(t)] \tag{C.7}$$

by substituting $\dot{x}_1(t)$ and $\dot{x}_2(t)$ expressions in (C.7), we have:

$$\begin{aligned} \dot{s}(t) = {} & [\ddot{y}_d(t) + \lambda \dot{y}_d(t)] \\ & - [\lambda x_2(t) + x_3(t) + (\lambda \alpha_1 + \alpha_2) u(t) + \alpha_1 \dot{u}(t)] \end{aligned} \tag{C.8}$$

the equivalent control law $u_{eq}(t)$ to achieve $\dot{s}(t) = 0$ can be found as follows:

- let,

$$\begin{aligned} g_1 &= \alpha_1 \\ g_2 &= \lambda \; \alpha_1 + \alpha_2 \\ g_3 &= [\ddot{y}_d(t) + \lambda \; \dot{y}_d(t)] - [\lambda \; x_2(t) + x_3(t)] \end{aligned}$$

  and

$$v(t) = \frac{g_1}{g_2} \; \dot{u}(t) + u(t)$$

  Substituting the last expressions in (C.8), we find:

$$v_{eq}(t) = \frac{g_3}{\hat{g}_2}$$

  $v_{eq}(t)$ is interpreted as the augmented equivalent control to achieve $\dot{s}(t) = 0$ with the identified model parameters $\hat{g}_2$

[1] Experiments on the TEMs show that $\alpha_{i \in [1,2,3]} \neq 0$.

- as we do not know the exact model of the system, we introduce a correction term so that the following inequality equation is reinforced:

$$\frac{1}{2}\frac{d}{dt}\left(s(t)^2\right) = s(t)\ \dot{s}(t) \leq -\eta\,\|s(t)\| \tag{C.9}$$

This inequality is the sliding condition. It ensures us that the distance to the sliding surface decreases along all the trajectories, with a minimal speed given by η.

The augmented control law v_a is chosen to be:

$$v_a(t) = v_{eq}(t) - k\ \mathrm{sgn}(s(t))$$

- now, we can write (C.8) as follows:

$$\begin{aligned}\dot{s}(t) &= g_3 - g_2\ v(t)\\ &= g_3\left[1 - \frac{g_2}{\hat{g}_2}\right] + g_2\ k\ \mathrm{sgn}(s(t))\end{aligned}$$

since:

$$\begin{aligned}s(t)\ \dot{s}(t) &= s(t)\left[g_3\left[1 - \frac{g_2}{\hat{g}_2}\right] + k\ g_2\ \mathrm{sgn}(s(t))\right]\\ &\leq \left(g_3\ \left[1 - \frac{g_2}{\hat{g}_2}\right] + k\ g_2\right)\ \|s(t)\|\end{aligned}$$

by choosing the sliding gain k, such as:

$$g_3\ \left[1 - \frac{g_2}{\hat{g}_2}\right] + k\ g_2 \leq -\eta \tag{C.10}$$

the sliding condition (C.9) is satisfied. the control input u expression is then deduced by solving the differential equation $\left(\frac{g_1}{g_2}\ \dot{u}(t) + u(t)\right) - v_a = 0$, for which a simplified solution is:

$$u(t) = u_{eq}(t) + k\ \mathrm{sgn}(s(t)) \tag{C.11}$$

where

$$u_{eq}(t) = \delta\ \exp\left(-\frac{\hat{g}_2}{\hat{g}_1}t\right) + \frac{g_3}{\hat{g}_2} \tag{C.12}$$

$\hat{g}_1$ is the estimated value of g_1.

C.2 Experimental validation

The synthesized controller was first validated by computer simulation using the temperature identified model described by (4.10) to track an amplitude varying

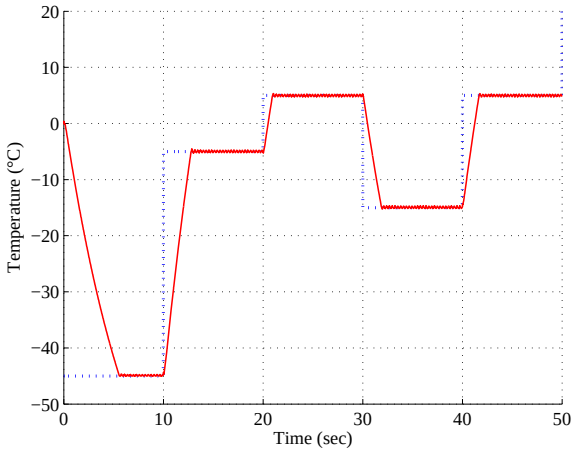

Figure C.1: Reference temperature (dashed) and estimated temperature (solid) of the Peltier pump.

reference. The controller parameters are initialized with $k = -0.9$, $\lambda = 250$ and $\delta = 20$. Fig. C.1 illustrates the simulation result.

The controller was then implemented in real experiments where the reference signals was varying from ± 10°C. The states x_2 and x_3 were computed using our observer. The reference and the measured TEM temperatures are shown in fig. C.2.

.

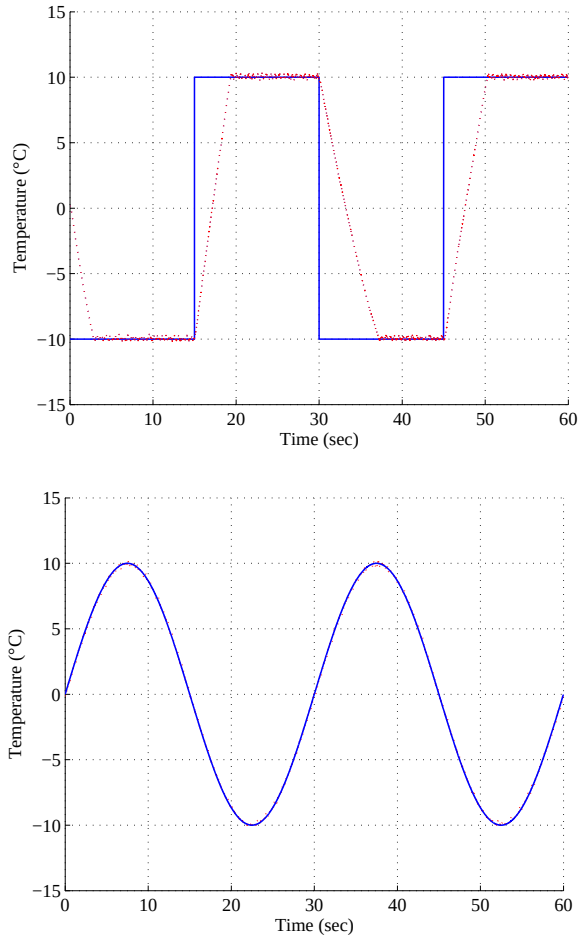

Figure C.2: Reference temperature (solid) and measured temperature (dashed) of the Peltier pump.

Appendix D

Publications

1. Mohamed Guiatni, Abdelhamid Drif and Abderrahmane Kheddar, *Thermoelectric Modules: Recursive non-linear ARMA modeling, Identification and Robust Control*, IEEE International Conference on Industrial Electronics: 568-573, Taiwan, 5-8 November , 2008.

2. Mohamed Guiatni, Abdelaziz Benallegue and Abderrahmane Kheddar, *Learning based thermal rendering for telepresence*, EuroHaptics (EH'08) : Springer Verlag 820-825, Madrid, Spain, 10-13 June, 2008.

3. Mohamed Guiatni and Abderrahmane Kheddar, *Theoretical and experimental study of a heat transfer model for thermal feedback in virtual environments*, IEEE/RSJ International Conference on Intelligent Robots and Systems (IROS): 2996-3001, Nice, France, 22-26 Sept, 2008.

4. Mohamed Guiatni, Abdelaziz Benallegue and Abderrahmane Kheddar, *Thermal Display for Telepresence Based on Neural Identification and Heat Flux Control*, Presence: Teleoperators and Virtual Environments, MIT Press, 156–169, Vol. 18, No. 2, 2009.

5. Mohamed Guiatni, Vincent Riboulet and Abderrahmane Kheddar, *Design and Evaluation of a Haptic Interface for Interactive Simulation of Minimally-Invasive Surgeries*, IEEE/ASME International Conference on Advanced Intelligent Mechatronics (AIM)), Singapore, 14-17 July , 2009, *Accepted*.

Bibliography

[Adelstein 1992] B.D. Adelstein and M.U.J. Rosen. *Design and implementation of a force reflecting manipulandum for manual control research.* Advances in Robotics, ASME DSC, vol. 42, pages 1–12, 1992. 35

[Aggarwal 2008] Rajesh Aggarwal, Indran Balasundaram and Ara Darzi. *Training Opportunities and the Role of Virtual Reality Simulation in Acquisition of Basic Laparoscopic Skills.* Journal of Surgical Research, vol. 145, no. 1, pages 80–86, 2008. 29

[Ahlberg 2002] G. Ahlberg, T. Heikkinen, L. Iselius, C.E Leijonmarck, J. Rutqvist and D. Arvidsson. *Does training in a virtual reality simulator improve surgical performance.* Surgical Endoscopy, vol. 16, no. 1, pages 126–129, 2002. 30

[Allard 2007] Jérémie Allard, Stéphane Cotin, François Faure, Pierre-Jean Bensoussan, François Poyer, Christian Duriez, Hervé Delingette and Laurent Grisoni. *SOFA - an Open Source Framework for Medical Simulation.* In Medicine Meets Virtual Reality, MMVR 15, February, 2007, pages 1–6, Long Beach, California, Etats-Unis, 2007. 107

[Arkin 1994] H. Arkin, L.X. Xu and K.R. Holmes. *Recent developments in modeling heat transfer in blood perfused tissues.* IEEE Transactions on Biomedical Engineering, vol. 41, no. 2, pages 97–107, 1994. 115

[Arsenault 2000] Roland Arsenault and Colin Ware. *Eye-hand co-ordination with force feedback.* In CHI '00: Proceedings of the SIGCHI conference on Human factors in computing systems, pages 408–414, New York, NY, USA, 2000. ACM. 13

[Astley 2000] O.R. Astley and V. Hayward. *Design constraints for haptic surgery simulation.* In IEEE International Conference on Robotics and Automation, pages 2446–2451, San Francisco, CA, April 2000. 41

[Bacon 2006] James Bacon, Neil Tardella, Janey Pratt, John Hu and James English. *The Surgical Simulation and Training Markup Language: An XML-Based Language for Medical Simulation.* Studies in health technology and informatics, vol. 119, pages 37–42, 2006. 107

[Baraff 1998] David Baraff and Andrew Witkin. *Large steps in cloth simulation.* In SIGGRAPH '98: Proceedings of the 25th annual conference on Computer graphics and interactive techniques, pages 43–54, New York, NY, USA, 1998. ACM. 107

[Basdogan 2001] C. Basdogan, C. Ho and M.A. Srinivasan. *Virtual Environments for Medical Training: Graphical and Haptic Simulation of Common Bile Duct Exploration.* IEEE-ASME Transactions on Mechatronics, vol. 6, no. 3, pages 267–285, 2001. 14

[Basdogan 2004] Cagatay Basdogan, Suvranu De, Jung Kim, Manivannan Muniyandi, Hyun Kim and Mandayam A. Srinivasan. *Haptics in Minimally Invasive Surgical Simulation and Training.* IEEE Computer Graphics and Applications, pages 56–64, March/April 2004. 14

[Baser 2006] Ozgur Baser, Erhan Ilhan Konukseven and Bugra Koku. *7 DOF Haptic Device Design.* In EuroHaptics 2006, pages 507–512, jul 2006. 39, 41

[Baumann 1998] Roger Baumann and Reymond Clavel. *Haptic Interface for Virtual Reality Based Minimally Invasive Surgery Simulation.* In IEEE International Conference on Robotics and Automation, pages 381–386, Leuven, Belgium, May 1998. 34

[Beaudoin 2008] Philippe M. Beaudoin, Yves Audet and Abdelhalim Bendali. *Characterizing a Thermoelectric Module as Part of a Semiconductor Course Laboratory.* IEEE Transactions on Education, vol. 51, no. 2, pages 330–336, May 2008. 73

[Bell 2007] Audrey K. Bell and Caroline G.L. Cao. *How Does Artificial Force Feedback Affect Laparoscopic Surgery Performance ?* In Human Factors and Ergonmics Society 51st Annual Meeting, pages 646–650, 2007. 14

[Benali-Khoudja 2003] Mohamed Benali-Khoudja, Moustapha Hafez, Jean Mark Alexandre, Jamil Benachour and Abderrahmane Kheddar. *Thermal feedback model for virtual reality.* In International Symposium on Micromechatronics and Human Science, pages 153–158, Nagoya, Japan, October 19-22 2003. 66, 67, 71

[Benali-Khoudja 2004] Mohamed Benali-Khoudja, Moustapha Hafez, Jean-Marc Alexandre and Abderrahmane Kheddar. *Tactile interfaces: a state-of-the-art survey.* In 35th International Symposium on Robotics, Paris, France, 22-23 Mars 2004. 14

[Berry 2007] Max Berry, Ted Lystig, Jonathan Beard, Hans Klingestierna, Richard Reznick and Lars Lonn. *Porcine Transfer Study: Virtual Reality Simulator Training Compared with Porcine Training in Endovascular Novices.* Cardiovasc Intervent Radiol, vol. 30, pages 455–461, 2007. 29

[Bholat 1999] O.S. Bholat, R.S. Haluck, W.B. Murray, P.J. Gorman and T.M. Krummel. *Tactile feedback is present during minimally invasive surgery.* Journal of the American College of Surgeons, vol. 189, pages 349–355, 1999. 13, 14

[Birglen 2002] Lionel Birglen, Clement Gosselin and Nicolas Pouliot. *SHaDe, A New 3-DOF Haptic Device*. IEEE Transactions on Robotics and Automation, vol. 18, no. 2, pages 166–175, April 2002. 39

[Bishop 1995] C.M. Bishop. Neural networks for pattern recognition. Oxford: Oxford University Press, 1995. 88, 89

[Boyd 2006] K. Brian Boyd, Jake Olivier and J.R. Salameh. *Surgical Residents' Perception of Simulation Training*. The American surgeon, vol. 72, no. 6, pages 521–524, 2006. 29

[Burdea 1996] Grigore C. Burdea. Force and touch feedback for virtual reality. John Wiley & Sons, Inc., New York, NY, USA, 1996. 36

[Cakmak 2000] H.K. Cakmak and U. Kühnapfel. *Animation and Simulation Techniques for VR-Training Systems in Endoscopic Surgery*. In Eurographics Workshop Animation and Simulation (EGCAS 2000), pages 173–185. Interlaken/CH, 2000. 14, 16

[Caldwell 1995] Darwin G. Caldwell, U. Andersen, C.J. Bowler and A.J Wardle. *A High Power Weight Dexterous Manipulator Using Sensory Glove Based Motion Control and Tactile Feedback*. Transaction of the Institute of Measurement and Control, vol. 17, no. 5, pages 234–241, 1995. 66, 67

[Caron 1997] François Caron. Analyse et conception d'un manipulateur parallèle sphérique à deux degrés de liberté pour l'orientation d'une caméra. Master's thesis, Université Laval, Quebec, Canada, Août 1997. 39

[Carrozza 2003] Maria Chiara Carrozza, Paolo Dario and Louis Phee Soo Jay. *Micromechatronics in surgery*. Transactions of the Institute of Measurement and Control, vol. 25, no. 4, pages 309–327, 2003. 114

[Carslaw 1959] Horiato Scott Carslaw and John Conrad Jaeger, editeurs. Conduction of heat in solids. Oxford , Clarendon Press , Oxford University Press, 1959. 72, 81

[Carsten 2002] N. Gutt Carsten, Zun-Gon Kim and Lukas Krahenbuh. *Training for Advanced Laparoscopic Surgery*. European Journal of Surgery, vol. 168, pages 171–177, 2002. 9

[Carter 2005] F. J. Carter, M. P. Schijven, R. Aggarwal, T. Grantcharov, N. K. Francis, G. B. Hanna and J. J. Jakimowicz. *Consensus guidelines for validation of virtual reality surgical simulators*. Surgical Endoscopy, vol. 12, pages 1523–1532, 2005. 27

[Castet 2008] Julien Castet and Jean-Loup Florens. *A Virtual Reality Simulator Based on Haptic Hard Constraints*. In EuroHaptics 2008, LNCS, Springer-Verlag Berlin Heidelberg, pages 918–923, Madrid, Sapin, 2008. 106

[Champion 2003] H. Champion and A. Gallagher. *Simulation in surgery: a good idea whose time has come.* British journal of surgery, vol. 90, no. 7, pages 767–768, 2003. 11

[Chiasson 2003] P. M. Chiasson, D. E. Pace, C. M. Schlachta, J. Mamazza and E. C. Poulin. *Minimally invasive surgery training in Canada: A survey of general surgery.* Surgical Endoscopy, vol. 17, pages 371–377, 2003. 9

[Cho 2007] Yoonju Cho, Kelvin Liang, Fopefolu Folowosele, Brain Miller and Nitish V. Thakor. *Wireless Temperature Sensing Cosmesis for Prosthesis.* In IEEE 10th International Conference on Rehabilitation Robotics, pages 672–677, Noordwijk, The Netherlands, 13-15 June 2007. 66

[Chopra 2008] S. Chopra, S. Kroeze, E. Mayer, R. Aggarwal, A. Darzi and A. Patel. *Virtual Reality Simulator - Answer to Training Needs of European Urology Residents.* European Urology Supplements, vol. 7, no. 3, pages 259–259, 2008. 30

[Ciccarella 1989] Gianfranco Ciccarella and Piero Marletti. *Model Reference Adaptive Control of a Thermostatic Chamber.* IEEE Transactions on Industrial Electronics, vol. 36, no. 1, pages 88–93, February 1989. 71

[Citérin 2006] Johann Citérin, Aurélien Pocheville and Abderrahmane Kheddar. *A touch rendering device in a virtual environment with kinesthetic and thermal feedback.* In IEEE International Conference In Robotics and Automation, pages 3923 – 3928, Orlando, Florida, 15-19 May 2006. 71, 94

[Cohen 1977] M.L. Cohen. *Measurement of the thermal properties of the human skin.* Journal of Investigative Dermatology, vol. 69, no. 3, pp. 333-338, 1977. 66

[Colgate 1994] J. Edward Colgate and J. Michael Brown. *Factors Affecting the Z-Width of a Haptic Display.* In IEEE Conference on Robotics and Automation, pages 3205–3210, May 1994. 109, 110

[Colgate 1997] J. Edward Colgate and Gerd G. Schenkel. *Passivity of a Class of Sampled-Data Systems: Application to Haptic Interfaces.* Journal of Robotic Systems, vol. 14, no. 1, pages 34–47, 1997. 109

[Conti 2003] F. Conti, F. Barbagli, R. Balaniuk, M. Halg, C. Lu and D. Morris. *The CHAI Libraries.* In Proceedings of Eurohaptics 2003, pages 496–500, Dublin, IE, July 2003. 107

[Cotin 1999] S. Cotin, H. Delingette and N. Ayache. *Real-Time Elastic Deformations of Soft Tissues for Surgery Simulation.* IEEE Transactions on Visualization and Computer Graphics, vol. 5, no. 1, pages 62–73, 1999. 14

[Defer 1998] Didier Defer, Emmanuel Antczak and Bruno Duthoit. *The characterization of thermophysical properties by thermal impedance measurements taken under random stimuli taking sensor-induced disturbance into account.* IOP Publishing Ltd, Meas. Sci. Technol., pages 496–504, 1998. 87

[Deml 2006] Barbara Deml, Andreas Mihalyi and Gunter Hannig. *Development and Experimental Evaluation of a Thermal Display.* In 6th Internationnal Conference EuroHaptics, Paris, France, 2006. 67

[Domuracki 2008] K.J. Domuracki, C.J. Moule, H. Owen, G. Kostandoff and J.L. Plummer. *Learning on a simulator does transfer to clinical practice.* Resuscitation, vol. 80, no. 3, pages 346–349, 2008. 29

[Drif 2005] Abdelhamid Drif, Johann Citérin and Abderrahmane Kheddar. *Thermal bilateral coupling in teleoperators.* IEEE/RSJ International Conference on Robots and Intelligent Systems, August 2-6, 2005. 66, 68, 71, 91, 102

[Duriez 2006] C. Duriez, F. Dubois, A. Kheddar and C. Andriot. *Realistic haptic rendering of interacting deformable objects in virtual environments.* IEEE Transactions on Visualization and Computer Graphics, vol. 12, no. 1, pages 36–47, 2006. 111

[Ellis 1996] R.E. Ellis, O.M. Ismaeil and M.G. Lipsett. *Design and Evaluation of a High-Performance Haptic Interface.* Robotica, vol. 14, pages 321–327, 1996. 34, 35, 37

[Eltaib 2003] M.E.H. Eltaib and J.R. Hewit. *Tactile sensing technology for minimal access surgery – a review.* Mechatronics, vol. 13, pages 1163–1177, 2003. 14, 15

[Faure 2007] François Faure, Jérémie Allard, Stéphane Cotin, Paul Neumann, Pierre-Jean Bensoussan, Christian Duriez, Hervé Delingette and Laurent Grisoni. *SOFA: A modular yet efficient simulation framework.* In Surgetica: Computer-Aided Medical Interventions: tools and applications, pages 101–108, Chambéry, France, November 2007. 107

[Feygin 2002] David Feygin, Madeleine Keehner and Frank Tendick. *Haptic Guidance Experimental Evaluation of a Haptic Training Method for a Perceptual Motor Skill.* In 10th Symposium on Haptic Interfaces for Virtual Environment and Teleoperator Systems, pages 40–47, Washington, DC, USA, 2002. IEEE Computer Society. 13

[Fischer 1990] P. Fischer, R. Daniel and K. Siva. *Specification and design of input devices for teleoperation.* In IEEE International Conference on Robotics and Automation, pages 540–545, 13-18 May 1990. 35, 36

[Gallagher 1999] AG. Gallagher, N. McClure, J. McGuigan, I. Crothers and J. Browning. *Virtual reality training in laparoscopic surgery - a preliminary*

assessment of minimally invasive surgical trainer virtual reality (MIST-VR). Endoscopy, vol. 31, no. 4, pages 31–313, 1999. 8, 29

[Gallagher 2005] Anthony G. Gallagher, E Matt Ritter, Howard Champion, Gerald Higgins, Marvin P. Fried, Gerald Moses, C Daniel Smith, and Richard M. Satava. *Virtual Reality Simulation for the Operating Room, Proficiency-Based Training as a Paradigm Shift in Surgical Skills Training.* Annals of Surgery, vol. 241, no. 2, pages 364–372, 2005. 11

[Gerovichev 2002] Oleg Gerovichev, Panadda Marayong and Allison M. Okamura. *The Effect of Visual and Haptic Feedback on Manual and Teleoperated Needle Insertion.* In MICCAI02: Proceedings of the 5th International Conference on Medical Image Computing and Computer-Assisted Intervention-Part I, pages 147–154, London, UK, 2002. Springer-Verlag. 14

[Goktekin 2004] Tolga Gokce Goktekin, Murat Cenk Cavusoglu, Frank Tendick and Shankar Sastry. *GiPSi: An Open Source/Open Architecture Software Development Framework for Surgical Simulation.* In LNCS 3078, pages 240–248. Springer-Verlag Berlin Heidelberg, 2004. 107

[Gosselin 2005] Florian Gosselin. *Optimisation des interfaces haptiques : problémes, meťhodes, applications.* In 17 éme Congrés Français de Mećanique, Troyes, 29 aug - 2 sep 2005. 35

[Gurusamy 2009] K.S. Gurusamy, R. Aggarwal, L. Palanivelu and B.R. Davidson. *Virtual reality training for surgical trainees in laparoscopic surgery (Review).* The Cochrane Collaboration, John Wiley and Sons, Ltd., vol. 1, 2009. 29

[Hafez 2007] Moustapha Hafez. *Tactile interfaces : technologies applications and challenges.* Visual Comput, vol. 23, pages 267–272, 2007. 14

[Hale 2004] Kelly S. Hale and Kay M. Stanney. *Deriving Haptic Design Guidelines from Human Physiological, Psychophysical, and Neurological Foundations.* IEEE Computer Graphics and Applications, pages 33–39, 2004. 36

[Harvey 2007] R. D. Harvey, D. G. Walker and K. D. Frampton. *Enhancing Performance of Thermoelectric Coolers Through the Application of Distributed Control.* IEEE Transactions on Components and Packaging Technologies, vol. 30, no. 2, pages 330–336, June 2007. 73

[Hashizume 2002] M Hashizume, M Shimada, M Tomikawa, Y Ikeda, I Takahash, R Abe, F Kaga, N Gotoh, K Konishi, S Maehara and K Sugimachi. *Early experiences of endoscopic procedures in general surgery assisted by computer-enhanced surgical system.* Surgical Endoscopy, vol. 16, no. 8, pages 1187–1191, 2002. 14

[Hasson 2001] H.M. Hasson, T. Schollmeyer and K. Vanhecke. *Experience with the laparoscopic training simulator 2000 (LTS2000).* In 30th Meeting of the

American Association of Gynecologic Laparoscopists (AAGL), page S24, San Francisco, CA, 2001. 27

[Hayward 1994] Vincent Hayward, Jehangir Choksi, Gonzalo Lanvin and Christophe Ramstein. *Design and Multi-Objective Optimization of a Linkage for a Haptic Interface.* Advances in Robot Kinematics and Computationed Geometry, pages 359–368, 1994. 35

[Hayward 1995] Vincent Hayward. *Toward a seven axis haptic device.* In International Conference on Intelligent Robots and Systems, page 3133, Washington, DC, USA, 1995. IEEE Computer Society. 35, 36, 41

[Hayward 1996] Vincent Hayward and Oliver R. Astley. *Performance measures for haptic interfaces.* In The 7th International Symposium on Robotics Research, pages 195–207. Springer Verlag, 1996. 36

[Hayward 1998] V. Hayward, P. Gregorio, O. Astley, S. Greenish and M. Doyon. *Freedom-7: A High Fidelity Seven Axis Haptic Device With Application To Surgical Training.* In Experimental Robotics V, Casals, A., de Almeida, A. T. (eds.), Lecture Notes in Control and Information Science, Springer-Verlag, pages 445–456, 1998. 34

[Henry 2006] D. Henry, S. Druon, P. Fraisse and A. Crosnier. *Conception et Validation d'une Architecture Haptique Indépendante des Modèles.* CIFA'06: Conférence Internationale Francophone d'Automatique, 2006. 110

[Hertz 1991] J. Hertz, A. Krogh and R. G. Palmer. Introduction to the theory of neural computation. Addison Wesley, 1991. 89

[Ho 2004] Hsin-Ni Ho and Lynette A. Jones. *Material Identification Using Real and Simulated Thermal Cues.* In 26th Annual International Conference of the IEEE EMBS, pages 2462– 2465, September 2004. 66, 67

[Ho 2006a] Hsin-Ni Ho and Lynette A. Jones. *Contribution of thermal cues to material discrimination and localization.* Perception and Psychophysics, vol. 68, no. 1, pages 118–128, 2006. 66

[Ho 2006b] Hsin-Ni Ho and Lynette A. Jones. *Thermal Model for Hand-Object Interactions.* In Symposium on Haptic Interfaces for Virtual Environment and Teleoperator Systems, pages 461–467, March 2006. 66, 67, 68, 86, 87

[Ho 2007a] Hsin-Ni Ho and Lynette A. Jones. *Development and evaluation of a thermal display for material identification and discrimination.* ACM Trans. Appl. Percept., vol. 4, no. 2, pages 13–24, 2007. 68

[Ho 2007b] Hsin-Ni Ho and Lynette A. Jones. *Infrared Thermal Measurement System for Evaluating Model-Based Thermal Displays.* pages 157–163, 2007. 67

[Hodes 2005] Marc Hodes. *On One-Dimensional Analysis of Thermoelectric Modules (TEMs).* IEEE Transactions on Components and Packaging Technologies, vol. 28, no. 2, pages 218–229, June 2005. 73

[Hodes 2007] Marc Hodes. *Optimal Pellet Geometries for Thermoelectric Refrigeration.* IEEE Transactions on Components and Packaging Technologies, vol. 30, no. 1, pages 50–58, March 2007. 71

[Hogle 2008] Nancy J. Hogle, Warren D. Widmann, Aku O. Ude, Mark A. Hardy and Dennis L. Fowler. *Does Training Novices to Criteria and Does Rapid Acquisition of Skills on Laparoscopic Simulators Have Predictive Validity or Are We Just Playing Video Games?* Journal of Surgical Education, vol. 65, no. 6, pages 431–435, 2008. 30

[Incropera 2006] F.P. Incropera, D.P. DeWwitt, T.L. Bergman and A.S. Lavine. Fundamentals of heat and mass transfer. JOHN WILEY and SONS, Sixth Edition, 2006. 80, 87

[Jones 2002] Lynette A. Jones and Michal Berris. *The Psychophysics of Temperature Perception and Thermal-Interface Design.* In HAPTICS '02: Proceedings of the 10th Symposium on Haptic Interfaces for Virtual Environment and Teleoperator Systems, pages 137–142, Washington, DC, USA, 2002. IEEE Computer Society. 66, 67

[Jones 2003] Lynette A. Jones and Michal Berris. *Material Discrimination and Thermal Perception.* pages 171–178, 2003. 66, 67

[Jones 2008] Lynette A. Jones and Hsin-Ni Ho. *Warm or Cool, Large or Small? The Challenge of Thermal Displays.* EEE Trans. Haptics, vol. 1, no. 1, pages 53–70, 2008. 66, 121

[Kabadayi 2006] Sakir Kabadayi. Design of a six degrees of freedom haptic interface. Master's thesis, Sabanci University, Istanbul, Turkey, 2006. 42

[Katsuura 1998] T. Katsuura, R. Tabuchi, K. Iwanaga, H. Harada and Y. Kikuchi. *Estimation of thermal sensation during varied air temperature conditions.* Applied Humain Sciences, vol. 17, no. 2, pp. 73-78, 1998. 66

[Khalil 1999] Wissama Khalil and Etienne Dombre. Modélisation, identification et commande des robots. Collection robotique, 1999. 48

[Khatri 2001] Prakash Khatri and John Ziemski. *'Dry-To-The-Touch' Thermal Grease.* In International Symposium on Advanced Packaging Materials, pages 236–239, 2001. 87

[Kheddar 2001] Abderrahmane Kheddar. *Teleoperation based on the hidden robot concept.* IEEE Transaction on Systems Man and Cybernetics, vol. 31, no. 1, pages 1–13, 2001. 94

[Kheddar 2004] Abderrahmane Kheddar, Abdelhamid Drif, Johann Citerin and Benjamin Le Mercier. *A multilevel haptic rendering concept.* In EuroHaptics, Munich, Germany, June 5-7 2004. 93

[Kühnapfel 2004] U. Kühnapfel, H. Çakmak, B. Chantier, H. Maaß, G. Strauss, C. Trantakis, E. Novatius, J. Meixensberger, K. Lehmann, H.J. Buhr, M. Lawo and G. Bretthauer. *HapticIO : Haptic Interface-Systems for Virtual-Reality Training in Minimally-Invasive Surgery.* 2004. 27

[Kim 2007] Keehoon Kim, J. Edward Colgate and Michael A. Peshkin. *A Pilot Study of a Thermal Display Using a Miniature Tactor for Upper Extremity Prosthesis.* In Frontiers in the Convergence of Bioscience and Information Technologies, pages 531–536, Washington, DC, USA, 2007. IEEE Computer Society. 66

[Kim 2008] Keehoon Kim, J. Edward Colgate and Michael A. Peshkin. *On the Design of a Thermal Display for Upper Extremity Prosthetics.* In Symposium on Haptic Interfaces for Virtual Environments and Teleoperator Systems, pages 413–419, Reno, Nevada, USA, 13-14 March 2008. 66

[Kuhn 1996] C. Kuhn, U. Kuhnapfel, H.G. Krumm and B. Neisius. *A virtual reality based training system for minimally invasive surgery.* In Proc. Computer Assisted Radiology (CAR96), pages 764–769, 1996. 107

[Labudovic 2004] Marko Labudovic and Jin Li. *Modeling of TE Cooling of Pump Lasers.* IEEE Transactions on Components and Packaging Technologies, pages 724–730, 2004. 72

[Lamata 2006] Pablo Lamata, Enrique J. Gomez, Fernando Bello, Roger L. Kneebone, Rajesh Aggarwal and Felix Lamata. *Conceptual Framework for Laparoscopic VR Simulators.* IEEE Computer Graphics and Applications, vol. 26, no. 6, pages 69–79, 2006. 28

[Lamata 2008] Pablo Lamata, Enrique J. Gómez, Félix Lamata Hernández, Alfonso Oltra Pastor, Francisco Miguel Sánchez-Margallo and Francisco del Pozo Guerrero. *Understanding Perceptual Boundaries in Laparoscopic Surgery.* IEEE Transactions on Biomedical Engineering, vol. 55, no. 3, pages 866–873, March 2008. 38

[Lartz 1994] D. J. Lartz, H. H. Cudney and T. E. Diller. *Heat flux measurement used for feedforward temperature control.* Proceeding of the 10th International Heat Transfer Conference, vol. 2, pp. 261-266, Brigthon, UK., 1994. 82

[Lawrence 1993] Dale A. Lawrence. *Stability and transparency in bilateral teleoperation.* IEEE Transactions on Robotics and Automation, vol. 9, no. 5, pages 624–637, 1993. 68

[Lawrence 1998] Dale A. Lawrence, Lucy Y. Pao, Anne M.Dougherty, Yiannis Paclou, Shane W. Brown and Stephen A. Wallace. *Human perception of friction in haptic interfaces.* In Symposium on Haptic Interfaces for Virtual Environment and Teleoperator Systems, pages 287–294, Anaheim, CA, March 1998. 35

[Laycock 2003] S. D. Laycock and A. M. Day. *Recent Developments and Applications of Haptic Devices.* Computer Graphics, Blackwell Publishing Ltd, vol. 22, no. 2, pages 117–132, 2003. 36, 39, 41

[Li 2006] Te-Mei Li. *On the design and developement of robotic mechanisms for laparoscopic surgery.* PhD thesis, Simon Fraser University, Burnaby, BC, Canada, 2006. 27, 37, 39

[Lineykin 2007] Simon Lineykin and Shmuel Ben-Yaakov. *Modeling and Analysis of Thermoelectric Modules.* IEEE Transactions on Industry Applications,Volume 43, Issue 2, pp. 505-512, March-april, 2007. 71

[Liu 2000] Jing Liu and Lisa X. Xu. *Boundary information based diagnostics on the thermal states of biological bodies.* International Journal of Heat and Mass Transfer, vol. 43, pages 2827–2839, 2000. 114

[Liu 2003] Alan Liu, Frank Tendick, Kevin Cleary and Christoph Kaufmann. *A survey of surgical simulation - applications, technology, and education.* Presence - Teleoper. Virtual Environ., vol. 12, no. 6, pages 599–614, 2003. 6, 14

[Liu 2008] Kuo-Chi Liu. *Thermal propagation analysis for living tissue with surface heating.* International Journal of Thermal Sciences, vol. 47, pages 507–513, 2008. 114

[Lorenzo 2005] Nicola Di Lorenzo and Jenny Dankelman. *Surgical Training and Simulation.* Business Briefing : Global Surgery - Future Directions, 2005. 11, 12

[Marghitu 2001] Dan B. Marghitu, editeur. Mechanical engineer's handbook. Academic Press, USA, 2001. 97

[Martorana 1975] Richard T. Martorana. *Thermoelectric Temperature Control of Instrumentation - A Sample Design.* IEEE Transactions on Industrial Electronics and Control Instrumentation, vol. IECI-22, no. 1, pages 96–105, February 1975. 73

[Martorana 2005] Richard T. Martorana. *Methodology for Extracting Thermoelectric Module Parameters.* IEEE Transactions on Instrumentation and Measurement, vol. 54, no. 4, pages 1548–1552, August 2005. 73

[Matsumoto 1997] S. Matsumoto, R. Ooshima, K. Kobayashi, N. Kawabe, T. Shiraishi, Y. Mizuno, H. Suzuki and S. Umemoto. *A tactile sensor for laparoscopic cholecystectomy.* Surgical Endoscopy, vol. 11, pages 939–941, 1997. 14

[McClusky 2005] D.A. McClusky, E.M. Ritter, A.B. Lederman, A.G. Gallagher and C. D. Smith. *Correlation Between Perceptual, Visuo-spatial, and Psychomotor Aptitude to Duration of Training Required to Reach Performance Goals on the MIST-VR Surgical Simulator.* The American Surgeon, vol. 71, no. 1, pages 13–21, 2005. 29

[McColl 2006] Ryan McColl, A.P Ian Brown, Cory Seligman, Fabian Lim and Amer Alsaraira. *Haptic Rendering and Perception Studies For Laparoscopic Surgery Simulation.* In 28th IEEE EMBS Annual International Conference, pages 833–836, New York City, USA, Aug 30-Sept 3 2006. 27

[Mettler 2006] L. Mettler, N.F. Zuberi, P. Rastogi and T. Schollmeyer. *Role and value of laparoscopic training devices in assessing nondominant and two-handed dexterity.* Gynecological Surgery, vol. 3, no. 2, pages 110–114, 2006. 29

[Miller 2000] Brian E. Miller, J. Edward Colgate and Randy A. Freeman. *Guaranteed Stability of Haptic Systems with Nonlinear Virtual Environments.* IEEE Transactions on Robotics and Automation, vol. 16, no. 6, pages 712–719, 2000. 110

[Mital 2008] Manu Mital and Ramana M. Pidaparti. *Breast Tumor simulation and parameters estimation using evolutionary algorithms.* Model. Simul. Eng., vol. 2008, no. 2, pages 1–6, 2008. 114, 120

[Monkman 1993] G.J. Monkman and P.M. Taylor. *Thermal Tactile Sensing.* IEEE Transactions on Robotics and Automation, vol. 9, no. 3, pages 313–318, June 1993. 66, 68

[Montgomery 2002] Kevin Montgomery, Cynthia Bruyns, Joel Brown, Stephen Sorkin, Frederic Mazzella, Guillaume Thonier, Arnaud Tellier, Benjamin Lerman and Anil Menon. *Spring: A General Framework for Collaborative, Real-time Surgical Simulation.* In Medicine Meets Virtual Reality, pages 23–26. IOS Press, 2002. 107

[Morris 2007] Dan Morris, Hong Tan, Federico Barbagli, Timothy Chang and Kenneth Salisbury. *Haptic Feedback Enhances Force Skill Learning.* In Second Joint EuroHaptics Conference and Symposium on Haptic Interfaces for Virtual Environment and Teleoperator Systems, pages 21–26, Washington, DC, USA, 2007. IEEE Computer Society. 29

[Neto 2003] A.G.S. Neto, L.A.L. de-Almeida, A.M.N. Lima and G.S. Deep. *Recursive ARMA modeling for thermoelectric modules.* In 20th IEEE Instrumentation and Measurement Technology Conference (IMTC'03), pages 919 – 923, Vail, CO, USA, 20-22 May 2003. 71, 73

[Ng 2004] Eddie Y-K Ng and N.M Sudharsan. *Computer simulation in conjunction with medical thermography as an adjunct tool for early detection of breast cancer.* BMC Cancer, vol. 4, no. 17, 2004. 114

[Ottensmeyer 1997] M. Ottensmeyer and J. Salisbury. *Hot and cold running VR, adding thermal stimuli to haptic experience.* Proceedings of the PHANToM Users Group, 1997. 67

[Ottermo 2005] Maria V. Ottermo, Oyvind Stavdahl and Tor A. Johansen. *Electromechanical Design of a Miniature Tactile Shape Display for Minimally Invasive Surgery.* In First Joint Eurohaptics Conference and Symposium on Haptic Interfaces for Virtual Environment and Teleoperator Systems, pages 561–562, Washington, DC, USA, 2005. IEEE Computer Society. 14

[Panait 2008] Lucian Panait, Robert L. Bell, Kurt E. Roberts and Andrew J. Duffy. *Designing and Validating a Customized Virtual Reality-Based Laparoscopic Skills Curriculum.* Journal of Surgical Education, vol. 65, no. 6, pages 413–417, 2008. 24

[Paruch 2007] M. Paruch and E. Majchrzak. *Identification of tumor region parameters using evolutionary algorithm and multiple reciprocity boundary element method.* Eng. Appl. Artif. Intell., vol. 20, no. 5, pages 647–655, 2007. 114, 120

[Payandeh 1997] Shahram Payandeh. *Force Propagation Models in Laparoscopic Tools and Trainers.* In 19th International Conference - IEEE/EMBS, pages 957–960, Chicago, IL. USA, Oct. 30 - Nov. 2 1997. 8

[Pham 2005] Thai Pham, Lincoln Roland, K. Aaron Benson, Roger W. Webster, Anthony G. Gallagher and Randy S. Haluck. *Smart Tutor: A Pilot Study of a Novel Adaptive Simulation Environment.* Stud Health Technol Inform, vol. 111, pages 385–389, 2005. 29

[Puangmali 2008] Pinyo Puangmali, Kaspar Althoefer, Lakmal D. Seneviratne, Declan Murphy and Prokar Dasgupta. *State-of-the-Art in Force and Tactile Sensing for Minimally Invasive Surgery.* IEEE Sensors Journal, vol. 8, no. 4, pages 371–381, 2008. 13, 14, 30

[Rasmussen 1983] J. Rasmussen. *Skills, rules and knowledge; signals, signs and symbols, and other distinctions in human performance models.* IEEE Transactions on Systems, Man, and Cybernetics, vol. 13, no. 3, pages 257–266, 1983. 11

[Richards 2000] C. Richards, J. Rosen, B. Hannaford, C. Pellegrini and M. Sinanan. *Skills evaluation in minimally invasive surgery using force/torque signatures.* Surgical Endoscopy, vol. 14, no. 9, pages 791–798, Sep 2000. 14, 38

[Rosen 1999] Jacob Rosen, Mark MacFarlane, Christina Richards, Blake Hannaford and Mika Sinanan. *Surgeon-Tool Force/Torque Signatures - Evaluation of Surgical Skills in Minimally Invasive Surgery.* In Medicine Meets Virtual Reality, IOS Press, pages 1–9, San Francisco, CA, October 1999. 38, 58

[Rosen 2000] Jacob Rosen, Massimiliano Solazzo, Blake Hannaford and Mika Sinanan. *Objective Evaluation of Laparoscopic Surgical Skills Using Hidden Markov Models Based on Haptic Information and Tool/Tissue Interactions.* In American College of Surgeons Annual Meeting - Washington State Chapter, June 2000. 38, 58

[Rosen 2002] Jacob Rosen, Jeffrey D. Brown, Lily Chang, Marco Barreca, Mika Sinanan and Blake Hannaford. *The BlueDRAGON: A System for Measuring the Kinematics and the Dynamics of Minimally Invasive Surgical Tools In-Vivo.* In IEEE International Conference on Robotics and Automation, pages 1876–1881, Washington, DC, May 2002. 38

[Rosen 2005] Jacob Rosen, Mitch Lum, Denny Trimble, Blake Hannaford and Mika Sinanan. *Spherical Mechanism Analysis of a Surgical Robot for Minimally Invasive Surgery - Analytical and Experimental Approaches.* Studies in Health Technology and Informatics - Medicine Meets Virtual Reality, pages 442–448, January 2005. 37

[Russell 1985] Robert Andrew Russell and Frank J. Paoloni. *Robot Sensor for Measuring Thermal Properties of Gripped Objects.* IEEE Transactions on Instrumentation and Measurements, vol. 34, no. 3, pages 458–460, September 1985. 66

[Russell 1988] Robert Andrew Russell. *Thermal sensor for object shape and material constitution.* Robotica, vol. 6, no. 1, pages 31–34, 1988. 66, 67, 68

[Salhab 2005] M Salhab, W Al Sarakbi and K Mokbel. *The evolving role of the dynamic thermal analysis in the early detection of breast cancer.* International Seminars in Surgical Oncology, vol. 8, no. 2, 2005. 114

[Salisbury 2004] Kenneth Salisbury, Francois Conti and Federico Barbagli. *Haptic Rendering: Introductory Concepts.* IEEE Comput. Graph. Appl., vol. 24, no. 2, pages 24–32, 2004. 110

[Satava 1993] R.M. Satava. *Virtual reality surgical simulator: the first steps.* Surgical Endoscopy, vol. 7, no. 3, pages 203–205, 1993. 11

[Savija 2003] I. Savija, J. R. Culham and M. M. Yovanovich. *Review of Thermal Conductance Models for Joints Incorporating Enhancement Materials.*

Journal of Thermophysics and Heat Transfer, vol. 17, no. 1, pages 43–52, January-March 2003. 87

[Schijven 2003] M. Schijven and J. Jakimowicz. *Virtual reality surgical laparoscopic simulators*. Surgical Endoscopy, Springer-Verlag New York Inc, vol. 17, pages 1943–1950, 2003. 8

[Schütze 2001] Jörg Schütze, Herman Ilgen and Wolfgang R. Fahrner. *An Integrated Micro Cooling System for Electronic Circuits*. IEEE Transactions on Industrial Electronics, vol. 48, no. 2, pages 281–285, April 2001. 71

[Seymour 2002] Neal E. Seymour, A. Gallagher and S. Roman. *Virtual reality training improves operating room performance: results of a randomized, double-blinded study*. Annals of Surgery, vol. 236, pages 458 – 464, 2002. 11

[Seymour 2005] Neal E. Seymour. *Virtual reality in general surgical training*. European Surgery, vol. 37, no. 5, pages 298–303, 2005. 30

[Seymour 2008] Neal E. Seymour. *VR to OR, A Review of the Evidence that Virtual Reality Simulation Improves Operating Room Performance*. World Journal of Surgery, vol. 32, pages 182–188, 2008. 29

[Sherman 2005] V. Sherman, L. S. Feldman, D. Stanbridge, R. Kazmi and G. M. Fried. *Assessing the learning curve for the acquisition of laparoscopic skills on a virtual reality simulator*. Surgical Endoscopy, vol. 19, pages 678 – 682, 2005. 24

[Slotine 1991] Jean-Jacques Slotine and Weiping Li. Applied nonlinear control. Prentice Hall Int. Inc., Englewood Cliffs, 2 édition, 1991. 140

[Solbrekken 2008] Gary L. Solbrekken, Kazuaki Yazawa and Avram Bar-Cohen. *Heat Driven Cooling Of Portable Electronics Using Thermoelectric Technology*. IEEE Transactions on Advanced Packaging, vol. 31, no. 2, pages 429–437, May 2008. 71

[Spaelter 2007] Ulrich Spaelter and Hannes Bleuler. *A Task Specific Kinematic Design Methodology With Application to a 4-DOF Haptic Interface*. In 12th IFToMM World Congress, Besançon, June 18-21 2007. 27, 37

[Stefanadis 2001] C. Stefanadis, C. Chrysochoou, D. Markou, K Petraki, D.B. Panagiotakos, C. Fasoulakis, A. Kyriakidis, C. Papadimitriou and P.K. Toutouzas. *Increased Temperature of Malignant Urinary Bladder Tumors In Vivo: The Application of a New Method Based on a Catheter Technique*. Journal of Clinical Oncology, vol. 19, no. 3, pages 676–681, 2001. 115, 119

[Stefanadis 2003] Christodoulos Stefanadis, Christina Chrysohoou, Demosthenes Panagiotakos, Elisabeth Passalidou, Vasiliki Katsi, Vlassios Polychronopoulos and Pavlos K Toutouzas. *Temperature differences are associated with*

malignancy on lung lesions: a clinical study. BMC Cancer, vol. 3, no. 1, pages 1–5, 2003. 115, 119

[Stehfest 1970] Harald Stehfest. *Algorithm 368: Numerical inversion of Laplace transforms [D5].* Communications of the ACM, vol. 13, no. 1, pages 47–49, 1970. 100

[Sternberg 2007] N. von Sternberg, M. S. Bartsch, A. Petersik, J. Wiltfang, W. Sibbersen, U. Tiede T. Grindel, P. H. Warnke, M. Heiland, P.A.J. Russo, H. Terheyden and P. Pohlenz. *Learning by doing virtually.* International Journal Oral Maxillofac Surgery, vol. 36, pages 386–390, 2007. 11, 29

[Stolzenburg 2007] Jens-Uwe Stolzenburg, Michael C. Truss, Robert Rabenalt, Minh Do, Thilo Schwalenberg, Paraskevi F. Katsakiori, Alan McNeill and Evangelos Liatsikos. *Training in Laparoscopy.* European Association of Urology and European Board of Urology, pages 53–62, 2007. 11

[Strom 2003] P. Strom, A. Kjellin, L. Hedmanand E. Johnson, T. Wredmark and L. Fellander-Tsai. *Validation and learning in the Procedicus KSA virtual reality surgical simulator: Implementing a new safety culture in medical school.* Surgical Endoscopy, vol. 17, no. 2, pages 227–231, 2003. 22

[Tan 1992] Hong Z. Tan, Xiao-Dong Pang and Nathaniel I. Durlach. *Manual resolution of length, force, and compliance.* The First International Symposium on Haptic Interfaces for Virtual Environment and Teleoperator Systems, vol. 42, pages 13–18, 1992. 36

[Tan 1994] Hong Z. Tan, Mandayam A. Srinivasan, Brian Eberman and Belinda Cheng. *Human Factors for the Design of Force-Reflecting Haptic Interfaces.* Dynamic Systems and Control, vol. 55, pages 353–359, 1994. 35, 36

[Tavakoli 2004] M. Tavakoli, RV. Patel and M. Moallem. *Design Issues in a Haptics-Based Master-Slave System for Minimally Invasive Surgery.* In IEEE Internalional Conference on Robotics and Automation, pages 371–377, New Orleans. LA, April 2004. 40

[Tavakoli 2005] M Tavakoli, RV Patel and M Moallem. *Haptic interaction in robot-assisted endoscopic surgery: a sensorized end-effector.* International Journal of Medical Robotics and computer assisted surgery, vol. 1, no. 2, pages 53–63, 2005. 13

[Tendick 2000] F. Tendick, M. Downes, T. Goktekin, M.C. Cavusoglu and D. Feygin. *A virtual environment testbed for training laparoscopic surgical skills.* Presence: Teleoperators and Virtual Environments, vol. 9, no. 3, pages 236–255, 2000. 27

[Tholey 2004] Gregory Tholey, Jaydev P. Desai and Andres E. Castellanos. *Force Feedback Plays a Significant Role in Minimally Invasive Surgery: Results and Analysis.* Annals of Surgery, vol. 240, no. 6, pages 1–8, 2004. 29

[Tholey 2006] Gregory Tholey and Jaydev P. Desai. *Design and Development of a General Purpose 7 DOF Haptic Device.* In Symposium on Haptic Interfaces for Virtual Environment and Teleoperator Systems, pages 95–101, Alexandria, Virginia, USA, March 25-26 2006. 35

[Toole 1999] R.O Toole. *Measuring and Developing Suturing Technique with a Virtual Reality Surgical Simulator.* Journal of the American College of Surgery, vol. 189, pages 114–128, 1999. 14

[Tuchschmid 2006] S. Tuchschmid, M. Grassi, D. Bachofen, P. Fruh, M. Thaler, G. Szekely and M. Harders. *A Flexible Framework for Highly-Modular Surgical Simulation Systems.* In ISBMS, LNCS, pages 84–92. Springer-Verlag Berlin Heidelberg, 2006. 107

[Upton 2002] Graham Upton. *Laparoscopic surgery simulation realism in a PC.* In The 13th International Training and Education Conference. Lille, France, 2002. 8

[Wagner 2002] C.R Wagner, N. Stylopoulos and R. Howe. *The Role of Force feedback in surgery: analysis of blunt dissection.* In Symposium on Haptic Interfaces for virtual Environment and teleoperator systems, pages 68–74. Orlando FL, 2002. 14

[Walker 2008] Sean Walker and J. Kenneth Salisbury. *Difference-based estimation of support friction.* In IEEE/RSJ International Conference on Intelligent Robots and Systems, pages 59–64, September 22-26 2008. 46

[Wang 2004] D. Wang and Y. Zhang. *Effect of haptic device's position resolution on stability.* In EuroHaptics Conference, pages 377–380, Munich, Germany, June 5-7 2004. IEEE Computer Society. 36

[Wayand 2004] Wolfgang Wayand. *The History of Minimally Invasive Surgery.* Business Briefing : Global Surgery, pages 37 – 38, 2004. 7, 8

[Wentink 2003] M. Wentink, L.P.S. Stassen, I. Alwayn, J.A.W. Hosman and H.G. Stassen. *Rasmussen's model of human behaviour in laparoscopy training.* Surg Endosc, vol. 17, pages 1241 – 1246, 2003. 29

[Woodrum 2006] Derek T. Woodrum, Pamela B. Andreatta, Rajani K. Yellamanchilli, Lauren Feryus, Paul G. Gauger and Rebecca M. Minter. *Construct validity of the LapSim laparoscopic surgical simulator.* The American Journal of Surgery, vol. 191, pages 28–32, 2006. 8

[Xin 2006] H. Xin, J. S. Zelek and H. Carnahan. *Laparoscopic surgery, perceptual limitations and force: A review.* In First Canadian Student Conference on Biomedical Computing, Kingston, Ontario, March 17-19 2006. 8

[Xu 2005] Ruiping Xu and Lie Xu. *An experimental investigation of thermal contact conductance of stainless steel at low temperatures.* Cryogenics, Elsevier Ltd., vol. 45, pages 694–704, 2005. 87

[Xu 2008] F. Xu, T. J. Lu and K. A. Seffen. *Biothermomechanical behavior of skin tissue.* Acta Mechanica Sinica, vol. 24, pages 1–22, 2008. 115

[Yamamoto 2004] A. Yamamoto, B. Cros, H. Hashimoto and T. Himchi. *Control of Thermal Tactile Display Based on Prediction of Contact Temperature.* IEEE International Conference on Robotic and Automation, pp.1536-1541, April 2004. 66, 67

[Yamamoto 2005] A. Yamamoto, H. Yamamoto and Toshiro Higuchi. *Thermal Tactile Presentation with On-Site Parameter Identification of Finger.* In IEEE International Symposium on Industrial Electronics, pages 1365–1370, June 2005. 66, 67

[Yao 2005] Hsin-Yun Yao, Vincent Hayward and Randy E. Ellis. *A Tactile Enhancement Instrument for Minimally Invasive Surgery.* Computer Aided Surgery, vol. 241, no. 1, pages 102–109, 2005. 14

[Yovanovich 1982] M. M. Yovanovich. *Thermal Contact Correlations.* Spacecraft Radiative Transfer and Temperature Control, Edited by T.E. Horton, Progress in Astronautics and Aeronautics, vol. 83, pages 82–95, 1982. 87

[Yovanovich 1997] M. M. Yovanovich, J. R. Culham and P. Teertstra. *Calculating interface resistance.* Electronics Cooling, vol. 3, no. 2, pages 24–29, 1997. 87

[Zhang 2000] Y. P. Zhang, X. G. Liang, Z. Wang and X. S. Ge. *A Method of Determining the Thermophysical Properties and Calorific Intensity of the Organ or Tissue of a Living Body.* International Journal of Thermophysics, vol. 21, no. 1, pages 207–215, 2000. 13, 114

[Zhang 2007] Jisheng Zhang, Jiting Li, Mileta M. Tomovic and Yuru Zhang. *Stability Control of Haptic Interface.* In ASME International Mechanical Engineering Congress and Exposition, Seattle, Washington, USA, November 11-15 2007. 112

[Zhao 2008] Qi Zhao, Jiaming Zhang, Ru Wang and Wei Cong. *Use of a Thermocouple for Malignant Tumor Detection.* IEEE Engineering in Medicine and Biology Magazine, vol. 27, no. 1, pages 64–66, 2008. 114, 115, 119, 121

[Zhong-Shan 2002] Deng Zhong-Shan and Liu Jing. *Analytical study on bioheat transfer problems with spatial or transient heating on skin surface or inside*

biological bodies. Journal of biomechanical engineering, vol. 124, no. 6, pages 638–649, 2002. 115

Design and Control of a Haptic Device for Minimally Invasive Surgery Simulation

Abstract:

The main objective of this thesis focuses on the construction of a new interface for Minimally Invasive Surgery training. This interface incorporates novel broad band sensory modalities that include visual, haptic and thermal technology, into the evolution of the next generation of surgical robotic and surgical simulator. Our particular novelty in this research is in using of thermal stimulation in a MIS applied perspectives. Several thermal exchange models have been designed, implemented and evaluated for telepresence and virtual reality applications. Interesting sensations have been recorded which have a direct bearing on the ability to distinguish between objects in the surrounding environment and particularly in the medical field where temperature sensing correlates with anomalies in some know diseases. A new haptic device is designed and realized by analyzing surgical tasks in terms of required dexterity, workspace, force and torque. The mechanical design constraints have been considered with respect to the general requirements for haptic interface design from what has been well established in the haptics literature. The overall device has been interfaced with an open source VR simulator (SOFA). We added in SOFA the necessary software dealing with thermal simulation using built-in data structure and methods. The integration was successful and a realistic simulation scenario with both visual and thermal feedback was achieved. Preliminary results using the overall simulation are presented.

Résumé:

L'objectif principal de cette thèse est de développer une nouvelle interface pour la simulation des procédures de chirurgie mini-invasive. L'interface développée introduit les modalités visuelle, haptique et thermique pour les futures générations de simulateurs et de robots chirurgicaux. La particularité de cette recherche réside dans l'utilisation de la stimulation thermique dans une perspective d'application pour la chirurgie. Dans ce cadre, plusieurs modèles de transfert de chaleur ont été développés, implémentés et évalués pour des applications de téléprésence et de réalité virtuelle. Des sensations intéressantes ont été enregistrées, ce qui a une conséquence directe sur la capacité de distinguer entre des objets dans l'environnement et particulièrement dans le domaine médical où la sensation thermique est en corrélation avec la présence d'anomalies dans certaines maladies. Un nouveau dispositif haptique est conçu et réalisé en analysant les tâches chirurgicales en termes de dextérité, d'espace de travail, de force et de couple exigés. Nous avons tenu compte des exigences générales de conception mécaniques des interfaces haptiques à partir de ce qui a été établi dans la littérature de l'haptique. Le dispositif complet a été interfacé avec un logiciel de simulation en réalité virtuelle (SOFA). Nous avons intégré dans SOFA le module nécessaire pour la simulation thermique. L'intégration était réussie et un scénario de simulation réaliste avec le retour d'information visuel que thermique a été réalisé. Des résultats préliminaires utilisant la simulation complète sont présentés.

Keywords: Minimally Invasive Surgery, Haptic Device, Thermal Rendering, Mechatronics, Heat flux, Thermoelectric Module, Surgery simulation, Virtual Reality, SOFA framework, Sensor calibration, Mechanical design.